A clinically driven characterization of pathological and non-pathological brain aging in the rhesus macaque model: impact of caloric restriction

By
Gail Stonebarger

A dissertation presented in partial fulfillment of the requirements for the degree Doctor of Philosophy in Behavioral Neuroscience

Oregon Health & Science University
3 June 2022

Dissertation advisory committee:

Chair: Dr. Jacob Raber
Mentor: Dr. Henryk Urbanski
Dr. Heather Bimonte-Nelson
Dr. Randy Woltjer
Dr. Deborah Finn
Final reader: Dr. Matthew Ford

Approved on: _____

Land Acknowledgment

Hypothesis-driven experiments and assays in this dissertation were performed on the unceded land of the primarily nomadic tribes of Cowlitz, Clackamas, Takelma, Upper Takelma, Latgawa, Shasta, Applegate, Galice, Cow Creek, Band of Umpqua, Quilsieton Band of the Chasta, Nahelta Band of the Chasta, Cownantico Band of the Scotons, Naalye Band of the Scotons, Upper Umpqua, Yoncalla, Tualatin, Yamhill, Luckiamute, Mary's River, Muddy River, Long Tom, Calapooia, Winnefelly, Mohawk, Tepoka, Chafan, Santiam, Pudding River, Northern Mollala, Cascades, Clowwewalla, Multnomah, Cathlamet, Skilloot, Southern Mollala, Athapaskan, Chinook, Coos, Kalapuya, Molale, Salishan, Alsea/Siuslaw, Atfalati, and Klickitat of the so-called Pacific Northwest.

Monkeys were housed on unceded lands of the Nacotchtank (Anacostan) and Piscataway tribes of so-called Bethesda, Maryland.

Tissue was processed on unceded lands of the Pawtucket, Mass-adchu-es-et, and Naumkeag tribes of so-called Boston, Massachusetts.

I acknowledge the continued systemic and interpersonal violence against Native tribes and individuals across Turtle Island and thank them deeply for their historical and continued caretaking of and relationship with currently colonized lands. All herein institutions have failed to properly acknowledge or pay reparations to the original caretakers of this land, and I emphasize that this is a systemic tragedy deserving of immediate and substantial attention. Native peoples have much higher rates of nearly all medical maladies and disease, in addition and due to drastically lower access to hospitals, testing facilities, mental health care, and medical clinics. This includes significantly higher transmission of and deaths due to the current COVID-19 pandemic, as well as Alzheimer's disease—the topic of this dissertation—even in the face of historical treaties which promise free and accessible healthcare to all First Nations peoples.

As the author of this dissertation, I acknowledge that control of the land on Turtle Island should be returned to its original stewards via the principles of the Land Back movement.

Reparations payments can and should be made to local tribes as well as the global Land Back movement. To find whose Native land you occupy, search the locations in which you live and work here.

*The views expressed on this page are of Gail Stonebarger

Table of Contents

Land Acknowledgement	2
List of Figures	5
List of Tables	6
Abstract	7
Chapter 1: Introduction	9
1 The aging brain	9
1.1 Cognitive aging	11
1.2 Brain changes in old age	12
2 Alzheimer's Disease	15
2.1 Pathological Hallmarks of AD	18
2.1.i Amyloid beta	19
2.1.ii Phosphorylated tau	21
2.1.iii Neuron loss	24
2.2 Therapeutic interventions	26
3 Caloric restriction	29
3.1 Ongoing long-term CR studies	30
4 Animal models of aging and AD	32
4.1 Preclinical rodent models of AD	32
4.2 The rhesus macaque model of normative and pathological brain aging	34
4.2.i Cognitive decline	35
4.2.ii Amyloid beta	36
4.2.iii Phosphorylated tau	36
4.2.iv Neuronal death	38
4.3 CR studies in the rhesus macaque	39
5 Methodological considerations	41
5.1 Animals	41
5.2 Tissue	44
5.3 Immunohistochemistry	47
5.4 Stereology	51
5.5 Data acquisition: Tau analysis	53
5.6 Data acquisition: PFC amylois plaques	61
5.7 Data acquisition: Neuronal counts	64
6 Study Aims	64
Chapter 2: Experiment 1 Amyloidosis and neuronal stability in the rhesus macaque prefrontal cortex	66
1 Study design and aims	66
1.1 Brain regions	66

1.2 Antibodies and quantification 67
1.3 Statistical analysis 67
1.4 Predictions 68
2 Results 69
2.1 Qualitative staining 69
2.2 Stereological analysis of plaques and neuron numbers 74
2.2.i BA 46 76
2.2.ii BA 32 78
2.2.iii Exploratory analyses 85
3 Summary 90
Chapter 3: Experiment 2 Braak staging and qualitative assessment of phosphorylated tau in the rhesus macaque 92
1 Study design and aims 92
1.1 Identification of regions of interest 93
1.2 Detailed methodology: Antigen retrieval 93
1.3 Detailed methodology: Human tissue 95
1.4 Identification of NFTs 95
1.5 Braak staging 95
1.6 Predictions 96
2 Results 100
2.1 Rhesus macaques followed clinical AD patterns of spread 100
2.2 AT8 non-NFT phenotypes: intracellular, plaques, dystrophic neurites, and glial tau 105
2.2.i Intraneuronal staining 105
2.2.ii Plaques and dystrophic neurites 105
2.2.iii Glial tauopathy 107
3 Summary 108
Chapter 4: Discussion 110
1 Staining patterns 110
1.1 NeuN 110
1.2 4G8 112
1.3 AT8 115
2 Presence and spread of NFTs 119
3 Lack of diet effects 120
4 Summary 123
5 Utilization of the herein characterization 127
6 Future directions 129
7 Conclusion 132
Acknowledgements 134
References 136

List of Figures

1: Changing population dynamics 10

2: Physical brain changes in AD patients, in the transverse plane 14

3: Amyloidogenesis and tau tangle formation across aging 17

4: Braak and Braak postmortem staging system of AD 24

5: Visual representation of the lifespan of the rhesus macaque compared to NIA study dietary condition onset 44

6: Visualization of proteins of interest using brightfield IHC 51

7: Presence of p-tau phenotypes in rhesus macaque hippocampus and surrounding cortex across a range of ages: the first attempt at characterizing tauopathy in the rhesus macaque HPC 55

8: Tau rating system for preliminary tau analysis of AT8-stained rhesus macaque brain sections compared to comparable human tissue 58

9: NeuN and 4G8 immunostaining phenotypes in the rhesus macaque PFC 70

10: NeuN immunostaining in the occipital cortex of the rhesus macaque 71

11: 4G8 immunostaining phenotypes in the rhesus macaque PFC 73

12: Age-related changes in the density of amyloid beta plaques in the rhesus macaque PFC 75

13: Sex and genetic origin effects in BA 46 77

14: Aβ plaque and neuron density in BA 32 of the cingulate 78

15: Aβ plaque and neuron density in BA 32 of the cingulate 79

16: No differences in CAA between dietary treatment groups, sexes, or genetic origins 81

17: Correlations between BA 46 and BA 32 83

18: Sex and genetic origin effects in BA 32 84

19: Relationships between age and Ab extracellular and vascular deposits (plaques and CAA) in the rhesus macaque anterior cingulate cortex 85

20: Linear regressions of measured outcomes across amount of time spent on CR 87

21: Linear regressions of plaque load in the PFC across age in old (20-29.9 years) and oldest-old (30-45 years) monkeys 89

22: T-test comparisons between old and oldest-old monkey PFC plaque burden 90

23: Characterization of p-tau staining of NFTs in rhesus macaque brains using primary antibody AT8 98

24: Clinical presentation and progression of “pure” AD 101

25: Extracellular tauopathy detected immunohistochemically unsing AT8 antibody in the rhesus macaque brain 104

26: Glial tauopathy in the rhesus macaque brain detected immunohistochemically using AT8 antibody 106

27: Glial tauopathy in the aged rhesus macaque 108

28: NeuN immunostaining in the occipital cortex of the rhesus macaque 112

29: Two proposed pathways by which neuronal and glial p-tau inclusions form 118

30: Hallmarks of AD compared to non-pathological human aging and the naturally aging rhesus macaque 131

List of Tables

1: Subject table 47
2: Immunohistochemistry protocol 48
3: Spread and density of NFTs in the aged rhesus macaque using AT8 102

ABSTRACT

This dissertation focuses on brain aging and neurodegeneration, specifically in the context of healthy brain aging versus Alzheimer's disease (AD). To study these processes, a translational model of human aging is necessitated; therefore, this dissertation will focus on the rhesus macaque's utility in modeling clinically normative and pathological brain aging. Protein-level consequences of central nervous system (CNS) aging in monkeys will be experimentally explored and discussed in comparison to concomitant clinical phenotypes. Findings are also interpreted in the context of brain function. Research completed in this dissertation will be further contextualized within neuropathological hallmarks across CNS diseases of aging. Calorie restriction (CR) has been proposed as a behavioral intervention to slow the progression of age-related symptomology, or even alleviate diseases of aging. CR has also been shown to extend lifespan in lower mammals. To this end, I observe herein whether CR has impacts on the rhesus macaque model of extreme brain aging. These studies utilize a cohort of the oldest known rhesus macaques, of which some were maintained on CR diets. Chapter 1, the Introduction, will provide an overview of the value of the rhesus macaque model in studying aging, a justification of methodology, and description of animals used throughout. Chapter 2: Experiment 1 evaluates amyloidosis—a classical hallmark of AD—in two clinically implicated phenotypes in the prefrontal cortex (PFC), along with parallel analyses of neuronal loss in the neocortex. Chapter 3: Experiment 2 takes steps to identify the presentation and progression of hippocampus (HPC) tauopathy in this model, and then expands these findings into the PFC. In Chapter 4, the Discussion, findings in this dissertation will be synthesized, and assimilated within the existing preclinical and clinical literature. Across both experiments, no difference was seen between the CR group

and control group, which suggests that CR may in fact be beneficial due to the lack of overeating, rather than the reduction in caloric intake from baseline. The natural progression of rhesus macaque brain aging appears to model clinically normative humans, as evidenced by a lack of overt dementia, sub-threshold levels of amyloidosis, and very sparse seeding patterns of tauopathy, which overall do not occur until after the average lifespan of the rhesus macaque. I did replicate and expand upon existing literature, showing that amyloid beta plaques increase across age, and that there is no neuronal loss, even in the oldest monkeys. Additionally, CR beyond the ideal caloric intake had no effect on these brain aging hallmarks, even in the presence of some metabolic effects. Amyloidosis, tauopathy, and neuronal death will be further discussed within the context of aging in the absence of dementia, and a critical analysis of the lack of dietary treatment differences. Finally, I include future directions for investigation into rhesus macaque models of AD.

Chapter 1

Introduction

1. The aging brain

As modern medicine progresses, the human lifespan has increased significantly (World Population Ageing, 2017). Fluctuations in population dynamics, including changes in mortality, result in distinct predictable phases of population demographics. As visualized by the U.S. Census Bureau in Figure 1, population fertility and mortality rates interact to change the population demographics as well as the average age of the total population across time. Lowered rates of infant mortality, stable and falling fertility rates (i.e., on average each person with a uterus gives birth to two or fewer offspring), and decreased mortality are occurring to varying degrees across a majority of the world. These variables contribute to alterations in the mean and mode population age; representations of population aging (rather than individual aging) can be seen in Figure 1.

Using projections from the U.S. Census Bureau, by the year 2050 nearly one in four people in the United States, two fifths of the Japanese population, and nearly one in three Spaniards is expected to be 65 years of age or older, for example (U.S. Census Bureau, 2020). Over the next few decades, there is a projected increase in the total number of old people globally, and the proportion of aged people will likely increase by 5% or more, even while overall population grows in a majority of countries around the world (U.S. Census Bureau, 2020); in fact, by 2030, there may globally be more persons over the age of sixty than there are young people between the ages of ten and twenty-

four years old (World Population Ageing, 2017). The overall aging of the population is likely to have major impacts on health care systems. With this understanding, an urgent need arises to comprehend aging on a physiological level, so as to provide proper medical care for a large proportion of the global population.

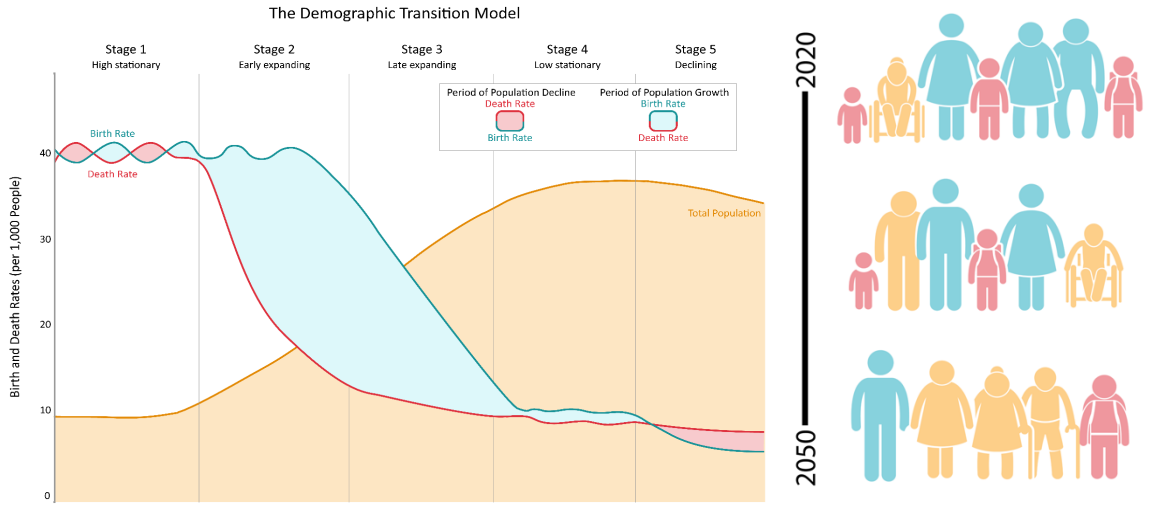


Figure 1: Changing population dynamics. a) The Demographic Transition Model. Stages represent a typical progression in population dynamics (i.e., the interaction of birth rate and death rate) in relation to total population. Stage one involves fluctuating but high birth and death rates, resulting in a small but stable total population. Stage two encompasses the time in which death rates drop dramatically, generally due to stabilizing social conditions, such as improved healthcare and access to resources. During this time, birth rates remain high, which increases the total population number. Stage three occurs when death within the population stabilizes at a low rate, but the overall population continues to increase. Birth rates in this stage, while falling, are still relatively high, especially compared to the low death rate. Stage four indicates a period of population stability, as both birth and death rates are steady. The final phase of stereotypical demographic transitioning is stage five, in which the total population begins to slowly decline, owing to the birth rate falling below that of the death rate across the population. Image sourced from U.S. Census Bureau, Population Division, International Programs. b) Example of a population aging across three generations, from the year 2020 to 2050. Red avatars represent those born in the generation being shown, blue avatars are adults, and yellow avatars represent those over the age of 65. The proportion of the population shown in yellow increases, even while overall population fluctuates. Graphics from U.S. Census Bureau, 2020.

1.1 Cognitive aging

One of the most common complaints amongst aging adults is the decline of cognitive capability and memory (Harada et al. 2013). Under normative, non-pathological aging conditions, there is still evidence of gradual but detectible cognitive decline, which we now know begins as early as the third or fourth decade of life (Harada et al. 2013; Dumas 2015; Schott 2017; Salthouse 2019). While many elderly adults develop overt dementias, a large percentage of the population does not become demented, but still experiences what is considered normal age-related cognitive decline (Dumas 2015; Schott 2017). This process of natural, healthy brain aging is important to understand in order to develop behavioral and pharmacological treatments to aid in independent living and overall functioning, especially given the increasingly expanding stage of old adulthood. It had previously been theorized that these changes begin after the age of 65 years, a cutoff which signifies the end of "working age adulthood" and begins the period of aged adulthood (Murphy 1989; U.S. Census Bureau, 2020).

However, more contemporary data show that in the non-pathologically aging human, some aspects of cognition are spared, while others decline at varying rates and starting at various timepoints in the aging process (Harada et al. 2013; Salthouse 2019). For example, crystalized intelligence refers to skills, ability, and knowledge which are well-practiced and over-learned. This type of intelligence remains stable or even improves across the sixth and seventh decades of life, as individuals gain experiences and continue to practice (Harada et al. 2013; Dumas 2015; Salthouse 2019). Crystalized intelligence is unaltered, or can even improve in the healthy aging brain, while a different type of cognitive capacity, fluid intelligence, begins to decline over the course old adulthood. Fluid intelligence represents an innate ability to learn new information,

process and solve problems in relation to one's environment (Harada et al. 2013). Fluid cognitive ability can be broken into various categories such as processing speed, memory, attention, reasoning, and multiple others, as well as into further subcategories, to represent a dynamic, adaptive way of exploring the world (Harada et al. 2013). Specific types of fluid intelligence begin to become impaired at differing times across the lifespan; i.e., general processing speed begins to deteriorate as early as the third decade of life, and continues to decline indefinitely, while other types of cognition follow separate time courses (Harada et al. 2013). One contrasting example of an aspect of cognition following a different course of decline is that the amount of time needed to make a complex decision during driving seems to be impaired in elderly adults more so than young and middle-aged participants (Salvia et al. 2016). Varying trajectories across different types of cognitive aging allude to a complex and multifaceted pattern of brain aging.

1.2 Brain changes in old age

One helpful tool to measure changes across age *in vivo* is magnetic resonance imaging (MRI). Structural MRI allows investigators and clinicians to observe gray matter and white matter structures in the brain. Functionally, blood oxygen levels in the brain can be measured in real time *in vivo* using functional magnetic resonance imaging (fMRI). The blood-oxygen-level dependent contrast, or BOLD signal, detects increases in blood flow (needed to supply glucose to the active neurons) as a proxy for neuronal activation. This technique has revealed notable divergences in activation patterns in old patients, from what is seen in younger controls. For example, in aged adults, the frontal cortex is reliably overactive compared to younger controls during a plethora of the same

memory and attention tasks, seemingly to compensate for degeneration of other pathways (Park and Reuter-Lorenz 2009; Sambataro et al. 2012; Dumas 2015).

The root physiological causes of complex impairments in fluid intelligence are not fully known; however, there are many physical, as well as functional, brain changes that are known to occur over the course of normative brain aging. At times, functional, anatomical, cellular or molecular brain changes correlate with cognitive measures. These behaviorally-correlated alterations either directly or indirectly cause the behavioral changes seen, or they are compensatory or reactionary responses to upstream modifications in brain functioning. For instance, presence of neurofibrillary tangles (NFTs)—which will be discussed later—predicts dementia severity (Bierer et al. 1995). Modifications in brain form and function that are not directly correlated with cognitive outcomes, but are consistent across aging humans—such as accumulation of pathological protein amyloid beta—are still critical to explore, as they are likely to indicate either compensation mechanisms or pre-symptomatic brain changes.

Perhaps the most striking physical change in the brain across age is the loss of cortical volume. Even in very healthy elderly adults, gray matter and white matter volumes decrease, while ventricles enlarge (Resnick et al. 2003; Figure 2). This volumetric shrinkage is observable both longitudinally and in cross-section *in vivo* through magnetic resonance imaging (MRI), and can be easily identified in postmortem brains (Salat et al. 2004; Raz et al. 2005; Fjell et al. 2009; Fjell et al. 2014). There have been conflicting perspectives regarding the driving factor behind this volumetric loss; for years a primary hypothesis was that neuronal death caused volumetric shrinkage and cognitive impairment. It has now been accepted, however, that in non-demented individuals this phenomenon is *not* due to the loss of cortical neurons, but rather to

changes in cell size and synaptic density (West et al. 2004; Morrison and Hof 1997; 2002; Harada et al. 2013). Neurons show morphologic alterations as they age, including, but not limited to, reduction in complexity of dendritic arborization, decreased spine numbers, shortened dendritic length, and axonal degeneration (Dickstein et al. 2007; Dickstein et al. 2013; Harada et al. 2013; Fjell et al. 2014). These structural changes are now believed to underlie cortical thinning. Taken together, cognitive decline and cortical thinning in non-pathological aging are not due to neuron loss, as there is no substantial decline in neuron number across age even in the oldest non-demented patients. However, there is substantial evidence that alterations in synaptic connections, functional changes as visualized by fMRI, and decline in fluid intelligence are related in healthy aging.

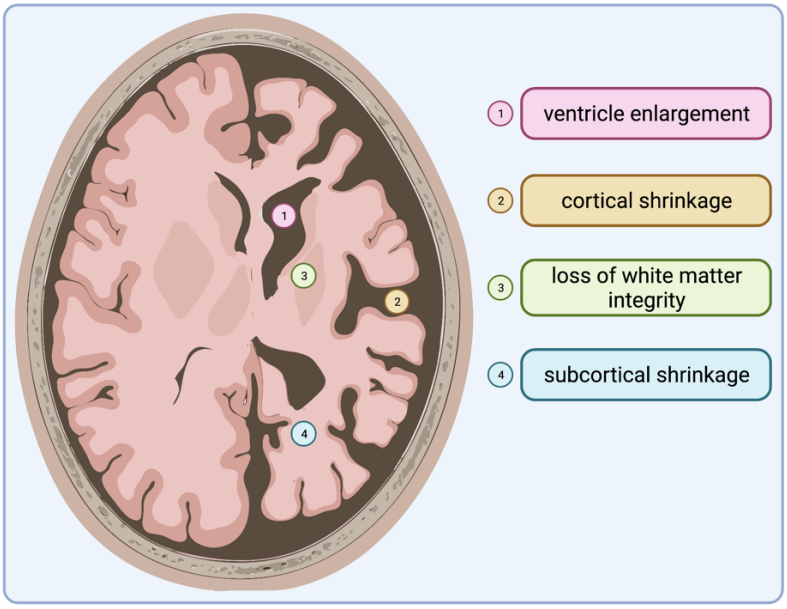


Figure 2: Physical brain changes in AD patients, in the transverse plane. The left hemisphere shows a healthy adult brain, while the right hemisphere shows major brain alterations due to neurodegeneration. These include: 1. Ventricle enlargement, 2. Cortical shrinkage, 3. Loss of white matter integrity, and 4. shrinkage of subcortical areas, notably the hippocampus. Created with BioRender.com

2. Alzheimer's Disease

On top of normative changes to physiology and slight cognitive decline involved in normal, healthy aging, half of adults in the United States aged 50–64 years consider themselves at least somewhat at risk for developing overt dementia such as Alzheimer's disease (AD), while 37% report having a family member with dementia (Maust et al. 2020). These concerns encompass the wide range of AD symptoms—including progressive memory loss, agitation, language deficits, depression, mood disturbances, and even psychosis—and are not unfounded, as a growing percentage of the population does develop AD (Schott 2017; Mehla et al. 2020). The most common symptoms of AD are the severe dementia and neuropsychiatric complaints involved in advanced AD, with 60–70% of dementia cases being attributable to AD (Dey et al. 2017).

Prior to overt AD, patients enter a stage called mild cognitive impairment (MCI), defined as the symptomatic, but predementia, phase of AD (Albert et al. 2011). In the clinic, MCI, like AD, diagnosis is based on behavioral and neuropsychological testing (Albert et al. 2011; Roberts and Knopman 2013). Additionally, it has been proposed that, by the time MCI is diagnosed, it may be too late to reverse current or prevent future cognitive deficits (Boyle et al. 2012). Potentially in contrast to this, not all patients diagnosed with MCI progress to AD or other dementias; however, it is becoming increasingly common to use techniques such as CSF analysis or PET scans to confirm the presence of AD biomarkers; this helps to verify that this condition is due to a pre-AD environment rather than a different form of dementia (Albert et al. 2011; Alzheimer's Facts and Figures 2021). Notably, this system is still not always accurate, as many AD biomarkers are present across normal aging as well. But, pre-AD MCI diagnoses are

considered to be more accurate within the last decade due to these confirmatory assays. Once pathology progresses to a full AD phenotype, clinical diagnosis becomes more straightforward, using both behavioral and neurological diagnostics and assessments of AD biomarkers (Alzheimer's Facts and Figures 2021). Risk factors for the progression of MCI to overt AD dementia are not well understood, and there are many conflicting studies regarding this topic (Roberts and Knopman 2013). Therefore, many studies consider MCI and AD groups separately, as opposed to a single progression from early/pre-AD to full AD symptomology. Even so, many studies show that MCI groups generally show pathology and brain changes which are intermediate phenotypes, between healthy agers and AD patients (as MCI is outside the primary scope of this dissertation, see Roberts and Knopman 2013 and Fjell et al. 2014 for more in-depth information).

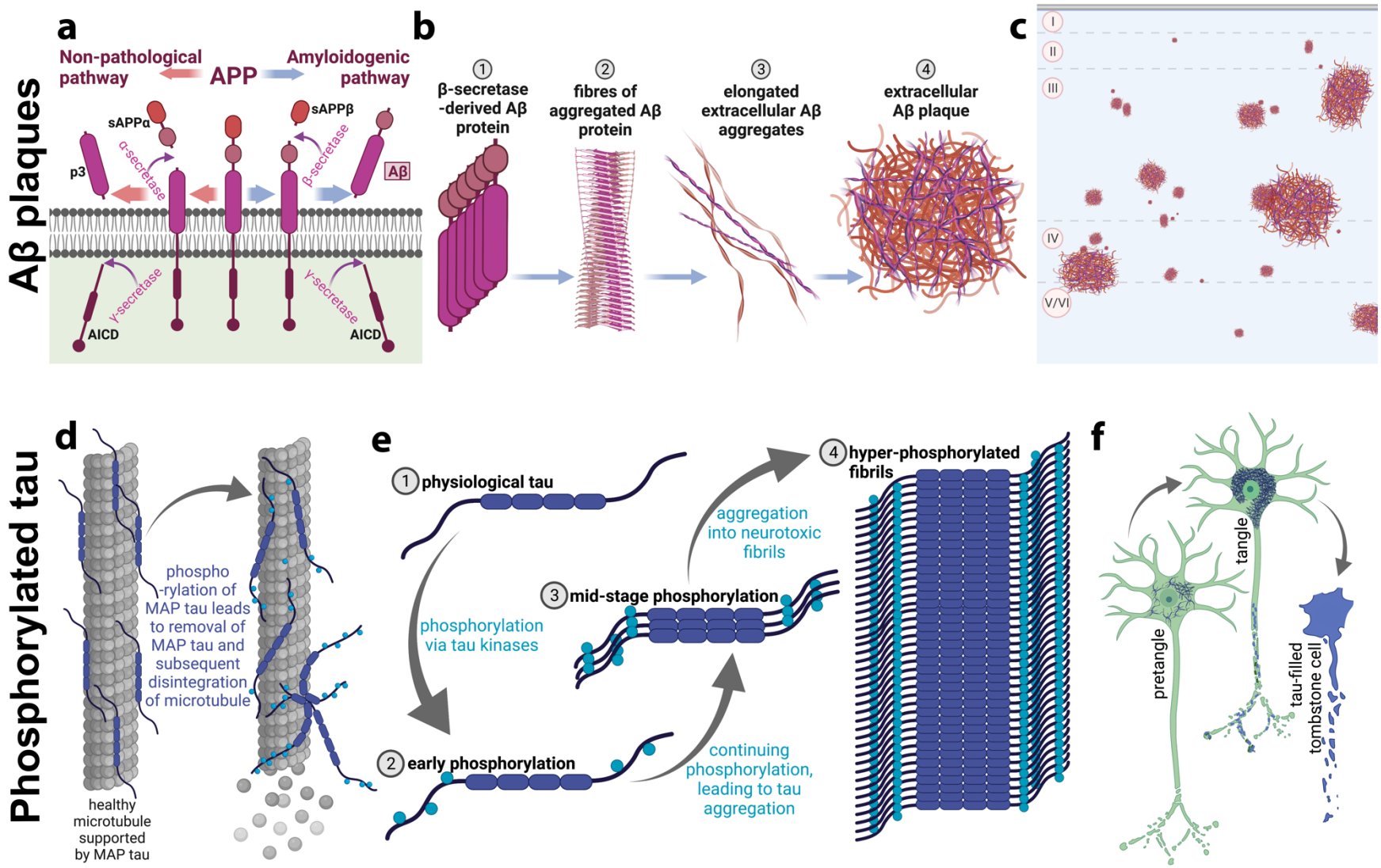

Aβ plaques
a
Non-pathological pathway
APP
Amyloidogenic pathway
sAPPα
sAPPβ
α-secretase
β-secretase
p3
Aβ
γ-secretase
γ-secretase
AICD
AICD
b
① β-secretase -derived Aβ protein
② fibres of aggregated Aβ protein
③ elongated extracellular Aβ aggregates
④ extracellular Aβ plaque
c
I
II
III
IV
V/VI
Phosphorylated tau
d
phospho -rylation of MAP tau leads to removal of MAP tau and subsequent disintegration of microtubule
healthy microtubule supported by MAP tau
e
① physiological tau
② early phosphorylation
③ mid-stage phosphorylation
④ hyper-phosphorylated fibrils
phosphorylation via tau kinases
aggregation into neurotoxic fibrils
continuing phosphorylation, leading to tau aggregation
f
pretangle
tangle
tau-filled tombstone cell

Figure 3. Amyloidogenesis and tau tangle formation across aging. In both old humans and old macaques, amyloidosis and tauopathy occur under normative and pathological aging conditions. Physiological proteins amyloid precursor protein (APP) and microtubule-associated protein tau undergo modifications during aging to form plaques and tangles, respectively. These processes occur in both humans and rhesus macaques across aging, resulting in parallel pathological aggregations of the same proteins in both species. (a-c) Show amyloidogenesis, while (d-f) represent processes involved in tau pathology. (a) Prior to aging, the transmembrane amyloid precursor protein is cleaved by α-secretase to form soluble amyloid precursor protein α (sAPPα; orange arrows; left), and subsequently cleaved further by γ-secretase, which creates p3 and APP intracellular domain (AICD). On the other hand, when APP is cleaved by β-secretase (blue arrows; right), soluble APPβ (sAPPβ) is formed before γ-secretase cleavage into AICD and Aβ, an insoluble pathological protein which is cleaved into the extracellular space. sAPPα, sAPPβ, and p3 are non-pathological APP fragments released extracellularly, while AICD is also physiologically relevant and is released into the intracellular matrix. (b) Aβ proteins begin to aggregate (1), create fibrils (2), form elongated fibers (3), and finally these fibers aggregate into insoluble extracellular plaques in the cortex (4). (c) A graphical representation of extracellular Aβ plaques in the neocortex. The top of the image represents the pial surface, with dashed horizontal lines signifying boundaries between cortical layers. Plaques vary in size and can be present in cortical layers II-VI. (d) On the left, microtubule-associated protein tau (tau) supports microtubules, a part of the neuronal cytoskeleton. When tau begins to be phosphorylated (on the right), the protein no longer adheres to the microtubule, leading to disintegration of the microtubule and subsequent degeneration of the neurites. (e) Tau (1) phosphorylation begins with early phosphorylation sites, which remove the protein from its role providing support to microtubules (2). These phosphorylated proteins are therefore present in the intracellular space, and free to be further phosphorylated by various tau kinases, which leads to intracellular aggregation (3). Eventually, hyperphosphorylation leads to formation of tau fibrils (4), which aggregate intracellularly. (f) Graphical representation of the clinical progression of intracellular tauopathy. In all three neurons, blue represents phosphorylated tau (p-tau). First, p-tau accumulates in the cell, visible via cytoplasmic immunoreactivity, and can be considered a pretangle. It can be presumed that early axonal degeneration is occurring, due to accumulation of detached tau in the cytoplasm. Then, when tauopathy progresses, the cytoplasm shows heavy, fibrillous tau aggregations, which exclude the nucleus and usually present as a teardrop-like shape as seen in the middle neuron. Additionally, at this stage, dystrophic neurites are visibly tau-filled (represented by blue axonal inclusions) and the neuron is presumed to be primarily non-functional. Finally, p-tau continues to fill the intracellular space until the neuron dies. At this stage, the nucleus is no longer distinguishable, and the cell membrane may be "leaking" tau into the extracellular space. The first two phenotypes are seen in very old monkeys, but progression to tombstone cells is uncommon. Figure created with BioRender.com. Published in Stonebarger et al. 2021

2.1 Pathological Hallmarks of AD

Some brain changes do appear to alter cognitive function, even in healthy aging humans (Furcila et al. 2018). However, patients with AD show some aforementioned cognitive symptoms at a younger age than non-demented counterparts, which sets AD patients onto a separate, pathological, brain aging trajectory. AD patients additionally present with overt neuron loss, which is not present in normative aging (Freeman et al.

2008). Accordingly, AD patients also reach higher levels of pathology than their non-AD peers (Duyckaerts et al. 2009). Two hallmarks of AD pathology are amyloid beta (Aβ): A protein which aggregates into extracellular plaques and is formed from cleavage of the APP, and phosphorylated tau (p-tau): A microtubule-associated protein which becomes hyperphosphorylated and accumulates intracellularly (Duyckaerts et al. 2009; see Figure 3 for protein modification and aggregation of each). Notably, these proteins are present in the non-AD aging brain as well; however, specific protein modifications are necessary for the clinical diagnosis of AD (Furcila et al. 2018).

2.1.i Amyloid beta

Aβ is one of two pathological proteins which define AD. Aβ plaques are present throughout cerebral cortices of healthy aging adults; however, they are found in far greater amounts in patients with AD (Edmonds et al. 2016). These plaques form via cleavage of a physiological protein, amyloid precursor protein (APP) into multiple domains including Aβ, and subsequent fibrilization and aggregation of Aβ protein. Figure 3(a-c) shows the progression of Aβ from transmembrane APP to senile plaques in the cortex.

The physiological function of Aβ's upstream protein APP is still not fully understood. It is a transmembrane protein which has almost exclusively been studied in relation to AD. However, APP is present throughout many body tissues, and various splice variants are present in differing ratios throughout the body (Dawkins and Small 2014). The protein cleaved from APP with α-secretase, sAPPα, has been shown to influence cell proliferation, neuritic outgrowth, synaptogenesis, and more. *In vitro*, it alters growth of many cell types including fibroblasts and some B cells, and some studies

show that injection of sAPPα after traumatic brain injury can improve neuronal survival and recovery (Dawkins and Small 2014).

Clinically, Aβ plaques begin to form well before cognitive impairment from AD, and also exist in many cognitively normal people who are aging (Edmonds et al. 2016). For many decades, researchers have sought to lower the amyloid accumulation that is characteristic of AD, to prevent AD's severe cognitive decline. Especially recently, much preclinical and even clinical research has been done to test drugs designed to decrease Aβ production and aggregation, with very limited to no efficacy (i.e., Farlow et al. 2012; Salloway et al. 2014; Sevigny et al. 2016; Ostrowitski et al. 2017; Cummings et al. 2018; McDade 2019; Egan et al. 2019; Haass and Levin 2019). However, researchers continue to develop Aβ-lowering drugs; some posit that the inefficacy is due to study parameters and the lack of drug functionality, and therefore believe that this class of drug may be effective in treating or preventing prodromal to mild AD (McDade 2019; Decourt et al. 2021).

In support of this, aducanumab, an antibody shown to reduce amyloid beta accumulation, was FDA-approved using a fast-tracked pathway (U.S. Food & Drug Administration, 2021). This approval, however, was based solely on the surrogate endpoint of plaque reduction, so the therapeutic potential of aducanumab is unknown especially in the context of symptomatic relief. This is because Aβ plaques do not reliably correlate with cognitive decline, and this and previous amyloid-lowering drugs have failed to consistently slow dementia onset (Nelson et al., 2012; Sevigny et al., 2016; McDade 2019). In the wake of decades of unsuccessful Aβ-lowering drug trials, much focus has shifted towards preventing or reversing the accumulation the other pathological protein involved in AD, hyperphosphorylated tau (p-tau).

2.1.ii Phosphorylated tau

Microtubule-associated protein tau (MAPT, or tau) is a physiological protein which stabilizes axonal microtubles, and has other roles supporting neuronal function, such as signal transmission, axonal transport, and maintaining overall structural integrity of neurons (Lewis and Dickson 2016; Liang et al. 2022). Of late, research interest has grown in phosphorylation and dephosphorylation of tau, and it has become a promising target for therapeutic intervention to prevent or even reverse AD symptomology (Liang et al. 2022). Like many proteins, posttranslational modifications to tau, such as ubiquitination, acetylation, and phosphorylation become more common across aging (Neddens et al. 2018). The culmination of these phosphorylations is p-tau, which has been modified enough that it no longer performs its physiological functions. Immunohistochemistry, which is explained below, can be used to visualize specific protein conformations *ex vivo*. Using this system, monoclonal antibody AT8 is used to detect mid-stage phosphorylation of tau, at Ser202/Thr205, while PHF1, another monoclonal antibody, was developed to detect late-stage tau phosphorylation, at Ser396 (Neddens et al. 2018; Arbaciauskaite et al. 2021). By mid- to late-stage tau phosphorylation, tau is considered to be hyperphosphorylated. P-tau is detrimental due both to loss of function, and to the gain of neurotoxic properties (Crestini et al. 2022; Liang et al. 2022). Once tau is hyperphosphorylated, it aggregates to form fibrils which in some ways resemble Aβ fibrils (Lewis and Dickenson 2015). These fibrils aggregate intracellularly, rather than in the extracellular space (as amyloid does), and the predominant contemporary theory is that tau "seeds" (i.e., initially arises) in some neurons, and then is transferred between cells to propagate. As shown in panels (d-f) of Figure 3, tau first becomes hyperphosphorylated, then forms p-tau fibrils, which begin

to aggregate in the cytoplasm, fill the cell to form a neurofibrillary tangle (NFT) which alters neuronal functioning in a plethora of ways, and can eventually kill the cell (Kosik 1992; Gómez-Isla et al. 1997; Moloney et al. 2021). This is still somewhat contentious, as some aspects of this are yet to be proven, but a majority of researchers accept that p-tau propagates directly or indirectly between neurons to spread through the brain (Lewis and Dickson 2015; Crestini et al. 2022; Han et al. 2022). While healthy agers do show some NFTs, AD patients show higher levels and further spread of p-tau NFTs (Thal et al. 2006).

In 1991, Braak and Braak systematically determined a general trajectory of NFT spread in AD. Of note, in the same paper, they determined that Aβ seems to arise independently in various regions (later described in more depth by Thal et al. in 2000), while p-tau appears to begin at a central locus and spread (Braak and Braak 1991). Their system was broken into six stages: Stage I includes only the transentorhinal region, a Stage II AD diagnosis is given when the transentorhinal region and CA1 of the hippocampus (HPC) are affected with NFTs, and Stage III includes previous regions as well as the subiculum. AD progresses to Stage IV when NFTs are present in CA4 and CA2 of the HPC, to Stage V when neocortex is affected, and finally, in Stage VI AD, all regions of the cortex (notably, including the occipital cortex), in addition to all previously mentioned subcortical regions, are heavily affected by NFTs and significant cell death (Braak and Braak 1991). In their landmark publication, Braak and Braak divided these stages into pairs: Stages I-II are transentorhinal, Stages III-IV include limbic regions, and Stages V-VI are isocortical. Figure 4 is Braak staging from their seminal 1991 paper, which is still used in modern pathological examinations (Trejo-Lopez et al. 2021).

The mechanisms by which p-tau is toxic are still not well-understood, but NFTs interfere with cell signaling and can functionally alter neuronal morphology (Fricker et al. 2017; Fish et al. 2019; Wessling et al. 2020; Zhang et al. 2022). However, it was established multiple decades ago that NFTs correlate with cognitive decline (Bierer et al. 1995), whereas Aβ does not reliably or consistently correlate with cognitive measures (Nelson et al. 2012). Therefore, it has long been assumed that p-tau is directly or indirectly the cause of cell death and, consequently, cognitive decline in AD (Gómez0-Isla et al. 1997; Moloney et al. 2021).

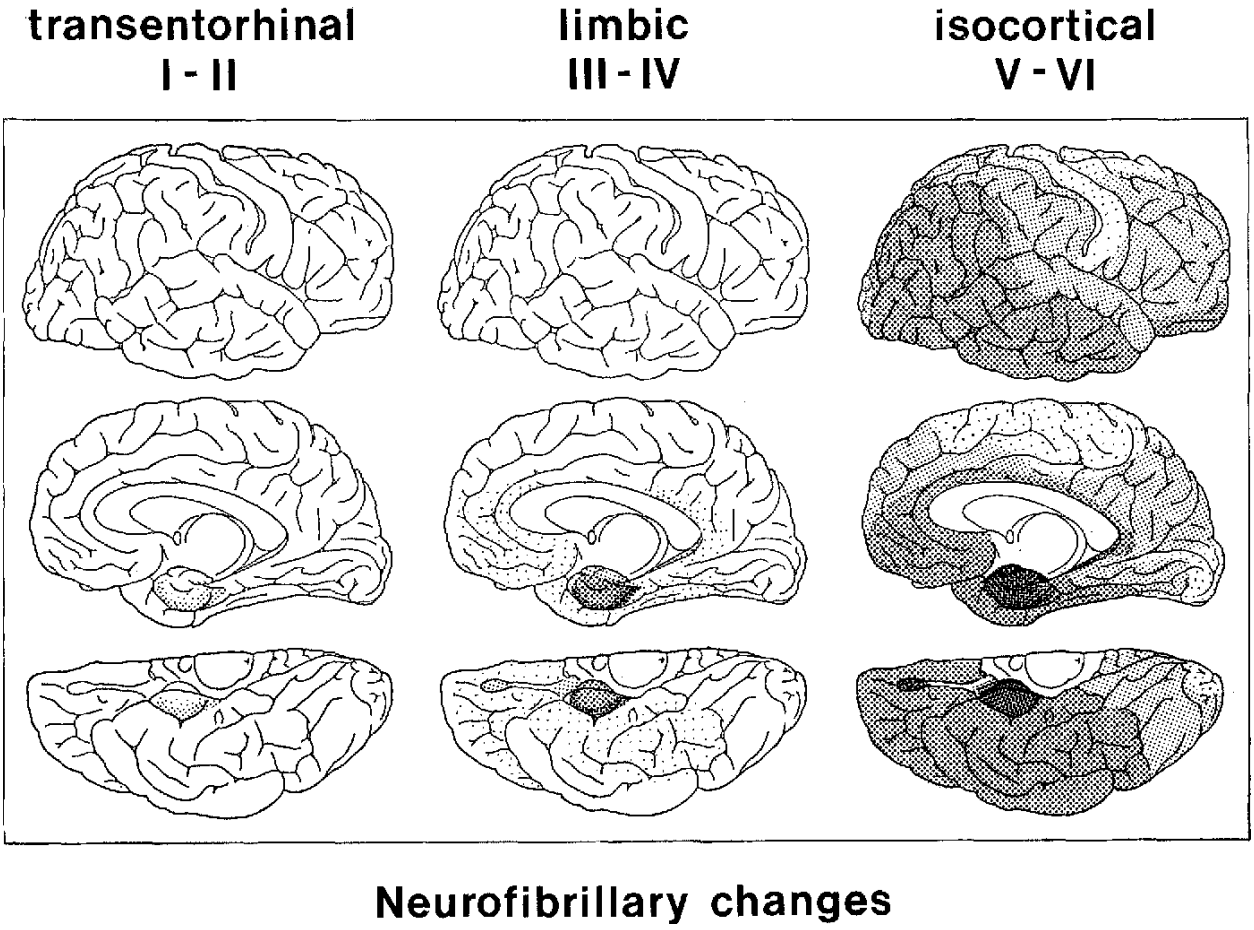


Figure 4: Braak and Braak postmortem staging system of AD. This figure from the landmark paper which established a contemporary method used to stage AD postmortem shows the spread of NFTs temporally in AD. Darker colors represent degree of severity, including NFT density and cell deaths. When NFTs are confined to transentorhinal regions, the patient is judged to be a Braak stage I/II. When limbic regions are involved, the patient has Braak stage III/IV, and finally, when isocortical regions are affected, AD has reached pathology stage V/VI

2.1.iii Neuron loss

Across normative aging, neuronal morphology and synapses are altered, which causes cortical thinning and slight cognitive impairment (Dickstein et al. 2007; Harada et al. 2013). Beyond this phenotype, neurodegenerative diseases—as the name implies—cause neuronal degeneration into cell death (Schliebs and Arendt 2011; Fricker et al. 2017; Li et al. 2022). Since the 1990's, there has been consistent interest in the causes

and consequences of neuronal cell death, especially in the wake of learning that notable neuronal death does not occur in healthy, non-pathological aging (Schliebs and Arendt 2011; Harada et al. 2013; Fricker et al. 2017; Li et al. 2022). A model, therefore, that has been proposed for the pathway to cell death in AD neurodegeneration is called the amyloid cascade hypothesis. This has been a predominant theory of AD neuropathology for multiple decades now (Selkoe 1991; Hardy and Higgins 1992; Price 1994; Selkoe and Hardy 2016; Haass and Levin 2019). The amyloid cascade hypothesis posits that the first event in a cascade that leads to clinical presentation of AD symptoms is the deposition of Aβ in the extracellular space. These deposits, by an unknown mechanism, induce hyperphosphorylation of tau and its subsequent deposition into neurons to form NFTs. These NFTs then lead to significant neuronal death, causing severe cognitive impairment seen in AD in the clinic (Hardy and Allsop 1991; Selkoe 1991). This idea is becoming more contentious, as various evidence arises that some amyloid species are toxic enough to induce cell death and p-tau and NFTs can precede or exist in the absence of Aβ plaques, along with other seeming contradictions to the theory (i.e., Price and Morris 1999; Price and Morris 2004; Haass and Levin 2019). Regardless of the cascade mechanism, it continues to be obvious that neuronal death is a consequence of pathological aging rather than normative aging, and is therefore a defining feature in AD cases (Harada et al. 2013; Schott 2017). Fully modeling AD preclinically would include all three major physical hallmarks of AD: amyloidosis, NFT accumulation, and neuronal death, as well as severe cognitive impairment (which, theoretically, should occur if all three of these hallmarks are present). Because the relationship between the four major hallmarks of AD is not fully understood, all three physical brain hallmarks are potential targets for therapeutic intervention.

2.2 Therapeutic interventions

In addition to the previously discussed Aβ -lowering aducanumab, there are some FDA-approved, as well as experimental treatments, that show some preclinical and clinical efficacy. There has been very limited efficacy in preventing the onset of some new memory-related AD symptoms with memantine, an N-methyl-D-aspartate (NMDA) receptor antagonist, cholinesterase inhibiters such as donepezil, and a recently approved combination of the two classes (Miziak et al., 2021). However, there are no current interventions which treat the etiology of or even prevent the progression of AD, in spite of many previously cited studies and clinical trials over the last three decades (McDade 2019).

Alternative (i.e., not synthesized in a laboratory; also referred to as natural, homeopathic, organic, traditional, ancient, and many other monikers) pharmacological interventions are gaining in popularity across medical fields, for a multitude of symptoms. There is some research on using ancient natural herbs to treat cognitive symptoms of various diseases, and aging in particular—and occasionally specifically in the context of AD (Dey et al. 2017; Mehla et al. 2020). Sage (*Salvia lavandulaefolia* and *Salvia officinalis*) and the Indian herb mandukparni (*Centella asiatica*; also referred to as jalbrahmi), among many others, have been used for centuries to improve memory and cognitive function (Mehla et al. 2020). Many of these plants and active compounds have recently been shown to have beneficial effects across aging in animal models and limited clinical trials, and current work focusing on the active compounds in these medicinal herbs is very promising for future interventions (for a review, see Mehla et al. 2020). One example, Brahmi (*Bacopa monnieri*) is a perennial creeping plant native to India that has been shown to have effective antidepressant, anticonvulsant, and

antimicrobial properties, along with many others (Aguiar and Borowski 2013). Importantly, Brahmi extracts have been shown in rodents to improve the formation and retention of memories and attenuate retrograde amnesia under various conditions. These properties seem to be due to a combination of multiple mechanisms of action in the brain, including enhancing protein kinase activity in the HPC, decreasing cerebral amyloid levels, protecting against aging-related changes in neurotransmitters, and more (Rastogi et al. 2012; Aguiar and Borowski 2013). This compound has shown clinical efficacy as well, with healthy elderly patients showing improved working memory and auditory memory, as well as decreased depression and anxiety compared to the control group (Calabrese et al. 2008). However, Brahmi is not tolerable to a portion of the population, as it can cause gastrointestinal tract irritation in various forms (Aguiar and Borowski 2013).

Another well-known medicinal compound is curcumin, or turmeric. Curcumin has been used since ancient times as an anti-inflammatory and has gained popularity recently as an overall health aid; in fact, it is now one of the most-studied plants for various diseases (Mehla et al. 2020). Similarly to Brahmi, preclinical studies over the last few decades have shown many anti-Aβ effects of curcumin in the brain, such as decreasing Aβ fibril production, reversing age-related neuronal hyperexcitability, preventing plaque aggregation, and encouraging dissolution of plaques (Lim et al. 2001; Chang et al. 2022). Behaviorally, curcumin exhibits beneficial effects on learning and memory as well as motor skills in multiple preclinical models (Moore et al. 2018; Gonzalez-Granillo et al. 2022; Uprety et al. 2022). Many various compounds show promise in both the improvement of cognition and attenuation of deleterious effects of brain aging, including dwarf morning glory (*Evolvulus alsinoides*), jyotismati (*Celastrus*

paniculatus), ashwaganda (*Withania somnifera*), and others reviewed in Mehla et al. 2020. None of these compounds are U.S. FDA-approved for treatment or prevention of diseases of aging, but some herbs are legally sold as supplements, even in the United States (Mehla et al. 2020). There are multiple Chinese and Indian herbal compounds that use multiple herbs synergistically and are used to treat AD. At least five of these compounds show promising effects in preclinical models, while two, mentat and Chinese Material Medica (CMM), have improved memory impairment, increased memory span, attenuated attention deficits, and improved learning ability in various human cohorts (Dey et al. 2017; Mehla et al. 2020).

Behavioral alterations towards healthy living have also been shown to consistently decrease the risk of, as well as slow progression of, AD (i.e., Podar et al. 2019; Decourt et al. 2022; Gregorini et al. 2022; Sendorovich et al. 2022). In some cases, these interventions can benefit caregivers, and the relationship between the patient and caregiver, as well, and caregiver wellbeing is also associated with patient outcomes (Attonsdotir et al. 2022; Bufalini et al. 2022; Byrne et al. 2022; Kępka et al. 2022). Sleep and diet have been two primary points of focus, as both of these have been highly implicated in various types of healthy and pathological aging (Cordone et al. 2019; Poddar et al. 2019; Cunnane et al. 2020; Lucey 2020; Oster 2020; Decourt et al. 2022). For example, a single night of sleep deprivation in old age can lead to increased toxic amyloid levels in cerebrospinal fluid (CSF) the next morning, and modifying sleep-wake cycles alters both p-tau and Aβ levels in CSF (Ooms et al. 2014; Lucey 2020). Caloric composition and intake have long been known to impact cognitive and physical aging, and these benefits are likely conferred under pathological aging conditions as well. Clinical studies have shown that across decades of aging, people who consumed

blueberries and strawberries regularly have slowed cognitive decline relative to their counterparts with diets that were less flavonoid-enriched, and numerous studies on the effects of nutrition, exercise, and sleep on aging and neurodegeneration have been conducted and showed promising results over the last fifty-plus years (Lettenour et al. 2007; Mancusco et al. 2007; Devore et al. 2012; Kępka et al. 2022; Korf et al. 2022; Vakulin and D'Rosario 2022). Early behavioral interventions have potential for highly efficacious treatment of AD and other age-related neuropathologies; further, determining the mechanisms through which benefits are conferred will elucidate options for new pharmacological interventions.

3. Calorie restriction

Calorie restriction (CR) is defined as a significant (generally between 10% and 40%) reduction in caloric intake below baseline, but without nutritive deficit (Mattison et al. 2017). In various animal models CR has long been studied as an intervention to attenuate aging processes in order to prolong healthspan and lifespan (McCay and Crowell 1934; Parrella et al. 2013; Kishi et al. 2015; Wahl et al. 2017). Since the middle of the twentieth century, interest has grown in CR as a way to delay aging. Many laboratory organisms, including yeast, fruit flies, spiders, nematodes, rats, and mice have shown lifespan extensions (Harper et al. 2006), but there are various mechanisms by which this extension may occur. While cardiometabolic effects are obvious outcomes to assess in relation to CR enhancements, and there are many benefits of CR on cardiometabolic health (Kraus et al. 2019), numerous studies show benefits of CR on the aging brain. For example, in rodents, CR has been shown to facilitate healthy brain

aging by mitigating hippocampal gene methylation, decreasing apoptosis, increasing neurogenesis, and improving cognitive function and motor performance (Ingram et al. 1987; Halagappa et al. 2007; Wahl et al. 2017; Gültekin et al. 2018; Hadad et al. 2018). Besides seemingly delaying natural aging processes in the brain, CR postpones onset of age-related disease characteristics (Weindruch et al. 1986; Weindruch and Walford 1982; Fontana et al. 2004; Mattison et al. 2017). However, some laboratory species as well as many wild-caught rodents don't show an extension of life, and in fact sometimes show a reduction in lifespan with CR (Harper et al. 2006). Due to these mixed data, it is unknown whether CR will be effective in elongating lifespan or healthspan in more complex mammals.

3.1 Ongoing long-term CR studies

Assessing the effects of CR in humans is understandably difficult as it is impossible to completely control the environment, adherence to diet regimens is poor, and participant retention is low. However, there is a contemporary well-known clinical study of CR in humans, with multiple phases so far: the CALERIE (Comprehensive Assessment of Long-term Effects of Reducing Intake of Energy) study. Upon entry to the study, participants were randomly assigned to a control group with a high–glycemic load diet (60% carbohydrate, 20% protein, 20% fat) or a 30% CR low–glycemic load diet (40% carbohydrate, 30% protein, 30% fat; Pittas et al. 2005). Study participants were provided food for the initial 24-week period, and asked not to consume other food; however, they were also asked to record other calories they consumed. This initial study was small, with only 32 participants completing the dietary regimen and follow-up measurements. However, since then, larger cohorts of clinical trials have been initiated.

In a following CALERIE study, two thirds of participants were assigned to a 25% CR diet, of which only a portion was provided by investigators. Additionally, the other third of participants who comprised the control group did not alter their diet, and continued to eat *ad libitum*, replicating the normal adult human condition (Rickman et al. 2011). These parameters were followed by 220 people for a year, to establish baseline weight loss: investigators did not want weight loss to confound the effects of "pure" CR, after benefits of weight loss were conferred (Rickman et al. 2011).

The current phase of the CALERIE trial, a multi-center clinical study of CR, has provided valuable insight on the effects of health parameters (Kraus et al. 2019). The current cohort of the CALERIE study is CALERIE 2, in which two thirds of randomly assigned participants were asked to adhere to a 25% CR diet for two years versus the last third, who continued to consume calories at *ad libitum* levels (Huffman et al. 2022). However, one of the difficulties inherent to clinical studies is the lack of control over many parameters, including adhesion to dietary regimens; to this end, the CR group averaged an 11.9% CR across the two years. Even so, many beneficial outcomes have been reported thus far.

Improved cardiometabolic health has so far been the primary outcome of this trial, but enhanced mood and sleep in the CR group indicate that there may be central effects as well (Martin et al. 2016; Kraus et al. 2019; Huffman et al. 2022). Compared to *ad libitum* controls, CR participants in the CALERIE 2 study have significantly improved general mood, sleep quality, general health, and sexual function (Martin et al. 2016). However, weight loss can also be correlated with these outcomes, and the individuals in the CR group of the CALERIE 2 study lost an average of 10% body weight over two years of treatment, even following the initial CALERIE studies which

attempted to control for weight loss (Martin et al. 2016; Huffman et al. 2022). Therefore, these beneficial central effects need to be more deeply probed to determine whether they are results of CR itself or of the accompanying weight loss.

4. Animal models of aging and AD

In order to make significant advances in our understanding of the pathways and neurodegenerative trajectories that underlie AD, and to develop safe and effective therapies, it is important to develop and characterize appropriate experimental animal models of AD. These preclinical models inform and drive novel investigations in the clinical realm, underscoring the importance of promoting cross-talk between preclinical and clinical science, as well as the critical nature of translational science for therapeutics.

4.1 Preclinical rodent models of AD

Rodents are the most commonly-used laboratory animals and have relatively short lifespans to allow for rapid experimental turnaround in aging studies. They do not, however, naturally develop measurable pathological features of AD such as Aβ plaques or p-tau tangles (LaFerla and Green 2012). Several methods have been employed to mitigate this lack of overt pathology, generally via modifications to genes which are known risk factors for AD, such as amyloid precursor protein (APP), apolipoprotein E, and presenilin (Webster et al. 2014). Other models involve adeno-associated virus (AAV) vectors and floxed genes (i.e., temporally controlled and mediated genes), induction of pathology via direct or indirect addition of Aβ and/or p-tau, or sometimes

direct insertion of clinical genes or proteins found in AD patients. For examples of these manipulations, see Alzforum (2021). These models allow great flexibility and temporal control over induction of AD characteristics which cannot be achieved with sporadically occurring clinical AD. Specific realms of memory can be probed on a basic level using rodent behavioral paradigms; for instance: set-shifting, spatial navigation, working memory, perseveration, and many other typically affected forms of cognition are measurable in rodents (Webster et al. 2014). These paradigms provide valuable insights into specific realms of memory as well as molecular mechanisms of aging. Conversely, some complex cognitive measures—such as the neurocognitive testing considered to be the clinical gold standard—are impractical or sometimes even impossible to use in characterizations of AD-like symptomology in rodents (Harada et al. 2013; Webster et al. 2014; Deb et al. 2017; Ingram and De Cabo, 2017; Colman 2018). Therefore, collectively, when assessing clinical hallmarks of AD, the rodent model provides a basis for informing studies in higher mammals.

Mice and rats are short-lived, allowing for study of the aging process in a relatively contracted time frame, but this abbreviated lifespan also limits chronological aging. For instance, 1-3 years (the average lifespan of a laboratory mouse; Dutta and Sangupta 2016) simply may not be enough time for pathological proteins such as Aβ or p-tau to accumulate and have neurodegenerative effects. As seen in the interactive visualization by Alzforum (2021), many mouse models do recapitulate aspects of AD—for example, APP processing (Figure 3[a-c]) via genetic induction—and they have been crucial to our understanding of mechanisms of aging and AD. To gain a holistic understanding of the disease, a more robust, naturally-occurring model is optimal. This model must also be highly clinically translational in order to probe complex cognitive

functioning, temporal dynamics, and non-cognitive neuropsychiatric symptoms. These shortcomings in rodent models may be complemented with the study of the rhesus macaque to model AD and aging. Taken together, the use of small laboratory rodents is paramount for studying cellular and molecular aspects of AD pathology, but a more complete clinically translational model is needed to recapitulate subtle behavioral symptoms and sporadic onset of both AD and normative aging mechanisms.

4.2 The rhesus macaque model of normative and pathological brain aging

The rhesus macaque (*Macaca mulatta*) is a nonhuman primate (NHP) that shows close genetic homology to humans (Rhesus Macaque Genome Sequencing Analysis Consortium, Gibbs et al. 2007), has a greatly extended lifespan relative to rodents (Bodkin et al. 2003; Mattison et al. 2017; Stonebarger et al. 2020), is capable of performing complex and prefrontal cortex (PFC)-dependent cognitive tests similar to those used in the clinic (Rapp and Amaral 1989; Peters et al. 1996; Moore et al. 2006; Nagahara et al. 2010) and also shows similar life stages; i.e., a prolonged childhood, adolescence, adulthood, and cognitive and hormonal aging declines (Downs and Urbanski 2006; Messaoudi et al. 2011; Sorwell et al. 2012; Mattison et al. 2017). For these reasons, the rhesus macaque may represent a more holistic and systems approach to studying mechanisms underlying human aging. Additionally, it has been commonly known for decades that rhesus macaques develop cortical and subcortical Aβ plaques—which represents the natural formation and aggregation of this protein—and there is evidence that this involves the same pathways as in human brain aging (Heilbroner and Kemper 1990; Uno 1993; Stonebarger et al. 2020).

4.2.i Cognitive decline

Because rhesus macaques are capable of more complex learning and memory tasks and have longer lifespans compared to rodents, they represent a valuable translational animal model with which to study longitudinal changes in cognitive function. For instance, many behavioral batteries include neuropsychological tests that closely resemble those used to clinically assess cognitive decline; i.e., monkeys are capable of performing testing with the same complexity and nearly identical parameters as multiple tests used in the clinic. To this end, many researchers have observed a gradual but significant decline in cognitive ability which occurs over the course of macaque late adulthood (Lai et al. 1995; Herndon et al. 1997; Moore 2003, Moore et al. 2006). For example, short-term memory, task-dependent memory, two-choice discriminations, abstraction, and set-shifting have all been shown to be impaired in old rhesus macaques compared to young, or even in some instances also compared to middle-aged monkeys (Bartus et al. 1978; Rapp and Amaral 1989; Lai et al. 1995; Herndon et al. 1997; Voytko 1999; Moore 2003). Importantly, as in humans, this decline is progressive such that “early aged” monkeys (19–23 years), “middle-aged” monkeys (24–29 years), and “oldest-old” (30+ years) show different levels of cognitive performance. Each age group shows impairments compared to the group directly younger in delayed non-match to sample tasks and non-spatial delayed recognition span test (Herndon et al. 1997; Harada et al. 2013). Like humans, variability in rhesus cognitive scores also increases with age (Moss et al. 2007; Schott 2017). However, even considering deficits seen in animals with the lowest cognitive scores, aging macaques do not appear to show decline of cognitive function as rapidly or to such severe impairment as humans with AD (Hara et al. 2012).

4.2.ii Amyloid beta

For decades, the progression and accumulation of Aβ extracellular plaques in the rhesus macaque has been well-documented. For example, in 1993 Uno reported amyloid plaques in 40–66% of rhesus macaques aged 20–30 years (Uno 1993), and as detection methods have improved in the last three decades, it may be that an even higher percentage of aged animals show amyloidosis. However, at least in the PFC, amyloidosis levels do not reach the threshold for clinical AD. For instance, brains of AD patients tend to show 10–20% area coverage of plaques in the PFC (O'Brien and Wong 2011; Smith et al. 2019). Nevertheless, a majority of studies using various methodologies have confirmed an increase in rhesus cerebral amyloid across age, which parallels findings in the clinic (Heilbroner and Kemper 1990; Uno 1993; Stonebarger et al. 2020). Moreover, building on this observation, there have been successful attempts to induce—rather than naturally replicate—a phenotype that more closely parallels the human AD brain environment in multiple species of macaques (Forny-Germano et al. 2014; Beckman et al. 2019). Altogether, these Aβ plaque data strongly suggest that the same aging processes occur in both human and rhesus macaques, but that they may be less developed in the rhesus brain.

4.2.iii Phosphorylated tau

Until recently, the rhesus macaque had been accepted as an incomplete model of AD, or potentially dismissed fully as a model of even natural clinical aging, due to the lack of neuronal p-tau detection. Indeed, for decades, rhesus macaques were considered not to develop p-tau naturally. This has presented a challenge in phylogenetically synthesizing the evolution of p-tau tangles—as chimpanzees, baboons, gorillas, and

cynomolgus monkeys have all shown evidence of cortical tauopathy (Schultz et al. 2000; Oikawa et al. 2010; Perez et al. 2013; Edler et al. 2020), along with some smaller simians such as marmosets and lemurs (Giannakopoulos et al. 1997; Sharma et al. 2019). Rhesus monkeys, a key evolutionary link, have not historically shown immunoreactivity to p-tau (Peters et al. 1996; Zhang et al. 2019). However, in 2018 Paspalas et al. reported detection of p-tau in the rhesus macaque entorhinal cortex, which has led to a resurgence in interest surrounding non-human primate p-tau. In addition to this initial landmark study, laboratories are currently researching both natural p-tau accumulation and tauopathy induction models in the rhesus macaque (i.e., Beckman et al. 2021; Datta et al. 2021). There is still much work to be done characterizing natural tauopathy in the rhesus macaque, but it has generally been observed that most monkeys do not live long enough to develop pathological tauopathy. For instance, most overt tauopathy appears to occur mainly in macaques over the age of 30 years, and very few primate facilities have a cohort of very old animals (Mattison et al. 2017; Paspalas et al. 2018; Stonebarger et al. 2021; Datta et al. 2021). Therefore, non-human primate induction models become highly relevant: if the same natural pathways that lead to tauopathy can be dysregulated or stimulated earlier in life, researchers can study the etiology and progression of the proteinopathy across many years, and monkeys would likely achieve more advanced states of tauopathy. This could mimic neurodegeneration or advanced stages of human brain aging, which can inform clinical progression of the disease; if researchers can induce tauopathy into a further progressed state in the macaque, the inverse processes are logical targets for early AD intervention. It should be emphasized that relatively few rhesus monkeys live beyond ~25 years, which is prior to the age at which they begin to show significant hippocampal tauopathy

(Le Bourg 2018; Paspalas et al. 2018; Datta et al. 2021); thus, the systematic study of p-tau induction will be critically important in further developing the macaque AD model. To facilitate induction models, patterns and mechanisms of natural p-tau accumulation need to be characterized in this species.

Taken together, the recent p-tau data question the traditional dogma that non-human primates do not develop AD due to a lack of p-tau accumulation. The primary physical AD hallmarks: clinically relevant p-tau intra-neuronal tangles and Aβ plaques, have now been observed in monkeys; so why don't they show a full cognitive AD phenotype?

4.2.iv Neuronal death

Mid- and late- stage clinical AD result in significant neuronal death in subcortical structures such as the hippocampus, and in the neocortex (Furcila et al. 2018). To fully capitulate an AD phenotype, the rhesus macaque would need to show significant cell loss in areas that are sensitive to aging. Thus far, data show no neuronal loss has been seen across multiple rhesus macaque brain regions, including the PFC, hypothalamus, and visual cortex (Peters et al. 1994, Peters 1998; Roberts et al. 2012; Giannaris and Rosene 2012; Stonebarger et al. 2020). Notably, the hippocampus has not to our knowledge been stereologically analyzed across age in the rhesus macaque. This brain region is highly sensitive to cognitive and pathological aging changes, critical to memory consolidation, and undergoes significant shrinkage in AD (Freeman et al. 2008; Squire et al. 2015). While the lack of neuron loss in all other analyzed areas seems to indicate that rhesus macaques do not naturally lose neurons as they age, it is interesting to note

that the multiple cohorts of rhesus monkeys have shown p-tau tangles in the hippocampus (i.e., Paspalas et al. 2018; Datta et al. 2021; Experiment 2 herein). Furthermore, in clinical studies it has been shown that p-tau tangles are associated with cell death—one of the primary drivers of cognitive decline in AD (Peters et al. 1994; Datta et al. 2021). Taken together, the overall consensus is that rhesus macaques do not show the distinctive neuronal loss that characterizes the later stages of AD in humans, and which is associated with dementia; however, there are still brain regions that show cell loss in humans with AD, yet to be assessed in the NHP.

4.3 CR studies in the rhesus macaque

To more easily identify and explore the mechanisms by which CR affects the brain and body, it is necessary to have available a preclinical animal model for which environmental factors such as diet, temperature, photoperiod, and medication can be strictly controlled. Described in more detail below, the nonhuman primate (NHP) fulfills these requirements. To this end, two National Institutes on Aging -funded, controlled longitudinal studies on CR in NHPs both began in the 1980's in separate facilities, in the hopes of determining whether beneficial effects of CR seen in many laboratory animals translate to higher order mammals (Kemnitz et al. 1993; Mattison et al. 2005; Mattison et al. 2017). Both studies utilize the rhesus macaque monkey (*Macacca mulatta*), but the parameters differ in significant ways. At the National Institute on Aging (NIA), diet was initiated in 121 monkeys at differing times in the lifespan, ranging from juvenile to old adulthood, to detect whether there are critical windows within which CR is effective in delaying aging (Mattison et al. 2017). At the University of Wisconsin (UW), monkeys entered the study during adulthood, as a way to control for developmental effects CR

may have. A further difference in the studies is the dietary control group utilized. UW control monkeys had *ad libitum* access to chow for 6-8 hours per day, while NIA controls were fed at calculated approximated healthy caloric amounts based on the National Research Council publication *Nutrient Requirements of Nonhuman Primates* (1978). Age-, sex-, and body weight- matched controls were given a 30% CR compared to this diet, such that CR animals were consuming 70% of the calories that their matched control counterparts ate. Notably, both groups received supplemental vitamins to ensure a complete nutritional diet. The UW control group was designed to mimic a clinical study design, in which a control group people would not change their eating habits (and have access to any food they would generally eat) and a CR group would follow guidelines to limit their caloric intake (Kemnitz et al. 1993). Conversely, NIA investigators limited control animals to a calculated healthy caloric intake so as to prevent obesity, which has many detrimental brain and cardiometabolic effects outside of just a lack of beneficial CR effects (i.e., Dye et al. 2017). While *ad libitum* access to food is common, both in preclinical laboratory animals and in human day-to-day life, to experimentally limit access prevents overeating and its subsequent obesity. Obesity and overeating (clinically known as hyperphagia) have been shown to have detrimental cognitive and metabolic effects, including widespread inflammation, vascular dysfunction, and impairment on a number of cognitive domains (Gardener et al. 2020; Tanaka 2020). Therefore, it was important to eliminate these two variables by limiting each animal's caloric intake to healthy levels. In this way, we can study CR compared to normal calorie consumption, rather than compare CR animals to obese animals. Because NIA controls were not allowed to become obese, investigators used the control group as a "pure" control, without the confounds of obesity, albeit one less similar to a

CR design in humans (Mattison et al. 2005, Mattison et al. 2017). Both studies have definitive justifications and therefore slightly different outcomes and interpretation of data. Animals in this dissertation are from the NIA CR study, so group differences are more definitively related to CR, rather than a lack of obesity.

5. Methodological considerations

5.1 Animals

The rhesus macaque is the most widely studied NHP model of human aging with an average lifespan of 26 years (Colman 2018), and a maximum reported lifespan of 44.1 years (Stonebarger et al. 2020). As previously described, the rhesus monkey is a pragmatic preclinical model with which to study aging (save for the logistical issue of its long lifespan, which can span the careers of multiple principle investigators). Although it remains unclear why some monkeys from the herein cohort lived well beyond the reported average lifespan, postmortem tissue from these oldest-old animals provides valuable insights into very advanced NHP aging. For example, because aging is the primary risk factor for AD diagnosis (Matthews et al. 2019), there is increased likelihood of detecting clinical AD pathology such as neuron loss in the brains of these very old animals. In the current study, postmortem brain tissue was obtained from a subset of these aged NIA animals and examined for differences between diet groups (CR and control) and the effects of age (Mattison et al. 2017).

Therefore, to systematically assess the effects of CR on primate aging, 121 male and female rhesus macaques of varying genetic backgrounds and breeding sources were enrolled in the herein discussed longitudinal aging study. All procedures were

conducted in accordance with the Guide for the Care and Use of Laboratory Animals and approved by the NIA Intramural Research Program Animal Care and Use Committee (IACUC). Subjects included twenty-one rhesus macaques (six females; fifteen males) housed at the NIH Animal Center (Table 1). All females aged 26+ were assumed to be postmenopausal based on their low circulating levels of anti-Müllerian hormone, estradiol, and progesterone, as compared to previously reported values for this species (Downs and Urbanski 2006; Luna et al. 2020). These animals represented a subpopulation of the NIA longitudinal study of CR in NHPs, initiated in the late 1980s with approximately 120 subjects. Notably, this subset included all subjects with PFC brain tissue that was not over-fixed (and therefore unusable for the IHC protocol detailed below), that were available at the time of the current study. Age at death (ranging from 22 to 44 years) was not significantly different between the control ($n = 10$, mean = 31.29 years, SEM = ± 1.33 years) and CR ($n = 8$, mean = 32.49 years, SEM = ± 2.82 years) groups ($t = 0.414$, $p > 0.6$). Of note, blood pressure, which is associated with some clinical neuropathological conditions, did not change statistically over time in either control animals or those on CR (data not shown). As previously described, animals were housed in standard primate caging with controlled temperature and humidity and a 12-h light-dark cycle (Mattison et al. 2005; Mattison et al. 2012).

The diet was naturally sourced, with the potential advantage of having micronutrients such as phytochemicals and ultra-trace minerals included. However, there was the possibility for batch-to-batch variation (Ingram et al. 1990; Mattison et al. 2017). CR and control monkeys received the same food, supplemented with additional vitamins and minerals to ensure a 100% daily level for CR monkeys. Thus, with the larger food intake, these levels were exceeded in control monkeys. Control animals were

maintained on a diet to approximate natural ad libitum levels: a stable ration based on age and body size in order to avoid confounding obesity effects. Animals in the CR group were fed 30% less than individual sex-, age-, and weight-matched controls, and these diet conditions were maintained for the duration of the study from age of CR onset through death, which ranged from 1 to 15 years in duration.

Specially formulated monkey chow was distributed twice per day at 0630h and 1300h, which was supplemented with daily food enrichment. Drinking water was provided ad libitum. Approximately three hours after the 0630h meal, any unfinished food was removed and a low-calorie treat was provided. For the second meal, at 1300h, any left-over food was not removed, so animals had continued access during the dark cycle (1800h). However, in general, the monkeys tended to eat before lights-out. Because intermittent daily fasting was not a variable that was under consideration when the study began 30 years ago, if and when the afternoon ration was totally consumed was not monitored.

Animals began their diet regimen as either a juvenile/adolescent, adult, or old adult, as visualized in Figure 5. This was to determine whether there is an optimal window of CR induction; not only are life stages less distinct and identifiable in smaller models, but NHPs are more likely to respond physiologically similarly to humans than are rodents or nematodes, and therefore if a critical window exists, we are most likely to elucidate it using a NHP model. These dietary conditions were maintained continuously until natural death. See Table 1 for subject characteristics such as sex, genetic origin, and importantly, age at death. Sex and genetic origin were considered, but power is very low to detect differences between these groups, and none emerged. However, over one third of the large cohort as NIA is still alive, and as those brains are collected, more

complex effects of CR on the brain can be probed using immunohistochemistry methodology with the inclusion of many more subjects.

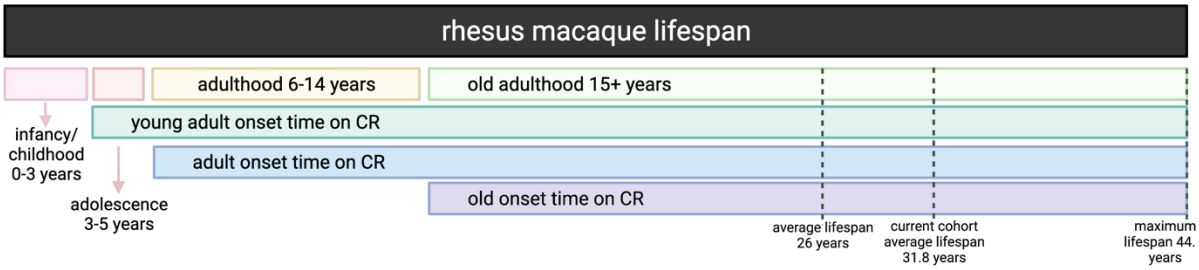


Figure 5: Visual representation of the lifespan of the rhesus macaque compared to NIA study dietary condition onset. The top row breaks the lifespan into developmental stages infancy/childhood (0-3 years), adolescence (3-5 years) adulthood (6-14 years), and old adulthood (15+ years). Dashed lines indicate the average species lifespan, the average lifespan of the cohort included in this dissertation, and the maximum recorded rhesus macaque lifespan, respectively, from left to right. The line labeled "young adult onset time on CR" represents the amount of the lifetime the young adult onset group ate a CR diet, while the subsequent two lines, "adult onset time on CR" and "old onset time on CR" represent the portion of the lifespan animals in the adult onset and old onset groups spent on a CR diet, respectively

5.2 Tissue

At necropsy, brains were collected, rinsed with 0.9% saline, and hemisected along the medial longitudinal plane. Immediately following collection, right hemispheres were immersed in 0.1 M phosphate buffer (pH 7.4) with 4% paraformaldehyde fixative while the left hemispheres were flash frozen for biochemical assay. The right hemispheres were maintained in fixative at 4°C for 5-9 days (notably, 3 animals in this study had longer fixation times, from 52-116 days, but have retained antigenicity). After fixation brains were rinsed in 0.1 M phosphate buffer and transferred to cryoprotectant consisting of 0.1 M phosphate buffer with 10% glycerol and 2% DMSO. After equilibration (1-2 days) they were transferred to 20% glycerol with 2% DMSO for 3-4 days after which they were blocked in the coronal plane posterior to the corpus callosum

and flash frozen in isopentane at -75°C, then stored at -80°C. This cryoprotection method almost totally eliminates freezing artifact and avoids the shrinkage inherent in sucrose cryoprotection (Rosene et al. 1986). For processing, the right hemisphere was removed from -80°C storage and cut into parallel sets of frozen sections, 8 at 30 μm thick and one at 60 μm so that adjacent sections in each series were spaced 300 μm apart. After cutting, each series of sections was transferred to cryovials containing 0.1 M phosphate buffer plus 15% glycerol, equilibrated overnight at 4°C and then stored at -80°C until processed. This method of storing frozen sections has been shown to preserve antigenicity for at least a decade (Estrada et al. 2017).

One eighth of one series through the frontal block of each animal was used to process each antibody (i.e., 4G8, NeuN, AT8, and PHF1). From this series, all sections containing the brain region of interest were selected, resulting in evenly spaced coronal sections at ~2.4 mm, which span the entire region.

Monkeys in the herein cohort represent a subset of animals from the larger study. Prior to the standardization of brain fixation procedures within the study, brains from many animals were not preserved in a way to retain antigenicity against primary antibodies (brain aging was not the original goal of the study, and therefore brain removal and fixation were not standardized until many animals were deceased). Therefore, this dissertation examines a smaller subset of rhesus macaques in which the above necropsy and fixation procedures were followed. This resulted in brain tissue from twenty-one animals that was ideally preserved for immunohistochemistry (IHC). One animal—CR022—was excluded from all prefrontal cortex (PFC) analysis, as all cryovials of this animal's tissue contained no intact PFC sections. This is presumed to be

a slicing or preservation error, as the rest of the brain is anatomically correct and intact, and some small but tattered PFC sections were present, but unable to be recovered.

Subject	Diet Group	Sex	Age at study entry (years)	Age at death (years)	Years in Study	Genetic Origin
CR025	CON	F	4.67	26.7	22.03	Indian
CR047	CON	F	7.70	32.8	25.10	Chinese
CR022	CON	M	3.24	28.7	25.46	Unknown
CR017	CON	M	3.75	30.1	26.35	Chinese
CR023	CON	M	1.82	28.8	26.98	Indian
CR026	CON	M	7.66	28.6	20.94	Indian
CR027	CON	M	2.05	27.9	25.85	Chinese
CR028	CON	M	14.07	41.2	27.13	Chinese
CR034	CON	M	3.83	32.7	28.83	Chinese
CR037	CON	M	2.39	30.0	27.61	Chinese
CR039	CON	M	4.78	34.1	29.32	Chinese
CR001	CR	F	1.84	22.4	20.56	Indian
CR020	CR	F	1.75	23.5	21.75	Indian
CR048	CR	F	7.60	33.0	25.40	Indian
CR049	CR	F	14.00	39.4	25.40	Indian
CR002	CR	M	16.25	40.3	24.05	Chinese
CR021	CR	M	1.76	28.7	26.94	Indian
CR024	CR	M	3.88	30.9	27.02	Chinese
CR033	CR	M	1.84	30.7	28.82	Indian
CR042	CR	M	1.81	31.9	30.09	Indian
CR038	CR	M	16.40	44.1	27.70	Chinese

Table 1: Subject table. Subjects are hierarchically organized, by treatment group followed by sex, and finally increasing age at death within sex. There is noticeable diversity between subjects, including in age at onset of treatment (range: 1.75-16.40 years), genetic origin (Indian and Chinese), both sexes, and amount of time in the study (range: 20.56-30.09 years)

5.3 Immunohistochemistry

All immunohistochemistry (IHC) reported here follows the same standard protocol, with slight modifications. Therefore, I will discuss the mechanisms through which this assay functions as well as provide an overview on the protocols used herein.

Table 2 communicates details of the brightfield protocol used; mechanisms by which these steps occur will be discussed below.

	Reagent	Length of incubation (minutes)	Number of rinses	Temperature (C)
1	Tris-buffered saline (pH 7.6)	10	3	RT (room temperature)
2	1% H2O2	45	1	RT
3	7.0 pH Tris-buffered saline	10	3	RT
4	Normal horse serum	60	1	RT
5	7.0 pH Tris-buffered saline	10	3	RT
6	Monoclonal primary antibody	overnight	1	4
7	7.0 pH Tris-buffered saline	10	3	RT
8	Horse anti-mouse secondary antibody	60	1	RT
9	7.0 pH Tris-buffered saline	10	3	RT
10	Avidin-biotin complex (ABC)	90	1	RT
11	7.0 pH Tris-buffered saline	10	3	RT
12	3,3'-diaminobenzidine (DAB)	5-10 (depends on primary antibody)	1	RT
13	7.0 pH Tris-buffered saline	5	5	RT

Table 2: Immunohistochemistry protocol. All studies used this protocol, with the addition of a heated antigen retrieval (AR) step after H2O2, in AT8 staining of the HPC only. However, control studies were performed to confirm the lack of difference in AT8 staining efficacy between tissue processed with an AR step and that without

Rhesus macaque tissue in this dissertation all derives from the same cohort of elderly animals, which allows for optimization of the protocol to focus on the individual antibody, rather than adjusting for fixation time and other tissue variables. While 4G8 (to visualize Aβ) and NeuN (to visualize neurons) are well-preserved and do not require any steps to make proteins available to bind, previous literature suggested that p-tau is only detectable in NHP tissue with the addition of an antigen retrieval step (Paspalas et al. 2018). Therefore, the first instance in our laboratory of AT8-positive staining in the

macaque occurred after a heated antigen retrieval (AR) procedure. For the detailed AR protocol utilized, see Experiment 2 design. Importantly, after full confirmation of specific staining, both using human positive controls and identifying characteristic morphological patterns of p-tau, we compared AT8 detection with and without AR. Following this comparison, it was obvious that AR is not, in fact, necessary for the detection of tauopathy in the current NHP tissue.

IHC is a process through which the endogenous immune system can be co-opted to identify and spatially visualize proteins of interest (see Adams 1992). First, an antibody against the protein of interest must be synthesized. The mammalian immune system naturally synthesizes antibodies that bind to unknown proteins and protect the host. To visualize a specific protein, the immune system of a host animal is "tricked" into creating natural antibodies against the protein of interest. That antibody is then applied to the tissue of interest, and binds to the protein of interest. After a series of steps described below, this initial binding site allows the protein of interest to be visualized wherever it is present in the tissue.

In the current studies, tissue is incredibly valuable, and we wanted an opportunity to test various analysis methods using the same sections. A very common method of IHC is to use 3,3'-diaminobenzidine (DAB) to create a pigment stain that does not fade over time (Adams 1992). Before primary antibody incubation, a hydrogen peroxide bath quenches all endogenous peroxidase activity in the tissue, so as not to interfere with the final DAB oxidation step, as described below. Between all steps, tissue is washed with buffer to remove any unbound excess from the previous step. Normal serum, which matches the species in which the secondary antibody was raised, blocks nonspecific binding of the secondary antibody by binding non-specific sites. In our

protocol (Table 2), normal serum is used as its own step in the assay, but many labs incubate the primary antibody and normal serum simultaneously, as they do not compete with each other. Following primary antibody incubation, which occurs for anywhere between a few hours and multiple days, depending on the strength and specificity of the primary used, the tissue is incubated with a secondary antibody. The secondary is a labeled antibody which detects an immunoglobulin that is specific to the host animal in which the primary antibody was raised. For example, if the primary was synthesized in a rabbit, the secondary antibody detects an immunoglobulin which is present on all rabbit antibodies. The secondary antibody is conjugated with the protein biotin. ABC is a complex which binds to the biotin on the secondary antibody, and also contains three further biotin groups. However, the other biotins bound to avidin are attached to a peroxidase. When DAB is added as the final step after washing away non-bound ABC, it is oxidized by biotin-bound peroxidase, which creates a dark brown precipitate that signals the presence and location of the protein of interest. See Figure 6 for a schematic of the end result of this enhancement process, ending in a visible precipitate.

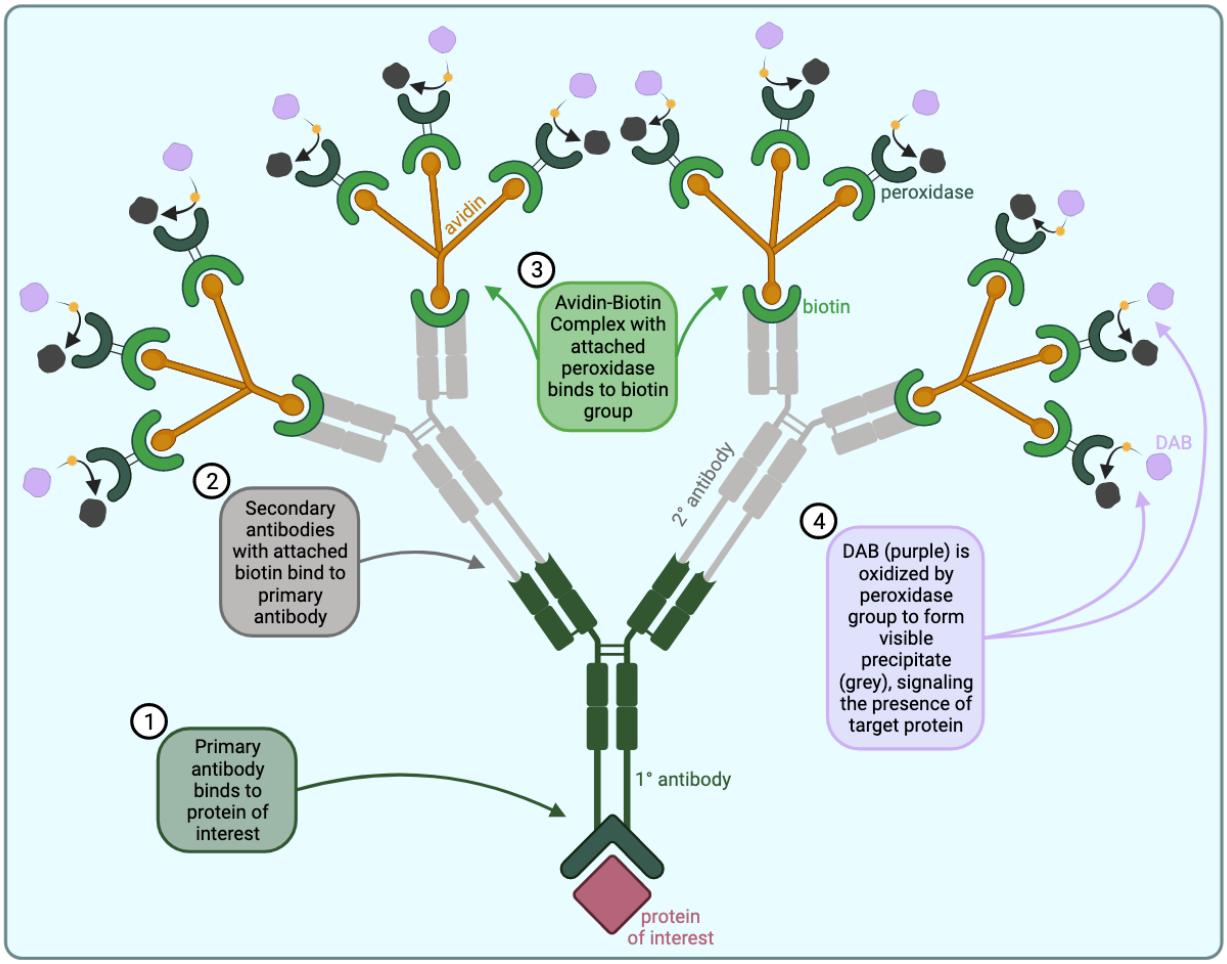


Figure 6: Visualization of proteins of interest using brightfield IHC. After primary antibodies are raised, 1. they bind to their target protein. 2. From there, a secondary antibody binds to the primary. The secondary is biotinylated, meaning antibodies are synthesized to have attached biotin groups. Avidin-biotin complex (ABC) is prepared such that three of the four avidin groups are bound to commercially available biotin with attached peroxidase. When the full ABC is added to tissue, 3. The remaining avidin in the complex binds a biotin group on the secondary antibody. 4. When the peroxidase is exposed to DAB in solution, the DAB is oxidized, which creates a visible, permanent precipitate at the site of the peroxidase. Of note, there are biotinylated primary antibodies which are acceptable for some very robust proteins, however the ABC is the contemporarily favored method of detection due to its signal enhancement. Created with BioRender.com

5.4 Stereology

To quantify the region occupied by amyloid plaques as well as number of neurons, both within the PFC, we used unbiased stereology. Stereological analysis is considered the gold standard in histological quantification and is used in many clinical

and preclinical settings (Brown 2017). Stereology used herein was performed using well-validated Stereo Investigator software (MBF Bioscience, Williston, VT) and is based on the premise of systematic uniform random sampling (SURS). True SURS functions such that every area of every structure of interest within the tissue has an equal chance of being sampled. Briefly, gross regions of interest are measured lengthwise perpendicular to the slicing plane. From this, sampling interval is determined, generally to include 8-10 sections through the area of interest, but this depends on the density and consistency of the stain of interest. The sampling interval, the number of sections between each sampled section, is referred to as T. From the front of the region of interest, a randomly selected number between 0 and T determines where sampling begins, and then sections are taken at every interval of T. Tissue in the current studies was sectioned at 30 μm, and T was 80. Selection of the first section in each individual was random within the first 80 sections. Therefore, SURS sections were 2.4 mm apart. SURS also refers to the placement of counting windows within the region of interest. Depending on the type of analysis as well as the density and uniformity of the objects or stain being analyzed, an area percentage for sampling is determined. Based on this calculated percentage, identical counting frames are placed—evenly spaced but at a random start—throughout the region of interest. Counting frame placement is therefore also both unbiased and systematic. To determine parameters of the counting frames, a pilot study of a subset of subjects is needed—being certain to include sections with very low-density stain—to determine the minimum counting area necessary for an accurate estimate of the full region. Small pilots like this are used to determine the coefficient of error (CE) using various parameters. When sampled sections are densely populated and uniform, a smaller percentage of the region needs to be counted. Versus, inconsistent or sparse

staining which may sometimes require the entire region to be "sampled" for an accurate estimate. Generally, prior similar studies are useful for determining a starting point for sampling area parameters (Brown 2017).

The optical fractionator is used to count discrete objects using symmetrical green and red edges of the counting frame, so neuronal number was estimated using this method.

5.5 Data acquisition: Tau analysis

P-tau has not been nearly as extensively characterized in this NHPs as in human pure aging or AD cases, as for multiple decades it was presumed that the rhesus monkey did not develop tauopathy (i.e., Uno 1993; Peters et al. 1996). As this was the case, there has been little evidence for the presence of p-tau in this species (Härtig et al. 2000)—that is, until recent studies renewed interest in p-tau accumulation in the macaque (Arnsten et al. 2021). Now, with brain tissue from a unique aged population of rhesus monkeys from the National Institute on Aging, we can further characterize p-tau accumulation in this primate research model and determine whether it recapitulates the clinical spread and severity of human AD. The presence of multiple forms of phosphorylated tau in multiple cohorts of aged animals was an exciting discovery for our laboratory. Gratitude to Dr. Donald Brown for his work early in optimizing monoclonal antibody AT8 in preserved monkey brain tissue. The initial analysis of tauopathy was performed on DAB-stained hippocampal sections from the CR cohort, as well as in a second cohort. This second set of brain tissue was processed very similarly to the CR study brains, wherein one half of the brain was flash frozen and one was saline rinsed then submerged in 4% paraformaldehyde to preserve proteins, and to be

sectioned for histological use. These animals were housed at Oregon National Primate Research Center (ONPRC) and were part of a cross-sectional aging series across the lifespan, wherein brains were imaged and/or collected from study and colony monkeys that were sacrificed for reasons other than brain collection. In this way, we have, over time, accumulated a large set of both fixed brain tissue and structural MRI scans at varying points across the rhesus macaque lifespan. Not only does this build a significant data set with which to explore normative development and aging of the brain, but it also makes the best use of an extremely intelligent and valuable animal model. This set of tissue will be referred to as the Aging Series (AS). Special thanks to Dr. Steven Kohama for his efforts towards accumulating this data set and for generously providing tissue from the older animals, as well as sections from young monkeys in this cohort to serve as controls.

Figure 7 contains data from the first analysis of tissue, which included two cohorts of animals, described in more detail below. Initially, after scanning tau-positive tissue from both cohorts, I identified ten different phenotypes of AT8 staining: astrocytes, microglia, white matter/oligodendrocytes, diffuse entorhinal cortex (ERC) staining (as was previously reported by Paspalas et al. in 2018), vasculature, HPC fibrils, cortical fibrils, plaques, light cytoplasmic neuronal staining, and circumscribed, dark neuronal staining. For this first analysis, each full section was examined and if any instance of a phenotype was present, it was counted. Therefore, each variable was a binary yes or no. Data gathered from animals are shown in Table 3. Subjects are shown in increasing order of age, from 5.79 to 44.1 years; however, ages are not to scale, so definite ages cannot be inferred from the visualization below. Animal numbers that begin with CR are part of the NIA CR study, while those without are ONPRC AS tissue.

Interestingly, even many young AS animals had at least one p-tau plaque, and/or light cytoplasmic AT8 reactivity. Monkeys with the most diverse types of AT8 staining are all old; however, there is no distinct order or pattern to which they begin to appear, cross-sectionally.

These data are not being included in any publications for many reasons. One major factor is the difficulty in analysis of binary outcomes, especially across many animals and many phenotypes. in addition to complexity in statistical analysis, quantifying such a large number of various phenotypes was not clinically relevant. To solve this problem, the following method of analysis was proposed.

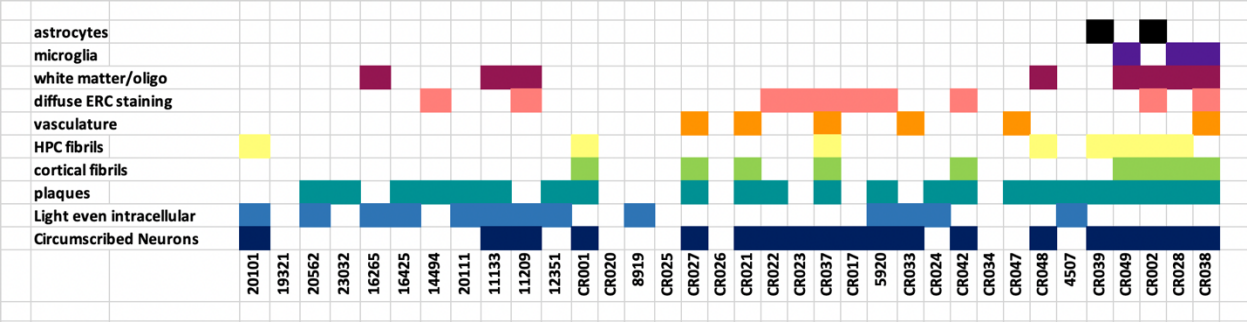
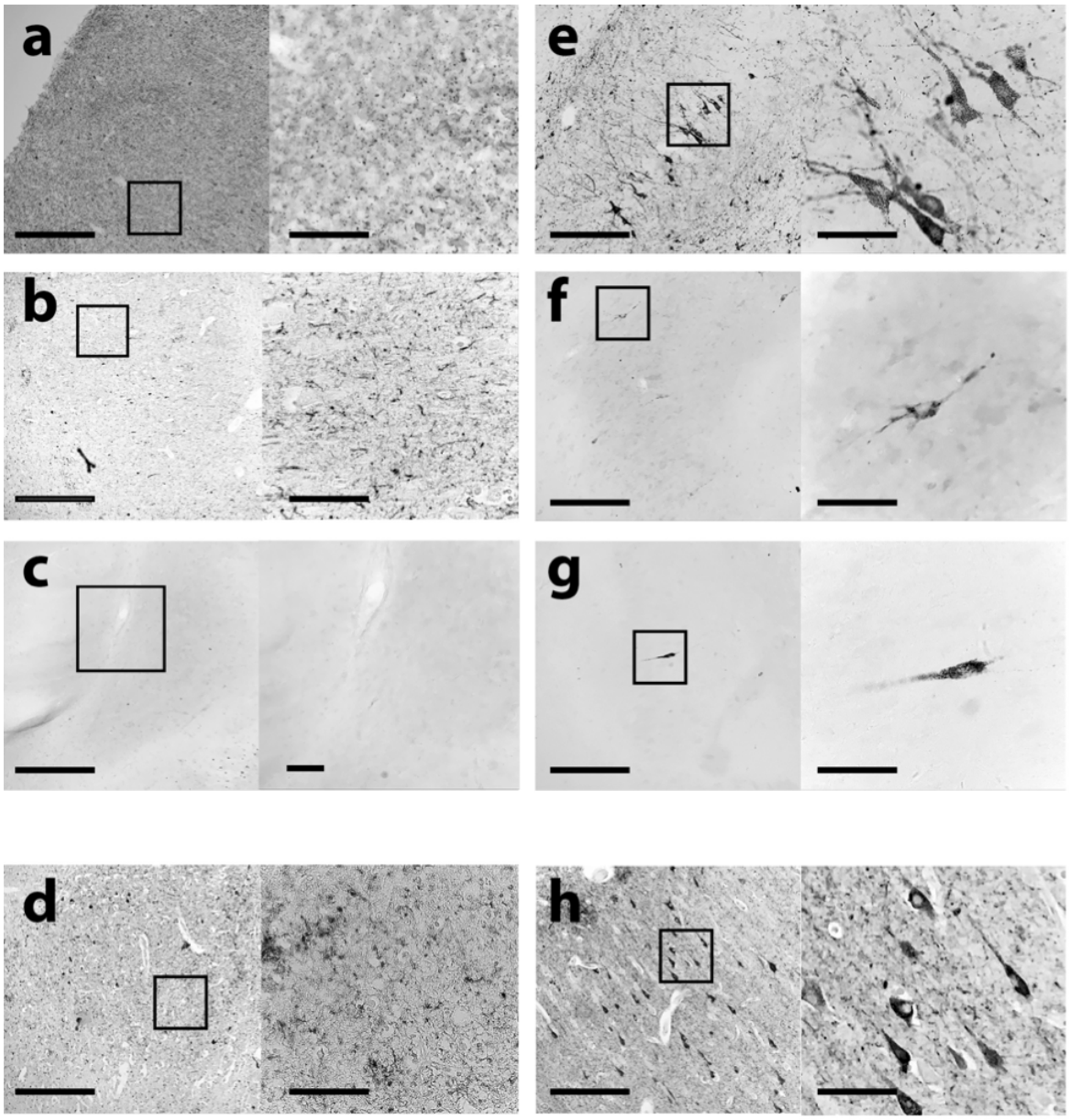


Figure 7: Presence of p-tau phenotypes in rhesus macaque hippocampus and surrounding cortex across a range of ages: the first attempt at characterizing tauopathy in the rhesus macaque HPC. Each title on the y axis labels one phenotype, and subjects are organized along the x axis from youngest to oldest. A filled-in cell indicates presence of the phenotype. Overall, older animals show a higher variety of AT8-positive phenotypes. Note that animals are listed only chronologically by age; there is no even interval by which age increases; therefore this is simply a visualization to observe a general pattern across aging.

A further attempt at quantifying tauopathy in old animals is exemplified in Figure 8. Originally, each animal was given a score for each of four primary non-glial morphologies visible with AT8: diffuse staining (which is common in the ERC, even in young adult animals; Paspalas et al. 2018), intraneuronal tau (including NFTs and pretangles), plaques, and dystrophic neurites. Scores ranged from 3, being most intense,

to 0, when the phenotype was fully absent. After scoring, examples were compared to human postmortem AD human tissue. Importantly, these scores also encompassed the entire area of available HPC sections, each of which includes many cortical and subcortical regions including the HPC, entorhinal cortex (ERC), subiculum, and temporal cortex, depending on where the section falls on the rostral-caudal axis.


a
e
b
f
c
g
d
h

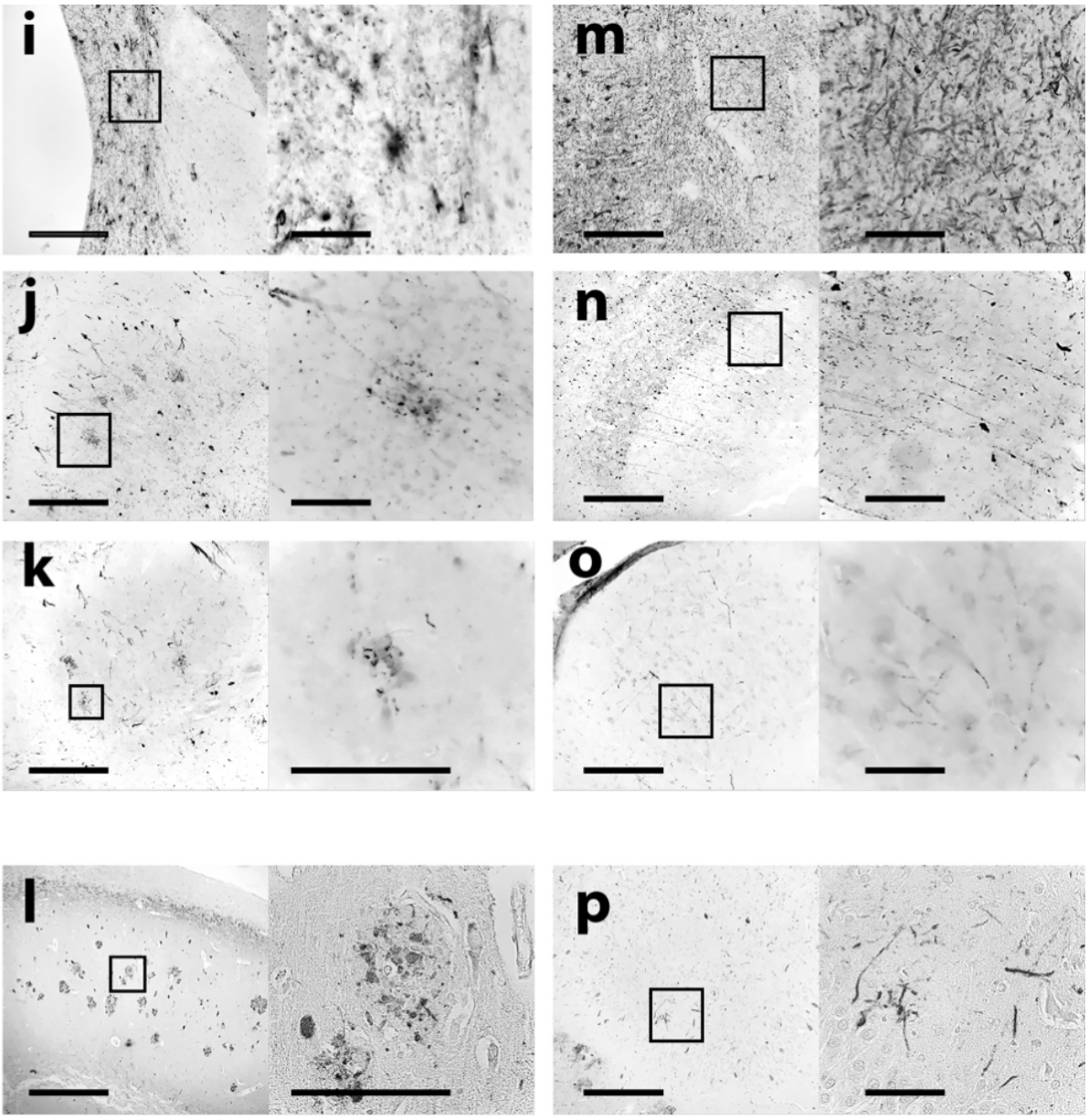


Figure 8: Tau rating system for preliminary tau analysis of AT8-stained rhesus macaque brain sections compared to comparable human tissue. In each paired column (divided by white lines), the images in the left column show low-power examples of each rating, while the adjacent image to the right is a high-power view of the phenotype. Panels are arranged so that in each column, the top section represents a "3" rating (most severe), the second row is the "2" rating, and the third row is an example of a "1" rating, wherein the phenotype exists in the tissue, but only in small amounts. "0" scores were not included, as a "0" rating indicates the absence of staining. The bottom row shows examples of each corresponding phenotype in an AT8-stained human postmortem hippocampal section. (a-d) Diffuse p-tau staining. (e-h) Intraneuronal p-tau. (i-l) P-tau-positive plaques. (m-p) Dystrophic neurites. Scale bar, low-power shots (left side of each column): 200 μm. Scale bar, high-power images (right side of each column): 30 μm.

Interestingly, in AS animals, tau accumulation anecdotally began earlier than in CR animals. This is likely that, because AS animals are fed *ad libitum* unless their diet is altered specifically for a study, they overeat and are consequentially more predisposed to pathology in general, especially in the aging process (i.e., Austad 2001). Figure 8 shows examples of ratings, using animals from both cohorts. Eventually, we decided not to introduce so many variables into the same study, with both groups. For instance, some noticeable differences between cohorts outside of dietary regimen (which had no overlap between cohorts, as no CR animals had *ad libitum* access to food) include:

- Balance of sexes: CR subjects were primarily male, and AS subjects included more females than males
- Age range: the oldest AS rhesus macaques were still closer to younger CR animals; i.e., ages only overlapped at the young end of CR and old end of AS
- General husbandry, including nutritional breakdown/food source, housing (i.e., single- or pair- housed, or size of colony)
- Social hierarchy: while not commonly accounted for outside of studies specifically studying social behavior, multiple studies have shown that social stress has impacts on immune and brain health in human and animal models (Bailey et al. 2017; Todorov et al. 2019; Varholick et al. 2019; Pavez-Fox et al. 2021), and there are multiple ways to directly or indirectly measure social status in macaques, with varying degrees of precision (Baxter et al. 2018; Robinson et al. 2018; Wooddell et al. 2020). This confound applies across both cohorts, but living in a colony setting (as most of AS animals did) compared to single- or pair-housing (how CR animals were housed), inherently alters and complicates analysis due to social structure and ranking

- Reproductive status of females. We were able to measure sex hormone levels in serum from CR females, to determine that the youngest was peri-menopausal and the rest were post-menopausal. Peri-menopause generally begins in the middle of the third decade of the female macaque lifespan, and has significant effects on aging (Downs and Urbanski 2006). Menopausal status has not been determined in the AS cohort, but seeing as many animals are too young for this phase of life, it would be difficult to effectively compare pathology in a cohort of younger, cycling females to that in older menopausal and peri-menopausal monkeys without controlling for menopause status, even regardless of other study differences.

Even further, including the entirety of a tissue section without regard to region does not provide sufficient information to compare to clinical cases. To mitigate these issues, I included only CR animals in the final analysis of the tissue, and to use a staging system which is regionally specific. After consultation with OHSU's clinical neuropathologist, Dr. Randy Woltjer, I decided to use the clinically relevant Braak and Braak staging system to qualitatively assess AT8 staining in the rhesus macaque. The purpose of this is to not only compare animals to each other within the cohort, but also to confer a diagnostic clinical relevance that has not occurred in prior NHP studies of tau. Therefore, patients with premortem AD diagnoses were immunohistochemically-stained with AT8 to directly compare p-tau at the same phosphorylation site between clinical AD cases and very old monkeys.

5.6 Data Acquisition: PFC amyloid plaques

PFC were stained with monoclonal antibody 4G8 (1:5000, Biolegend, San Diego, CA, USA) using DAB IHC described above in Table 2. The first analysis of amyloid plaques in Brodmann Area 46 (BA 46) was attempted using ImageJ software. When the tissue was first stained, we did not expect such a high amount of cerebral amyloid angiopathy (CAA) or intracellular staining in the PFC. Therefore, our first attempt at quantification of amyloid in the dorsolateral PFC and anterior cingulate was to use Fiji ImageJ software (supplement to ImageJ by National Institutes of Health, open source; Schindelin et al. 2012) to quickly calculate area coverage of the region. Briefly, using ImageJ, high-resolution scans were converted to 8-bit images and then the threshold was manually adjusted to—in theory—include amyloid plaques and exclude background noise, CAA, and intraneuronal staining. After thresholding, area of positive stain was calculated using the measure feature. Initially, a small pilot was run in which four sections were used. BA 46 surrounds the principle sulcus, so each section was digitally divided into seven sub-regions in order to check for dorsal-medial and also lateral-medial variation patterns. This protocol, however, was incredibly time consuming, little to no data exist to substantiate that BA 46 is divided into such small, arbitrary subsections, and no patterns had become evident. Therefore, BA 46 was analyzed as one contiguous region in each tissue section.

However, even the region was analyzed contiguously within a section, this method yielded somewhat inaccurate results for several reasons. Firstly, thresholds varied widely between subjects, and sometimes between brain sections of the same subject (but, not between sections on the same slide, which generally had similar thresholds). There are any number of reasons for this phenomenon. These particular

slides were scanned prior to a major software and hardware update to the high-resolution microscope slide scanner, and the scanning process at many times required manual focus and significant adjustments. Therefore, quality, contrast, and exposure were likely inconsistent enough to require a difference in post-scan image processing methodology. Additionally, there is likely some drift in ratings. Even though one researcher completed all ratings, some amount of drift is inevitable between the first subjects analyzed and those that were thresholded after significant experience in the process due to practice effects. Outside of variation in initial conversion of images, there were many artifacts (relative to the intended analysis of plaques) that could not be removed via the act of adjusting the greyscale threshold of the image.

Notable, dark intraneuronal 4G8 staining was prevalent, especially in younger animals. This staining pattern does not indicate non-specific staining, even though 4G8 detects Aß. Amyloid precursor protein (APP) is a physiological protein of which the primary function is not fully understood (Dawkins and Small 2014). This protein is then cleaved multiple times to form various fragments with differing actions depending on what enzymes are present (see Figure 3). Aß is a protein fragment of APP, and therefore any sequence present in Aß is inherently also present in upstream APP. There is also evidence of Aβ itself in neuronal cells, but the functional effects of this are not entirely known, so either of these scenarios are likely (LaFerla et al. 2007). However, to the eye, neuronal and extracellular staining are easy to differentiate based on size and stain morphology. While intraneuronal Aß does occur in AD patients, and potentially has functional implications at the synapse (i.e., Takahashi et al. 2010), our priority was quantifying Aß plaques, a primary AD hallmark. Further, a gross measurement of the area covered by all 4G8 staining is imprecise, as it gives no information regarding the

ratio of plaques: neuronal staining: CAA, which could be important. Due to these concerns, I decided to use the gold standard of area quantification in tissue, being stereology. Because stereology is completed manually, I was also able to measure cerebral amyloid angiopathy (CAA) in BA 32 using the same stereological protocol.

All analyses were done with the investigator blind to subject characteristic (age, sex, group, etc.). Blind, coded slides were scanned at × 20 objective in one z-plane using a Leica Aperio AT2 slide scanner (Wetzlar, Germany). Aβ plaques were manually quantified from these images using the area fraction fractionator (AFF) probe in Stereo Investigator 2018 (MBF Bioscience, Williston, VT, USA), and neuronal cells were quantified using the optical fractionator procedure found in the same program. AFF is a form of Cavalieri point counting based on a systematic random sampling grid, which uses manually determined areas of positive staining to estimate a fraction of the entire region. The same blinded investigator manually completed stereological counts on all sections of all animals, in order to eliminate inter-rater variability and to ensure consistent criteria were used to differentiate intracellular staining from amyloid plaques. In brief, the digitized histologically stained images were imported into Stereo Investigator, and counting frames systematically randomly placed across manually delineated ROIs in each brain section (determined with Scalable Brain Atlas Markov Cortical Regions Atlas 2014, regions 46d, 46v, 9-46d, and 9-46v for BA 46, and region 32 for BA 32). After counting was complete, we verified that sampling for each subject had Gunderson's coefficient of error (an estimate of the accuracy of the counting scheme) scores of < 0.10. Aβ plaques were determined to be positive if they were larger than a pyramidal neuron (i.e., to exclude intraneuronal Aβ) and ellipsoid (as opposed to

linear vasculature staining), and only plaque area inside the counting frame was marked positive.

5.7 Data Acquisition: Neuronal counts

Neurons in the PFC were visualized using a neuron-specific monoclonal antibody NeuN (1:2000, MilliporeSigma, Darmstadt, Germany). NeuN IHC also followed the protocol in Table 2. Stereology was completed using Stereo Investigator's optical fractionator flow.

Neurons were counted using the optical fractionator probe in the same program. All SURS principles and methodology also applies to the optical fractionator flow, outside of the researcher placing markers on identified neurons as opposed to determining whether grid points are positive or negative for 4G8. Neurons were counted if the nucleus was visible or if the cell was morphologically deemed to be a neuron (Bhattacherjee et al. 2019). The cell was only marked if it was contained within the counting frame, or if the cell body or visible processes contacted the green bottom or right edges of the frame. Neurons were not counted if cell bodies or processes were in contact with the red top and left edges, or if the nucleus was not identifiable. From this unbiased estimate, we obtained a measure of neuronal density.

6. Study aims

The goal of this dissertation is to characterize amyloidosis, neuronal stability, and spread of neurofibrillary tangles, using the oldest known rhesus macaques in the world. Some of these animals were calorie restricted by 30% for a significant portion of their

adult lives; therefore, I examine the effects of calorie restriction on the aforementioned hallmarks of Alzheimer's disease. Using these data, the rhesus model of aging will be compared to clinical healthy and pathological aging. I hypothesized that, due to being the oldest population of rhesus macaques, some animals would show Alzheimer's-like characteristics. The prevalence of AD in humans over the age of 85 years is nearly 50% (47%, ; if rhesus monkeys model clinical AD patterns, and rhesus monkeys age at a rate three times that of human patients, roughly seven animals in this cohort should show overt AD pathology. However, I also hypothesize based on previous studies that CR will mediate these effects such that fewer animals in the CR group will show severe pathology, or that pathological protein accumulation and neuron loss will be less severe in the CR group than controls.

Chapter 2

Experiment 1: Amyloidosis and neuronal stability in the rhesus macaque prefrontal cortex

Neuronal and senile plaque data from this chapter were published in September 2020, in the peer-reviewed journal *GeroScience* (Stonebarger et al. 2020).

Animal subjects used in this study were a part of an IACUC-approved longitudinal aging program at the National Institute on Aging, headed by Julie SM Mattison. Tissue was sectioned by and subsequently acquired through Douglas L Rosene at Boston University.

1. Study design and aims

1.1 Brain regions

I initiated my analysis with the PFC, which has been shown to contain a very high number of Aß plaques in aged rhesus monkeys (Heilbroner and Kemper 1990). Within the PFC, I focused on BA 46, a key cognitive area with well-documented sensitivity to aging in both humans and monkeys (Peters et al. 1994; Peters and Kemper 2012; Yuan et al. 2012; Primiani et al. 2014), and BA 32, a region with many implications in clinical aging (Gigi et al. 2007; Shamy et al. 2011; Dumas et al. 2013; Pimontel et al. 2020), and

which has not yet been fully characterized in aging monkeys. Importantly, because BA 32 is located within the same coronal sections as BA 46, it can serve as an internal comparison for each subject. I reasoned that if neuron death does occur in NHPs, it is likely to be revealed in the current cohort of very old monkeys, as it is exceedingly rare for macaques to live beyond the age of 40 years. However, three animals in this cohort lived beyond this age, with one other nearly reaching 40, at 39.4 years. This cohort has an average age of 31.8 years and contains some of the oldest known rhesus monkeys; therefore, any brain changes which occur due to rhesus macaque aging are likely to become evident within this population.

1.2 Antibodies and quantification

Monoclonal antibody 4G8 (1:5000; BioLegend, San Diego, CA, USA) was used to detect Aβ. To assess neuron numbers, PFC sections were immunostained for the neuronal marker NeuN (1:2000; MilliPoreSigma, Darmstadt, Germany). Antibodies were used on two different parallel sets of equally spaced tissue within each animal. Both markers were quantified using unbiased stereology, as discussed in Introduction section 5.3.

1.3 Statistical analysis

Notably, one animal of the original twenty-one had no viable PFC sections available and was therefore excluded from Experiment 1 analyses. Two animals of the remaining twenty subjects were excluded from all analyses as statistical outliers in high Aβ percent area coverage (i.e., area fractions of these animals were higher than 1.5x the determined interquartile range added to the third quartile), leaving a total of eighteen

animals with quantified plaques and neurons. Excluded animals were a male and a female in the early-30's age range and in the CR dietary group. Future studies with more animals will determine whether these animals represent true outliers or are indicative of a phenotype for which we do not yet have the power to detect.

Linear regressions and correlations were performed in GraphPad Prism (San Diego, CA), with alpha level set at 0.05. To calculate neurons per mm^3, the estimated total number of neurons per animal was divided by the sum of the area of all regions of interest (ROIs) for that animal, as calculated by Stereo Investigator software. Neurons per mm^3 was used instead of neuron count estimations to normalize data, as animals varied in number of available PFC sections due to varying brain size. Estimated area fraction of Aβ (i.e., fraction—or, percentage—of PFC that is filled with Aβ plaques) was calculated automatically by Stereo Investigator. Section 5.4 of the Introduction contains more detailed stereology justification and protocol.

1.4 Predictions

I hypothesized that Aß plaque load would increase with age in BA 46 and 32, and might possibly be attenuated by CR, while neuronal cell number, similar to previous studies, would be stable across age, even in the oldest-old animals. If neuronal loss occurs, I hypothesized I would observe it only in the oldest monkeys, and/or those with the highest plaque load.

2. Results

2.1 Qualitative staining

PFC neurons positively stained with anti-NeuN antibody occurred densely through the cortex but were absent in the underlying white matter. In the PFC, NeuN-positive neurons displayed three different patterns of staining: nuclear staining, cytoplasmic staining, or both (Figure 9). Since this pattern has not been previously reported, I ruled out a cohort effect using PFC sections from two additional male middle-aged (i.e., mid-20's) rhesus monkeys that were part of a separate aging study at Boston University and were processed identically to the NIA samples, also in our lab. They showed the same three NeuN phenotypes (data not shown). In contrast, the occipital cortex in both cohorts of animals showed a more traditional cellular staining pattern with more nuclear and less cytoplasmic NeuN expression (Figure 10).

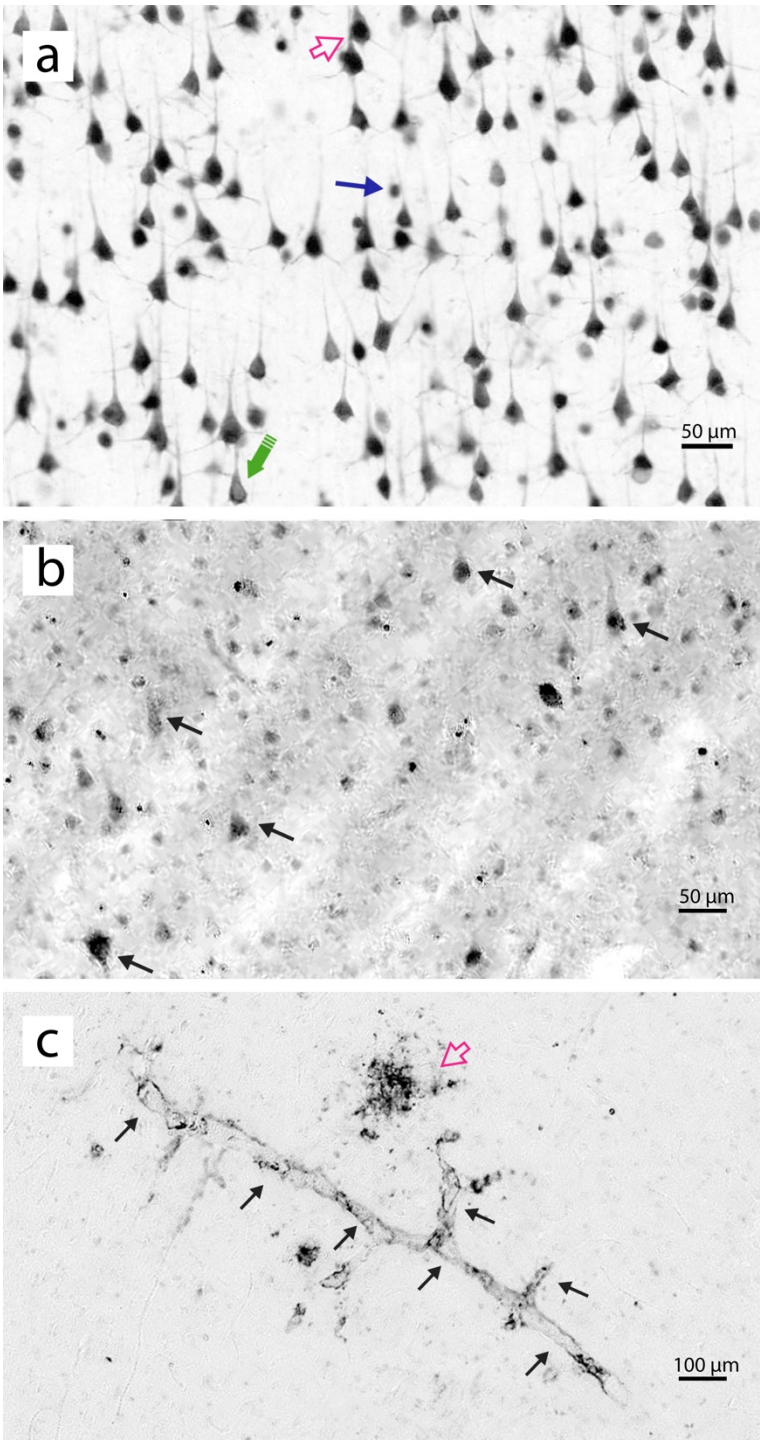


Figure 9. NeuN and 4G8 immunostaining phenotypes in the rhesus macaque PFC. (a) Phenotypes of NeuN staining. Open pink arrow indicates a neuron with both nuclear and cytoplasmic staining, closed blue arrow points to a cell with only nuclear staining, and the large green arrow emphasizes a neuron with only cytoplasmic staining. All animals showed all three phenotypes in the PFC. (b) 4G8 staining, which is presumed to be intracellular. Contrast has been enhanced to more clearly show the size and shape of staining. Arrows indicate examples of staining, which can be morphologically identified as pyramidal neurons. (c) 4G8 vasculature staining. Black arrows indicate the immunostained capillary, while the pink open arrow indicates a diffuse plaque. Scale bar in (a) applies to panel (b) as well: 50 µm. Scale bar (c) 100 µm. Published in Stonebarger et al. 2020

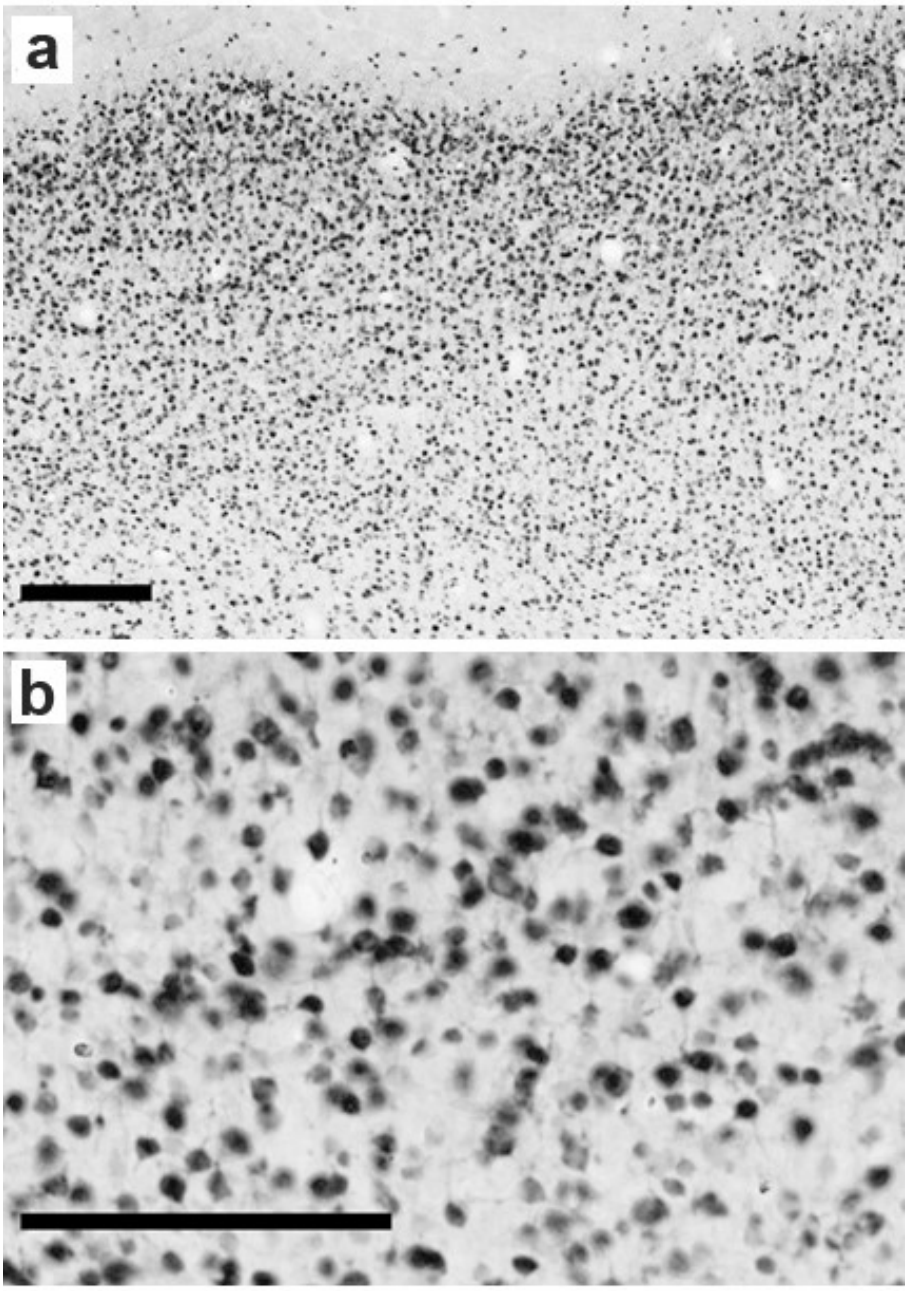


Figure 10. NeuN immunostaining in the occipital cortex of the rhesus macaque. Positive staining exclusively within the cell nuclei conforms to a traditional staining pattern for this antibody, and contrasts with the more widespread cellular staining pattern observed in the PFC (Figure 9). Scale bar (a, b): 200 mm. Published in Stonebarger et al. 2020.

Staining of Aβ with 4G8 also revealed multiple immunostaining patterns. As expected, Aβ plaques were detected only in cortical regions, but many animals also showed varying degrees of vasculature amyloidosis as well as presumed intracellular 4G8 labeling (Figure 11), neither of which were stereologically counted as positive plaque labeling. Of note, no major phenotypic differences were seen between BA 46 and BA 32. Across cortical regions, there were increases in 4G8 staining which were visible to the naked eye. For instance, Figure 12 shows representative examples of differences in PFC 4G8 staining between an animal that died at 22.4 years and one that survived until age 40.3 years. At both high and low magnifications, the cross-sectional increase in Aβ is obvious from late middle-age to the oldest-old animals.

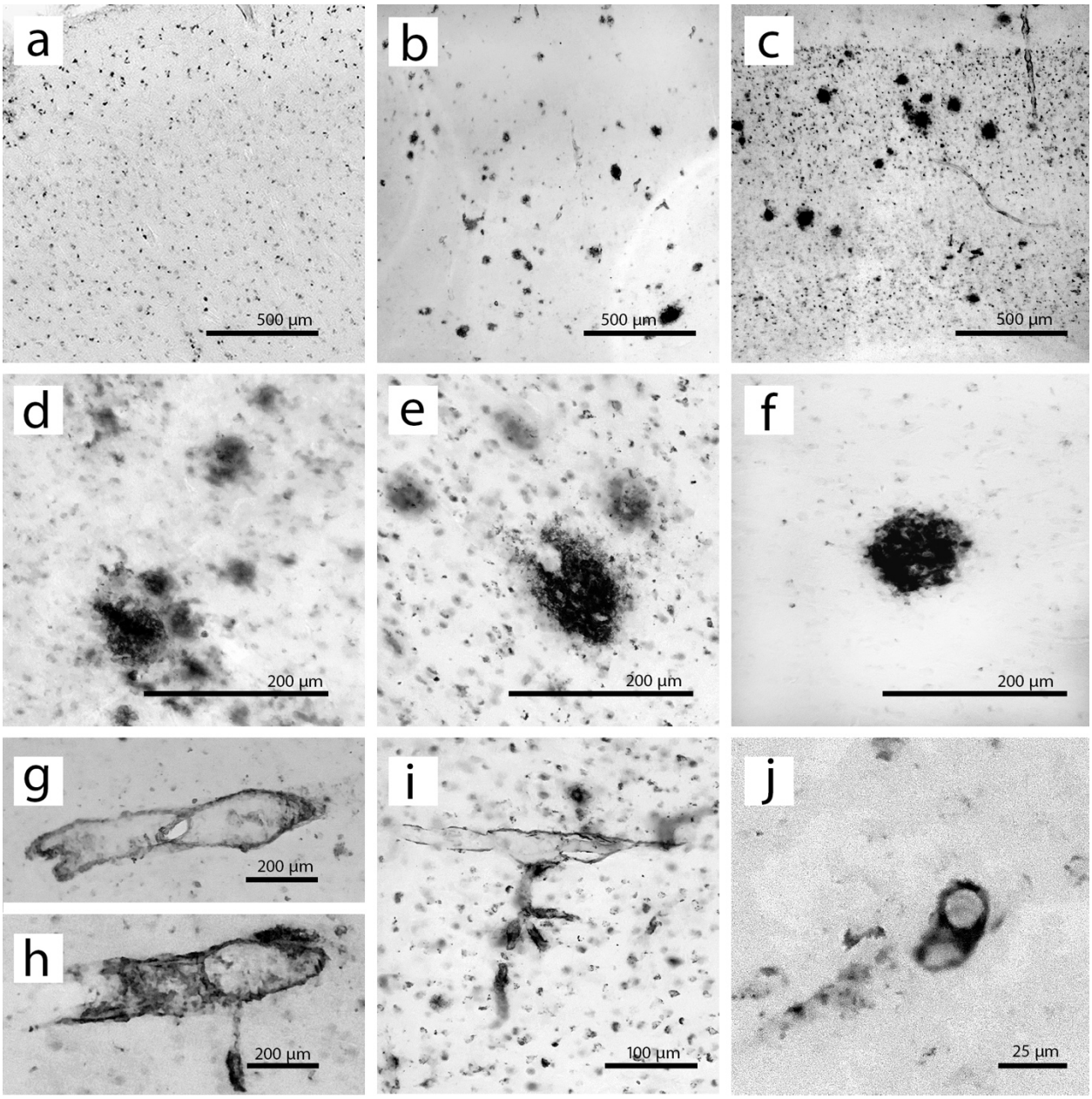


Figure 11. 4G8 immunostaining phenotypes in the rhesus macaque PFC. The top row shows full cortical sections from BA 46 in three animals, representing various staining phenotypes. All three images are shown at the same magnification, encapsulating all cortical layers, and with the pial surface at the top of the image. (a) 4G8 staining in a 30.7-year-old animal is nearly exclusively intracellular. (b) Only plaques and vasculature are stained in a 34.1-year-old animal. (c) 4G8-labeled plaques and vasculature as well as intracellular staining in a 41.2-year-old animal. The middle row contains some representative Aβ plaque phenotypes. d Multiple very diffuse plaques cluster together with light intracellular staining. (e) A larger plaque with distinctive intracellular 4G8 staining. (f) A singular plaque with very little intracellular staining surrounding it. The bottom panels are representative images of vasculature staining phenotypes. (g, h) Larger 4G8-positive blood vessels. (i) Smaller stained vasculature, with intracellular staining. (j) A 4G8-positive capillary in cross-section. Note the difference in scale between panel (j) and other panels. Published in Stonebarger et al. 2020

2.2 Stereological analysis of plaques and neuron numbers

After plaque density was quantified via Stereo Investigator's AFF and neuronal density was calculated via the optical fractionator, linear regression was applied to calculate whether trajectories of plaque accumulation and neuron number varied based on dietary treatment group. Pearson's correlations were used to evaluate relationships between measured outcomes (i.e., relationships between neuron density and plaque area fraction). Results showed that there were no differences in plaque accumulation due to sex or genetic origin (Chinese or Indian) from which rhesus monkeys in this study were derived, as the slopes of these linear regressions were not significantly different (Figures 13 and 18). Therefore, both sexes and both genetic origins were combined across subsequent analyses.

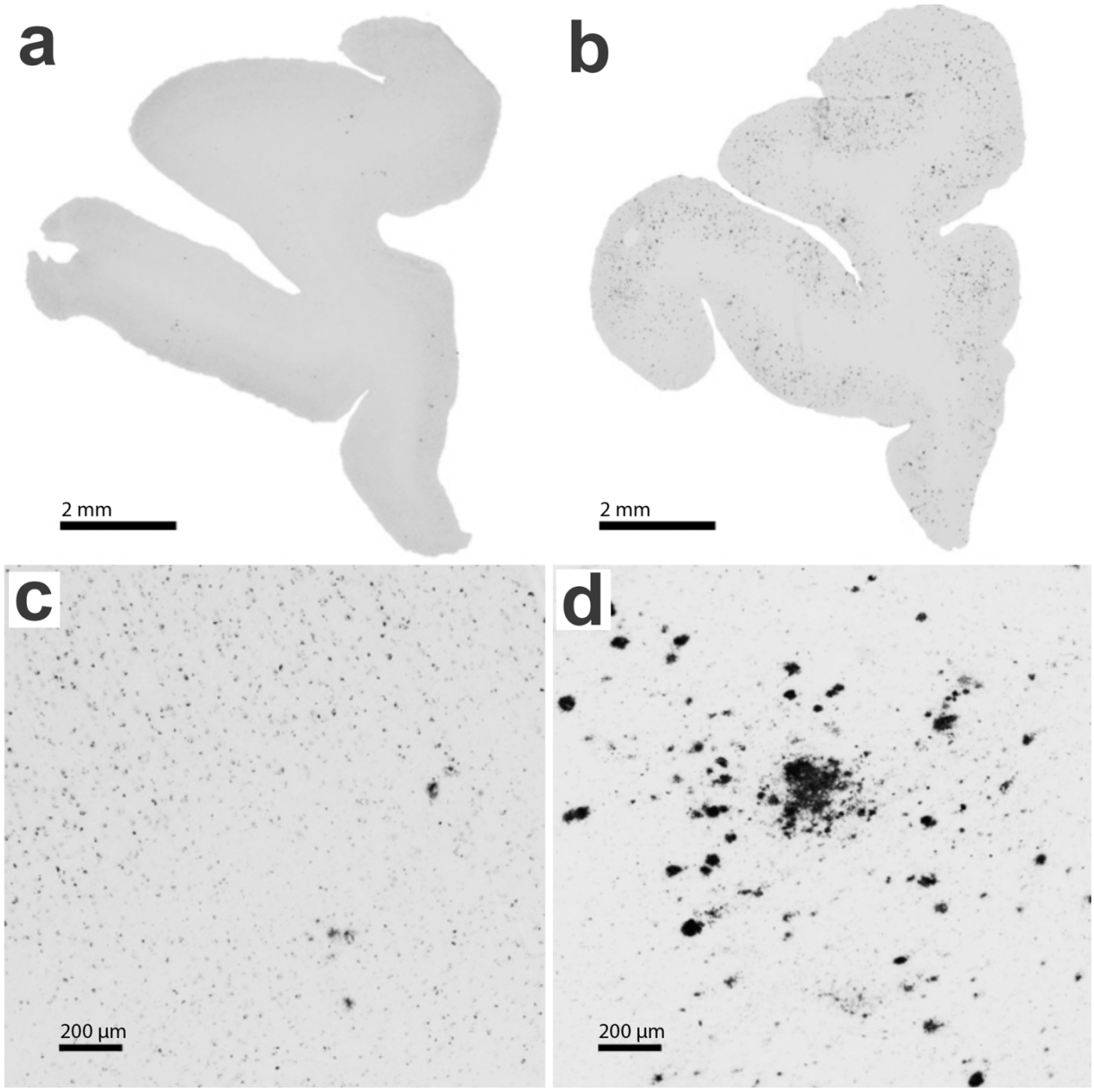


Figure 12. Age-related changes in the density of amyloid beta plaques in the rhesus macaque PFC. (a, b) Low-power representative micrographs depicting PFC sections from a 22.4-year-old and a 40.3-year-old animal, respectively. High-power representative photomicrographs emphasizing the difference in PFC plaque density between the same 22.4-year-old (c) and 40.3-year-old animal (d). Scale bars, 2 mm and 200 µm for the upper and lower panels, respectively. Published in Stonebarger et al. 2020

2.2.i BA 46

Aβ plaques

In BA 46, there were no significant effects of sex (F[1,14]=0.8586, p>0.3; intercept: F[1,15]=0.7781, p>0.3; Figure 13) or genetic origin (slope: F[1,14]=0.0343, p>0.8; intercept: F[1,15]=1.8420, p>0.1) on 4G8 plaque immunostaining. Aβ plaque load increased significantly as a factor of age (F[1,16] = 5.640, p = 0.030), consistent with previous observations. Additionally, there was no difference in plaque density across age in controls versus animals on CR (slope: F[1, 14] = 0.013, p > 0.9; intercept: F[1,15] = 0.198, p > 0.6; Figure 14).

Stability of neuronal density

Also in BA 46, NeuN-positive cells did not change in number across age based on sex (slope: F[1,14]=0.8473, *p*>0.3; intercept: F[1,15]=0.7273, *p*>0.4) or genetic origin (slope: F[1,14]=0.0343, *p*>0.8; intercept: F[1,15]=1.8420, *p*>0.1; Figure 13). Even in these extremely aged animals, neuron number was not significantly changed with age (F[1,16] = 0.139, p > 0.7), and the number was similar irrespective of dietary treatment (slope: F[1,14] = 0.365, p > 0.3; intercept: F[1,15] = 0.302, p > 0.5). Additionally, density of plaques and density of neurons were not significantly correlated in BA 46 (r = 0.196, p > 0.4; Figure 14). Thus far, there is only one report of neuronal loss in the rhesus macaque with loss indicated in PFC Brodmann Area 8a (Smith et al. 2004). However, data included in Stonebarger et al. (2020) included a larger cohort of monkeys across more of the lifespan, and this expanded cohort did not show age-related neuronal loss in BA8a of the PFC. Therefore, there appears to be no neuronal loss in the PFC across rhesus macaque aging.

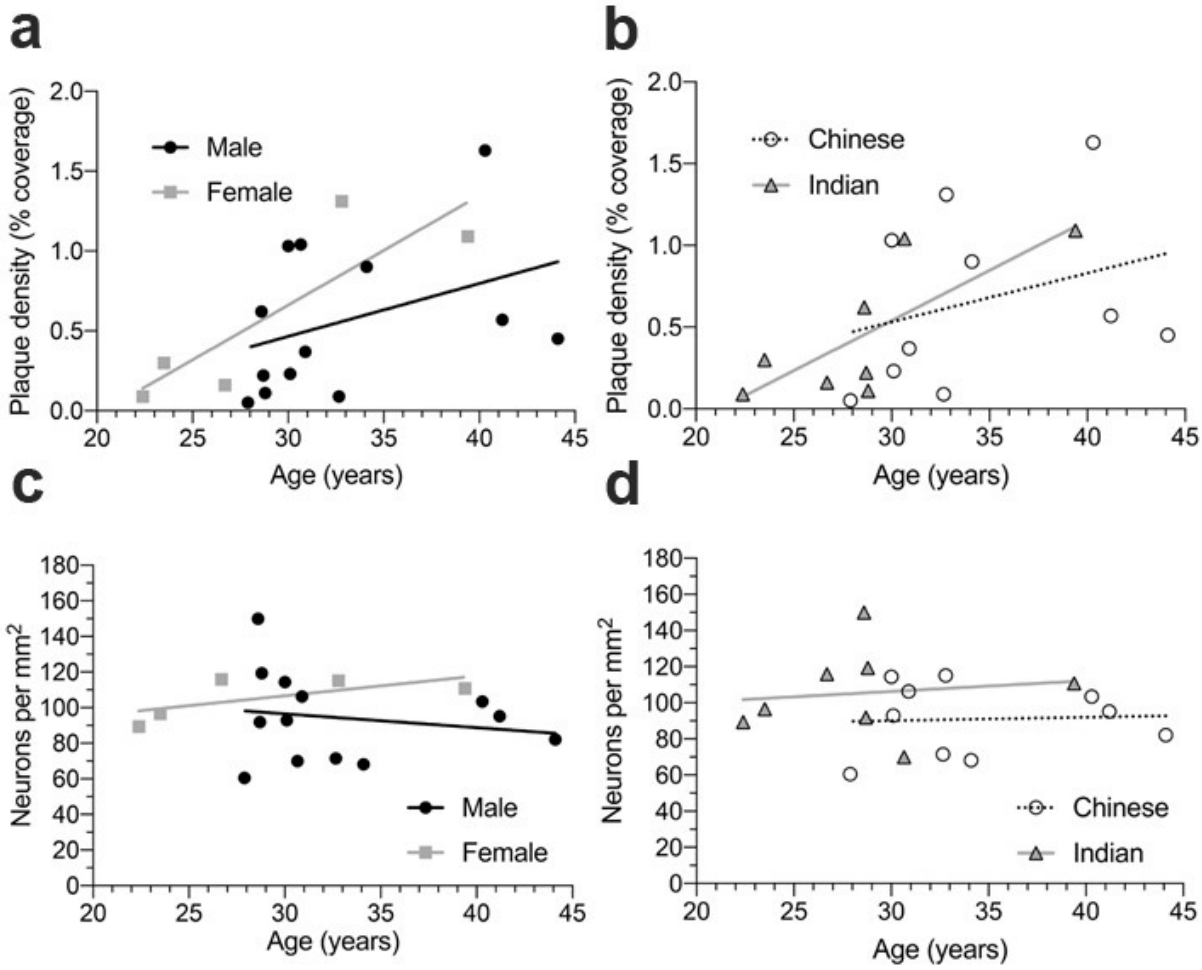


Figure 13. Sex and genetic origin effects in BA 46. There were no significant effects of (a) sex (slope: F[1,14]=0.8586, p>0.3; intercept: F[1,15]=0.7781, p>0.3) or (b) genetic origin (slope: F[1,14]=0.0343, p>0.8; intercept: F[1,15]=1.8420, p>0.1 on 4G8 immunostaining in BA 46. Likewise, NeuN-positive cells did not change in number across age based on (c) sex (slope: F[1,14]=0.8473, p>0.3; intercept: F[1,15]=0.7273, p>0.4) or (d) genetic origin (slope: F[1,14]=0.0343, p>0.8; intercept: F[1,15]=1.8420, p>0.1). Published in Stonebarger et al. 2020

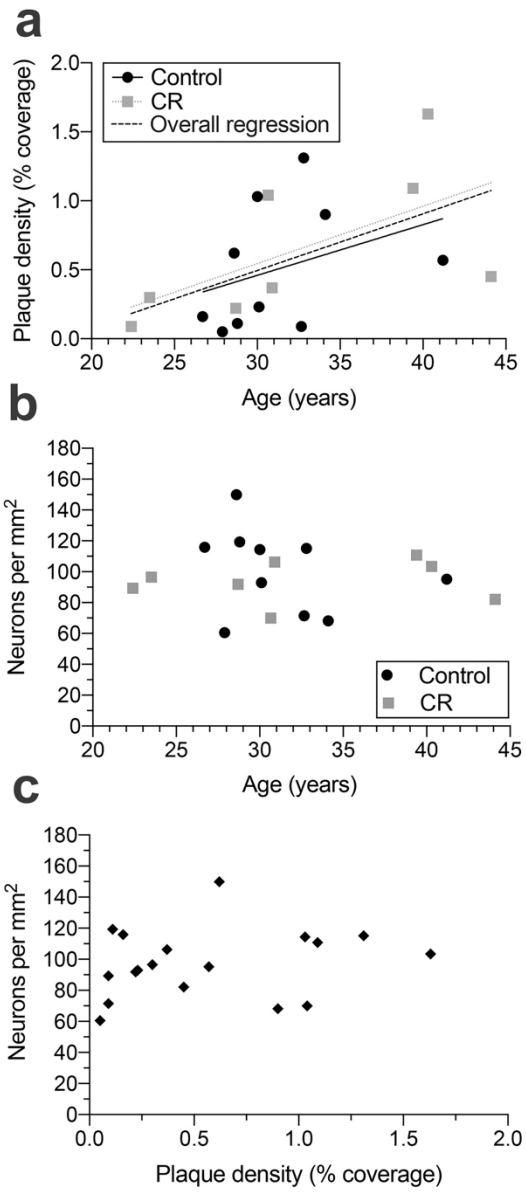


Figure 14. Aβ plaque and neuron density in BA 46 of the PFC. (a) There was a significant overall increase in plaque density with age (dashed line; F[1,16] = 5.640, p = 0.030; pooled regression equation: y = 0.040x–0.711), but no effect of dietary treatment (slope: F[1, 14] = 0.013, p > 0.9; intercept: F[1,15] = 0.198, p > 0.6). Solid black line indicates control group, while dotted gray line shows regression for the CR animals, in (a). (b) There was no significant age-related change in neuron number in BA 46 (F[1,16] = 0.139, p>0.7), nor significant differences between treatment groups (slope: F[1,14] = 0.365, p > 0.3; intercept: F[1,15] = 0.302, p>0.5). (c) There was no significant correlation between Aβ plaque density and neuron number in BA 46 (r = 0.196, p>0.4). Published in Stonebarger et al. 2020

2.2.ii BA 32

Aβ plaques

Using the same tissue sections and same stereological methodology, I first report no dietary group differences surfaced in area fractions (AF; a calculation of the percent area of the ROI that is immunoreactive) for Aβ plaques (slope: F[1,14]=0.003, *p*>0.9;

intercept: F[1,15]=0.164, p>0.6); Figure 15. There are also no differences between animals of different sexes or genetic origins in this cohort, in plaques (sex[slope: F[1,14]=0.154, p>0.7; intercept: F[1,15]=0.030, p>0.8]; genetic origin[slope: F[1,14]=0.423, p>0.5; intercept: F[1,15]=0.023, p>0.8]; Figure 18).

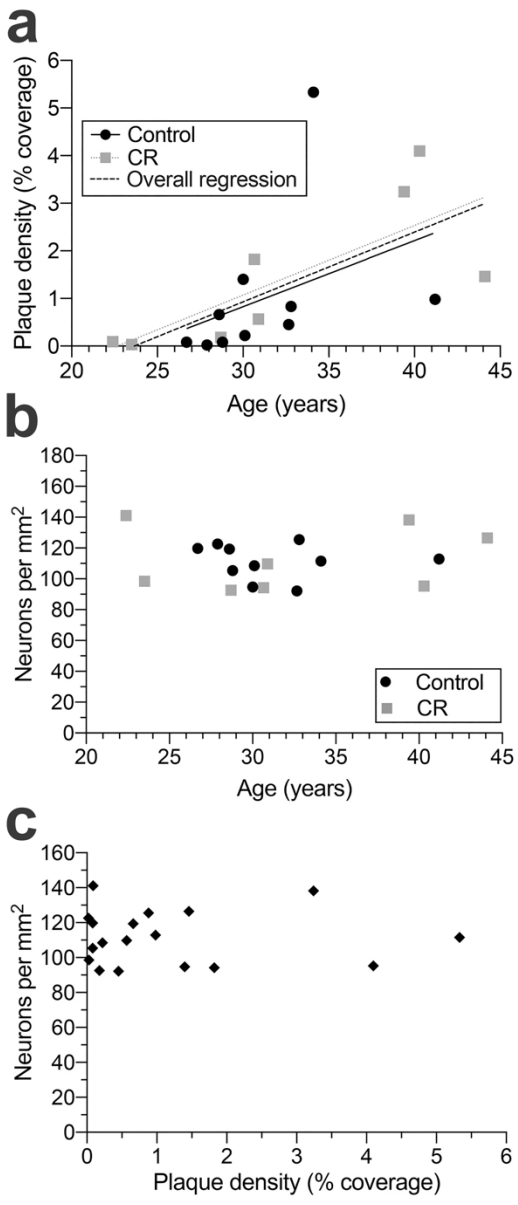


Figure 15. Aβ plaque and neuron density in BA 32 of the cingulate. (a) There was a significant overall increase in plaque density with age (dashed black line; F[1,16] = 7.797, p = 0.013; pooled regression equation: y=0.144x–3.391), but no significant effect of dietary treatment (slope: F[1,14] = 0.003, p > 0.9; intercept: F[1,15] = 0.164, p > 0.6). Dashed black line shows significant overall increase in Aβ plaques across age, solid black line represents the control group, while gray dotted line indicates CR group regression in (a). (b) There was no significant age-related change in neuron density in BA 32 (F[1,16] = 0.080, p > 0.7), nor significant differences between treatment groups (slope: F[1,14] = 0.176, p > 0.6; intercept: F[1,15] = 0.006, p>0.9). (c) There was no significant correlation between Aβ plaque density and neuron number in BA 32 (r = – 0.018, p>0.9). Published in Stonebarger et al. 2020

Cerebral amyloid angiopathy (CAA)

No dietary group differences surfaced in area fractions for CAA (Figure 16; slope: $F[1,14]=2.298$, $p>0.1$; intercept: $F[1,15]=0.117$, $p>0.7$). There are also no differences in CAA between animals of different sexes or genetic origins in this cohort (sex[slope: $F[1,14]=1.45$, $p>0.2$; intercept: $F[1,15]=0.283$, $p>0.6$]; genetic origin[slope: $F[1,14]=0.830$, $p>0.3$; intercept: $F[1,15]=0.551$, $p>0.4$]; Figure 16).

As reported above, Aβ plaque coverage in BA 32 increased significantly with age in this cohort of animals. The AF of CAA also increased significantly across age ($F[1,16]=9.164$, $p=0.008$, $R^2=0.328$; Figure 19), and these two measures were significantly correlated with each other ($F[1,16]=10.02$, $p=0.006$, $R^2=0.385$; Figure 19). In order to investigate whether the proportions of these two measures of amyloidosis within an animal vary across age, I also created a ratio score for each animal such that the AF of each subject's plaque coverage was divided by the AF of vasculature staining. This ratio did not significantly change across age ($F[1,16]=0.105$, $p>0.7$; Figure 19). CAA was not assessed in BA 46, but considering other measures followed the same patterns across regions, it is reasonable to assume that CAA measures would be correlated between regions. CAA was visibly present in relatively high amounts compared to the average clinical population, in both BA 46 and BA 32.

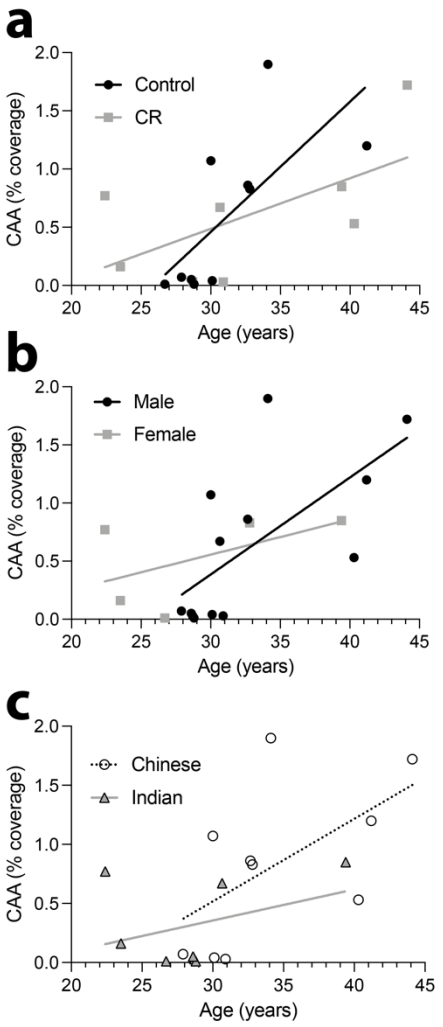


Figure 16. No differences in CAA between dietary treatment groups, sexes, or genetic origins. (a) Dietary treatment groups do not differ in accumulation of CAA across age (slope: $F[1,14]=2.298$, $p>0.1$; intercept: $F[1,15]=0.117$, $p>0.7$). (b) Sexes do not differ in CAA accumulation across age (slope: $F[1,14]=1.45$, $p>0.2$; intercept: $F[1,15]=0.283$, $p>0.6$). (c) No effect of genetic origin on CAA across age (slope: $F[1,14]=0.830$, $p>0.3$; intercept: $F[1,15]=0.551$, $p>0.4$].

Stability of neuronal density

Neuron counts as defined by NeuN staining showed no sex differences in the main outcome (Figure 18); that is, slope (i.e., trajectory of neuron change across age; $F[1,14]=0.013$, $p>0.7$). However, the intercepts of regressions representing male and female animals are statistically different ($F[1,15]=7.980$, $p=0.0128$). It is unclear whether this occurred due to 1) the three youngest animals being female, 2) unequally-sized groups, i.e., ~3x the number of males as females are included in the analyses, or 3) representation of the same number of neurons condensed into a smaller brain volume in

females than that of males. Previous studies have shown that male macaque brains have a larger overall volume (Franklin et al. 2000); therefore, if the number of neurons is equivalent between sexes, females will inherently have a higher density of neurons in the cortex. This seems to be the most likely explanation. However, as I am interested in whether neuron loss occurs due to aging, the lack of difference between slopes—and statistically insignificant regressions—is representative of the lack of difference in trajectories between males and females, which is the main outcome of the study. Therefore, different intercepts in this case does constitute a sex difference in aging trajectories. When animals are combined into one group representing a cross-section of aging, there is a significant overall increase in Aβ plaque density in BA 32 across age ($F[1,16] = 7.797$, $p = 0.013$; Figure 15). As in BA 46, neuronal number did not change with age ($F[1,16] = 0.080$, $p > 0.7$) and was similar irrespective of dietary treatment (slope: $F[1,14] = 0.176$, $p > 0.6$; intercept: $F[1,15] = 0.006$, $p>0.9$). Despite relatively high plaque density in BA 32, there was no significant decrease in neuron density with age ($F[1,16] = 0.080$, $p > 0.7$), nor were Aβ plaque density and neuron density significantly correlated ($r = -0.018$, $p > 0.9$; Figure 15b & 15c). I did not observe any dietary treatment effect for either measure in BA 32 (Aβ plaque density: slope: $F[1,14] = 0.003$, $p > 0.9$; intercept: $F[1,15] = 0.164$, $p > 0.6$ and neuron density: slope: $F[1,14] = 0.176$, $p>0.6$; intercept: $F[1,15] = 0.006$, $p > 0.9$).

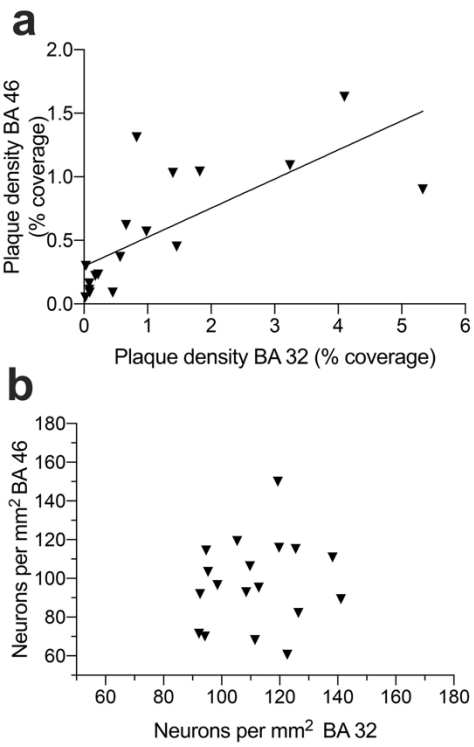


Figure 17. Correlations between BA 46 and BA 32. (a) Aβ plaque density is significantly correlated between BA 46 and BA 32 ($r = 0.727$, $p < 0.001$). (b) No significant correlation exists between neuron number in BA 46 and BA 32 ($r = 0.147$, $p > 0.5$). This is thought to be due to cytoarchitechtonic differences between regions, as all layers of cortex were quantified

Interestingly, plaque densities in BA 46 and BA 32 were significantly correlated ($r = 0.727$, $p < 0.001$; line of best fit: $y = 0.229x + 0.296$; Figure 17). However, when comparing density of neurons between BA 46 and BA 32, there was no significant correlation between areas ($r = 0.147$, $p > 0.5$; Figure 17).

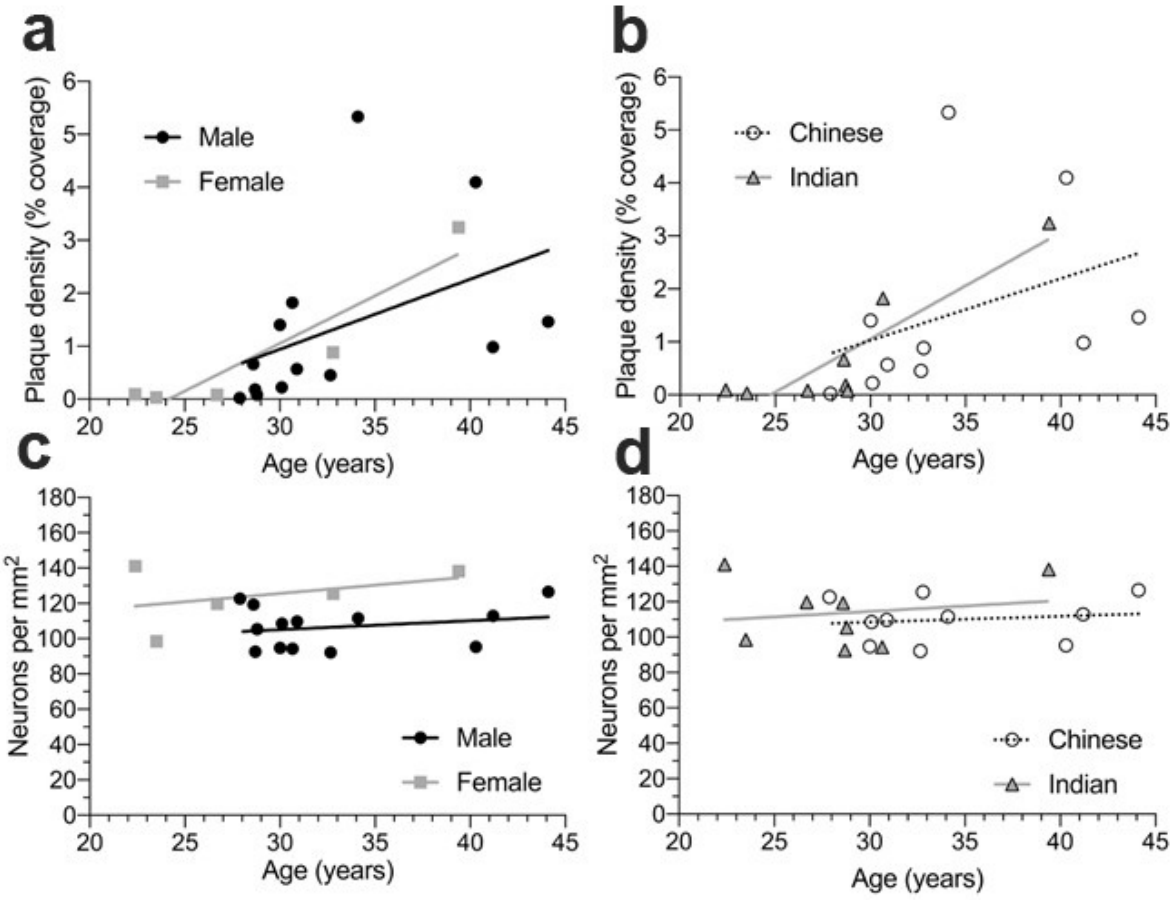


Figure 18. Sex and genetic origin effects in BA 32. Sex by age effects were nonsignificant in (a) 4G8 plaque immunostaining (slope: $F[1,14]=0.1537$, $p>0.7$; intercept: $F[1,15]=0.0313$, $p>0.8$). There were no effects of genetic background on (b) 4G8 (slope: $F[1,14]=0.4233$, $p>0.5$; intercept: $F[1,15]=0.0226$, $p>0.8$). (c) NeuN showed no sex differences in the main outcome; that is, slope (i.e., trajectory of neuron change across age; $F[1,14]=0.013$, $p>0.7$). However, the intercepts of regressions representing male and female animals are statistically different ($F[1,15]=7.980$, $p=0.0128$). It is unclear whether this occurred due to 1) the three youngest animals being female, 2) unequally-sized groups, i.e., ~3x the number of males as females are included in the analyses, or 3) representation of the same number of neurons condensed into a smaller brain volume in females than that of males. Previous studies have shown that male macaque brains have a larger overall volume (Franklin et al. 2000); therefore, if the number of neurons is equivalent between sexes, females will inherently have a higher density of neurons in the cortex. This seems to be the most likely explanation. However, as we are interested in whether neuron loss occurs due to aging, the lack of difference between slopes—and statistically insignificant regressions—is representative of the lack of difference in trajectories between males and females, which is the main outcome of the study. Therefore, different intercepts in this case does constitute a sex difference in aging trajectories. (d) Genetic background has no effect across age on number of NeuN-positive cells (slope: $F[1,14]=0.0323$, $p>0.8$; intercept: $F[1,15]=0.5132$, $p>0.4$) densities. Published in Stonebarger et al. 2020

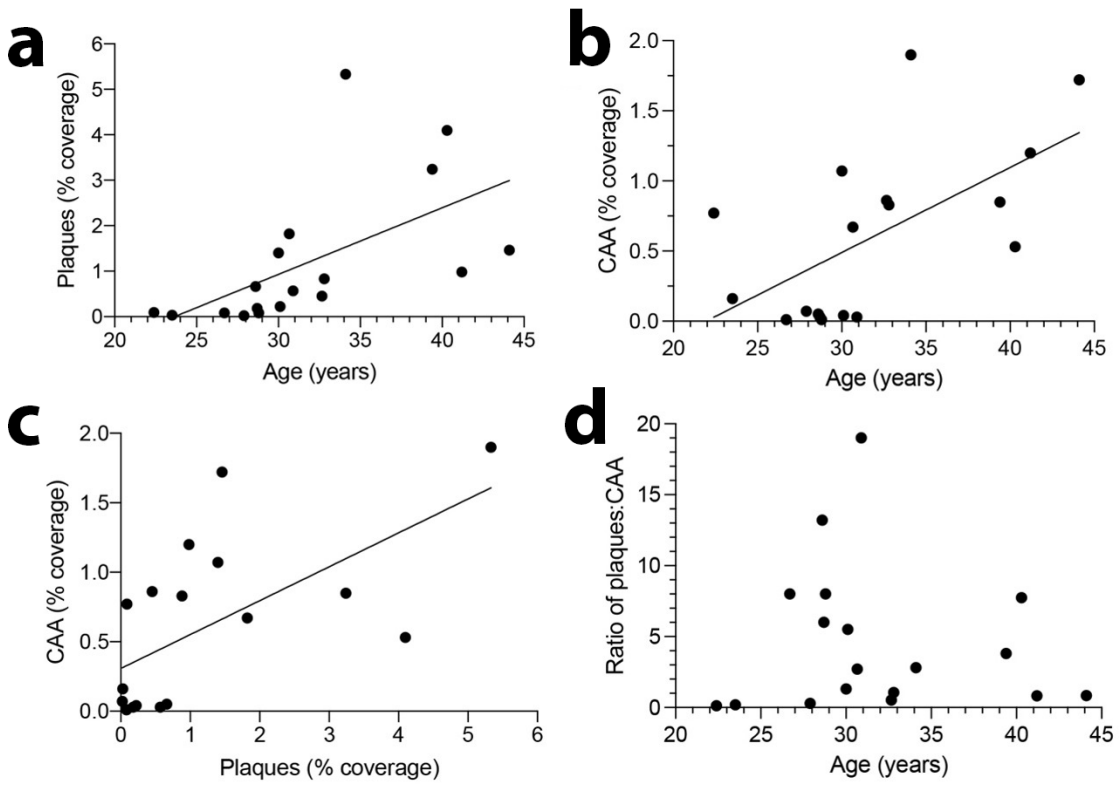


Figure 19. Relationships between age and Aβ extracellular and vascular deposits (plaques and CAA) in the rhesus macaque anterior cingulate cortex. (a) The area fraction (AF; a calculation of percent area) of Aβ plaques increased steadily across aging, beginning in the early-to mid-third decade of life ($F[1,16]=7.797$, $p=0.0130$). (b) The CAA immunoreactivity AF also increased significantly from early 20's through the maximum lifespan of nearly 45 years ($F[1,16]=9.164$, $p=0.008$). (c) AFs of CAA and Aβ plaques are correlated ($F[1,16]=10.02$, $p=0.006$, $R2=0.385$). (d) In order to examine the relationship between CAA and Aβ plaques across aging, we calculated the ratio of the AF for plaques to the AF for CAA for each animal. This ratio was investigated across age, and there is no relation between these variables ($F[1,16]=0.105$, $p>0.7$).

2.2.iii Exploratory analyses

While the cohort is currently a subset of the larger group of animals at NIA, I probed for potential effects in order to guide future hypothesis-driven studies on the larger set of subjects. For instance, I probed whether the amount of time an animal was on a CR diet affected accumulation of amyloid plaques or neuron number. In BA 46, there was no significant regression in plaque accumulation, and unsurprisingly due to a

lack of age-related neuronal loss, there were also no neuronal density differences based on the amount of time the animal was enrolled in the CR treatment group (Figure 20; Aβ plaques: $F[1,8]=2.046$, $p>0.1$; Neuronal density: $F[1,8]=1.764$. $p>0.2$). Similarly in BA 32, there was no significant change in plaques, CAA, or neuronal density due to time spent on a CR diet (Figure 20; Aβ plaques: $F[1,8]=2.220$, $p>0.1$; CAA: $F[1,8]=0.230$, $p>0.5$; Neuronal density: $F[1,8]=0.259$, $p>0.6$). Considering only ten animals were included in the current CR group, analyses are interesting to consider, but likely not powered enough to reveal whether differences appear. Considering there were no CR effects, plaque load increases across age, and amount of time on CR can be seen as a loose proxy for age, I would predict that in a large sample of CR animals, plaques and CAA may in fact *increase* when analyzed by number of years spent on a CR diet. However, there would likely be no difference between groups when compared to number of years the control group animals were enrolled in the study, supporting the theory that the effect is driven by age rather than amount of time spent in the dietary condition. However, much of the population which entered the study originally is still alive, so this will be an important factor to examine in a larger cohort, especially because I am significantly under-powered to divide animals into groups based on the developmental stage in which they began a CR diet.

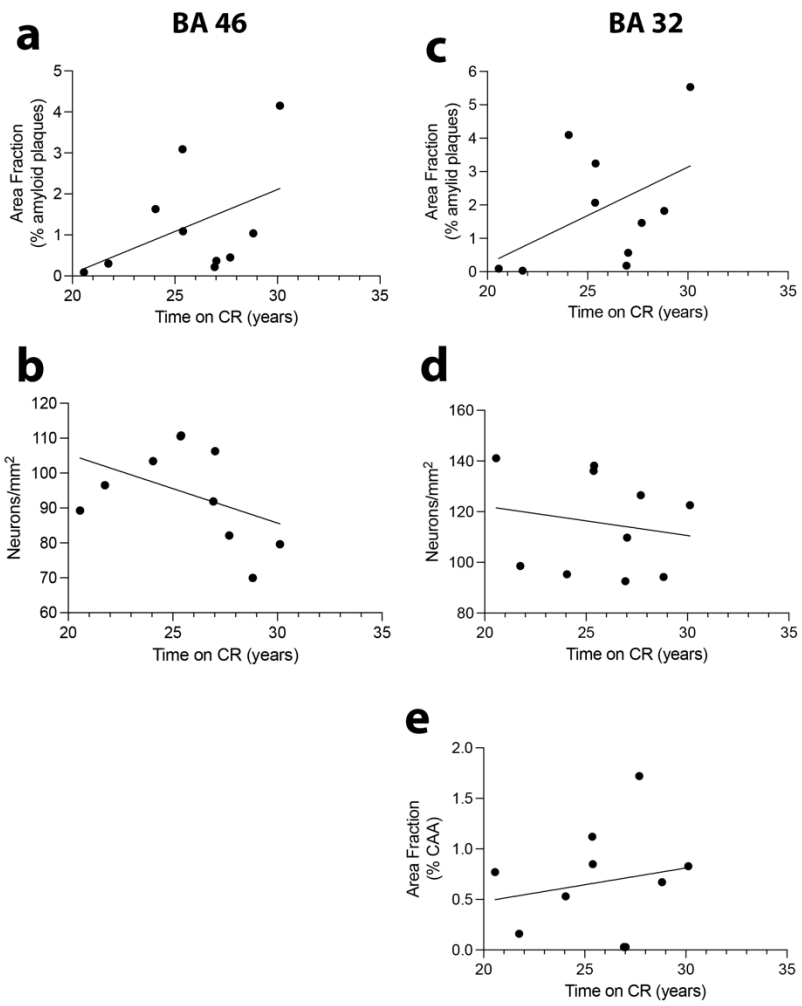


Figure 20. Linear regressions of measured outcomes across amount of time spent on CR. All regressions are nonsignificant. (a) Amyloid plaque load in BA 46. $F[1,8]=2.046$, $p>0.1$. (b) Neuronal density in BA 46. $F[1,8]=1.764$. $p>0.2$. (c) Amyloid plaque load in BA 32. $F[1,8]=2.220$, $p>0.1$. (d) Neuronal density in BA 32. $F[1,8]=0.259$, $p>0.6$. (e) CAA accumulation in BA 32. $F[1,8]=0.230$, $p>0.5$.

Additionally, because this sample represents extreme aging to an extent which has not previously been observed, I divided plaque load regression analyses into "old" and "oldest-old" groups, in which animals survived from 20-29.9 years, and 30-45 years, respectively. The purpose of this was to explore whether patterns of accumulation change when an animal enters an extreme aging state versus what occurs within a more expected lifespan. In BA 46, (Figure 21a) there were no slope or intercept differences (slope: $F[1,14]=7.543$, $p>0.9$; intercept: $F[1,15]=2.551$, $p>0.1$), nor significant

regressions of old rhesus macaques ($F[1,5]=0.214$, $p>0.6$) or the oldest-old population ($F[1,9]=0.225$. $p>0.6$). Further, there were no significant differences in BA 32 between regressions (slope: $F[1,14]=0.757$, $p>0.7$; intercept: $F[1,15]=0.322$, $p>0.3$) or increases in plaque load across age within either of the group, where old monkeys ($F[1,5]=1.858$, $p>0.3$) and oldest-old monkeys ($F[1,9]=1.011$, $p>0.3$) showed no increase in plaque load when analyzed separately (Figure 21b). Notably, as predicted, variability noticeably increased in oldest-old animals (i.e., standard error for the y-intercept in the oldest-old animals in BA 32 was greater than a full percentage: 1.099). Because there was no neuronal loss in either region, I did not analyze these data based on age grouping.

In order to compare age groupings to each other, I used independent t-tests to assess differences in group means. In both BA 46 and BA 32, oldest-old groups show both higher amyloid plaque burden and greater variance (BA 46 t-test: $t=2.944$, $df=16$, $p=0.010$; BA 46 F test: F, DFn, Dfd = 6.167, 10, 6; $p=0.037$. BA 32 t-test: $t=2.654$, $df=16$, $p<0.02$; BA 32 F test: F, DFn, Dfd = 54.20, 10, 6; $p<0.001$). Because variance differed significantly between groups, I used a Mann-Whitney rank-order test to compare groups, which also showed a significant difference in both cases (data not shown). These comparisons show that, even in a subset of animals, and in the absence of significant increases within a group, oldest-old animals still show more accumulation of amyloid plaques than tissue belonging to younger monkeys.

I emphasize here that these analyses were performed *ad hoc*, and should therefore be used to guide future hypothesis-driven analyses in larger populations of this overarching NIA study and others, rather than utilized as definitive results in this study.

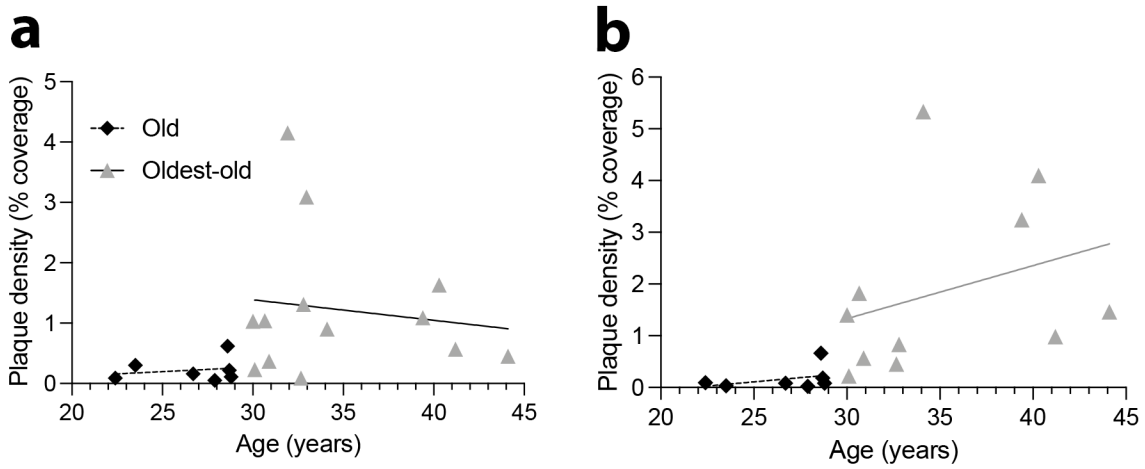


Figure 21. Linear regressions of plaque load in the PFC across age in old (20-29.9 years) and oldest-old (30-45 years) monkeys. (a) BA 46. No slope or intercept differences (slope: $F[1,14]=7.543$, $p>0.9$; intercept: $F[1,15]=2.551$, $p>0.1$) between regressions of old rhesus macaques ($F[1,5]=0.214$, $p>0.6$) and the oldest-old population ($F[1,9]=0.225$. $p>0.6$). (b) BA 32. No significant differences between regressions (slope: $F[1,14]=0.757$, $p>0.7$; intercept: $F[1,15]=0.322$, $p>0.3$) or increases in plaque load across age within either of the group: old monkeys ($F[1,5]=1.858$, $p>0.3$) compared to oldest-old monkeys ($F[1,9]=1.011$, $p>0.3$) showed no effect when comparing regression lines. Notably, as predicted, variability noticeably increased in oldest-old animals (i.e., standard error for y-intercept in the oldest-old animals in BA 32 was greater than a full percentage: 1.099)

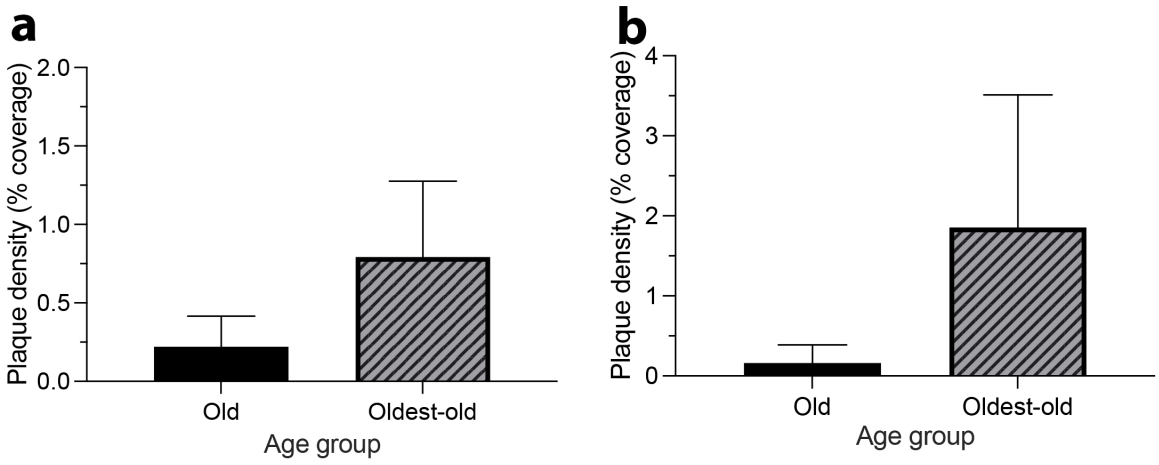


Figure 22. T-test comparisons between old and oldest-old monkey PFC plaque burden. When comparing age groups using unpaired t-tests, significant differences exist between plaque load in old (20-29.9 years) and oldest-old (30-45 years) animals in both analyzed PFC regions. a) BA 46. For BA46, t=2.944, df=16, p=0.010. As predicted, variance was also greater in the oldest-old group (F, DFn, Dfd = 6.167, 10, 6; p=0.037). b) BA 32. Old and oldest-old group means also differ significantly (t=2.654, df=16; p<0.02) and variance was also higher in the oldest-old group (F, DFn, Dfd = 54.20, 10, 6; p<0.001)

3. Summary

Using postmortem tissue from a cohort of extremely aged rhesus monkeys (22.4–44.1 years old, average age 31.8 years) from a longitudinal CR study, I measured immunohistochemically labeled amyloid beta plaques in Brodmann areas 32 and 46 of the prefrontal cortex, areas that play key roles in cognitive processing, are sensitive to aging and, in humans, are also susceptible to AD pathogenesis. I also evaluated these areas for cortical neuron loss, which has not been observed in younger cohorts of aged monkeys. I found a significant increase in plaque density with age, but this was unaffected by diet. Moreover, there was no change in neuron density with age or treatment. These data suggest that even in the oldest-old rhesus macaques, globally, Aβ simply does not accumulate enough in the rhesus brain to be overtly neurotoxic.

Old rhesus macaques also show a high prevalence of CAA, which indicates that they may be a reliable model for studying this phenomenon experimentally. Stereological analysis indicates that CAA does increase across age in the anterior cingulate (BA 32), and is also correlated with an increase in extracellular amyloid plaques. Both of these hold true in calorie restricted and control groups, with no statistical differences. No neuron loss has been observed in this region, and therefore we can surmise that an increase in CAA does not underly cell death. The rhesus model appears to be an excellent model for studying the deposition of amyloid beta into cerebral vasculature, and has excellent potential to facilitate investigation into both the etiology and outcomes of CAA. Hence, the rhesus macaque serves as a pragmatic animal model for normative human aging but is not a complete model of the neurodegeneration of AD. This model of aging may instead prove most useful for determining how even the oldest monkeys are protected from AD, and this information may therefore yield valuable information for clinical AD treatments.

Chapter 3

Experiment 2: Braak staging and qualitative assessment of phosphorylated tau in the rhesus macaque

Data from this chapter are in preparation for submission to the peer-reviewed journal *Alzheimer's and Dementia*.

Animal subjects used in this study were a part of an IACUC-approved longitudinal aging program at the National Institute on Aging, headed by Julie SM Mattison. Tissue was sectioned by and subsequently acquired through Douglas L Rosene at Boston University.

1. Study design and aims

No brain aging differences between dietary groups or sex have been identified in the current cohort; therefore, these animals were once again combined into one single cohort, comprised of males and females, enabling us to focus on the effects of pure aging rather than diet. Detailed subject information, including housing, diet, and individual characteristics, see Table 1 and Introduction section 5.1. HPC sections were available for all subjects, so no animals were excluded from analysis. HPC and PFC sections were IHC stained using primary monoclonal antibody AT8 (1:500, Biolegend, San Diego, CA), which detects middle- to late-stage phosphorylation sites on tau protein (Neddens et al. 2018) at Ser202/Thr205.

1.1 Identification of regions of interest

Regions of interest were identified using the Saleem and Logothetis 2nd edition brain atlas (Saleem and Logothetis 2012). After IHC staining, p-tau-positive sections were thionin-stained to confirm regional neuroanatomical accuracy. Gratitude to Dr. Alison Weiss for providing regionally labeled Nissl sections.

1.2 Detailed methodology: Antigen retrieval

As mentioned previously, we initially used a heated antigen retrieval immunohistochemistry to detect phosphorylated tau in pre-mounted rhesus macaque temporal cortex sections. All steps were performed at room temperature unless otherwise specified. Between each step of the process described below, the slide-mounted sections were rinsed three times with pH 7.6 Tris-buffered saline (TBS). During antigen retrieval and H_2O_2 steps (both described below), slides were contained in vertical slide racks, and transferred into 250 mL containers holding 200 mL of solution. For all following steps, slides were removed, tissue sections were circumscribed using a PAP wax pen, and slides were then laid horizontally in lidded plexiglass slide carriers containing water reservoirs so as to not allow tissue to dry. For steps in which slides were horizontal, solutions were dropped onto the tissue using a pipette, then to rinse and change solutions, liquid was aspirated off using vacuum suction and replaced with the next solution, such that tissue sections did not dry between steps.

After hippocampal sections were selected and mounted, the slides were allowed to dry overnight at room temperature. The next day, they were rehydrated and placed in slide racks. These racks were placed into containers of preheated 9.0 pH ETDA Tris

buffer, inside a steam cooker at 90°C. After 20 minutes, containers were removed from the steam cooker and placed on an agitation plate without changing buffer for 20 more minutes, to allow to gradually cool. Following this, slide racks were moved to a container of room temperature distilled water for ten minutes. This was repeated twice, for a total of three distilled water rinses, then slides were immersed for 30 minutes in a solution of 30% H_2O_2 in 100% methanol, to achieve a final concentration of 2% H_2O_2, in order to block endogenous peroxidase activity. After this, slide racks were rinsed three times in TBS, then slides were transferred to horizontal slide holders described above. Three hundred ml of 5% normal horse serum in TBS was pipetted onto each slide, and incubated for 30 min before slides were rinsed and solution was replaced with primary AT8 antibody (1:500, Thermo Fisher, Waltham, MA, USA), with incubation occurring overnight at 4°C, to reduce background staining. The next morning, following primary antibody incubation, secondary antibody (1:500, biotinylated horse anti-mouse secondary, Vector, Burlingame, CA) was applied for 60 minutes, followed by avidin-biotin complex prepared via manufacturer instructions (Vector, Burlingame, CA) for 90 minutes. Finally, sections were exposed to 3,3'-diaminobenzadine tetrahydrochloride (DAB) and H_2O_2 for 10 minutes and rinsed for a final time to prevent overdevelopment and background staining. Slides were allowed to dry overnight, then dehydrated in increasing concentrations of ethanol baths followed by xylenes, and finally cover-slipped and sealed using DPX mounting medium (Electron Microscopy Services, Hatfield, PA, USA).

1.3 Detailed methodology: Human tissue

Postmortem clinical brain tissues were obtained for comparison from the Oregon Brain Bank at Oregon Health & Science University (OHSU; Portland, OR). Donor subjects of either sex were enrolled and clinically evaluated in studies at the National Institutes of Health-sponsored C. Rex and Ruth H. Layton Aging and Alzheimer's Disease Center (ADC) at OHSU, in accordance with protocols that were approved by the OHSU Institutional Review Board (IRB). Informed consent was obtained from all participants before their enrollment in the studies at the ADC. Subjects were participants in brain-aging studies at the ADC and received annual neurologic and neuropsychological evaluations, with a clinical dementia rating assigned by an experienced clinician (Fracassi et al. 2021). All three cases shown herein are males with a “pure” AD diagnosis; i.e., no comorbid neurodegenerative disorders. Tissue was collected and prepared as described in Fracassi et al. 2021.

1.4 Identification of NFTs

For staging and density ratings, only cells containing dark, identifiably fibrillous staining in the cytoplasm of a neuron were classified as NFTs and used to rate the spread and density of p-tau pathology (see Figure 23 i-p for examples).

1.5 Braak staging

Braak staging of p-tau, based on postmortem analysis, is now widely used clinically to describe the progression of AD. (Braak and Braak 1991; Figure 4). Stage A (encompassing Braak stages I/II), the ERC and CA1 region of the HPC are the areas

affected first; Stage B (encompassing Braak stages III/IV), the subiculum and other hippocampal regions, follows; Stage C (encompassing stages V/VI) includes the neocortex. This classification represents early-, mid-, and late- stage AD, respectively (Braak and Braak 1991; Figures 4 and 24). To identify staging in our rhesus cohort, temporal sections, containing primary regions implicated in A and B stages, as well as neocortical PFC sections to represent stage C—or late involvement—were immunohistochemically stained. These regions of analysis are highlighted in a coronal view in Figure 23. As Braak staging has never been completed in a large cohort of aged rhesus macaques, I also observed the density of NFTs within an affected region and assigned a density rating (Figure 23). If any fully formed intraneuronal NFTs were observed, and up to four NFTs were visible within the field of view (FOV) at 4x objective, the region received a score of +. More than four NFTs per 4x FOV, but less than five NFTs per 10x FOV received a score of ++. Finally, five or more NFTs in a 10x objective were scored as +++. Examples of these density ratings are seen in Figure 23. Only NFTs were used to stage and rate p-tau progression; i.e., other phenotypes were not included in analysis. See Figure 23 i-p and section 2.3.ii for examples and a detailed description of NFT assessment. Staging and ratings of all AT8- and PHF1- stained sections were performed by the same blinded observer (GS) to avoid interrater variability and bias. Following this process, these data were confirmed by two other raters who also remained blinded to age and sex.

1.6 Predictions

Our qualitative focus on NFTs rather than other p-tau phenotypes directly parallels clinical postmortem surveys. This is the first analysis of Braak p-tau staging in

rhesus macaques, and it represents a significantly older and larger cohort than has been previously investigated. I hypothesized that NFTs would accumulate across age, and that spread of NFTs would mimic human AD pathology; therefore, I also compared the tauopathy in rhesus monkeys to clinical postmortem AD tissue. Examination of these three regions established whether the spread of p-tau in macaques is comparable to that seen in clinical AD, which follows a pattern beginning in the ERC, moving into the HPC, and finally to the neocortex, which is affected only in late-stage AD (Braak and Braak 1991).

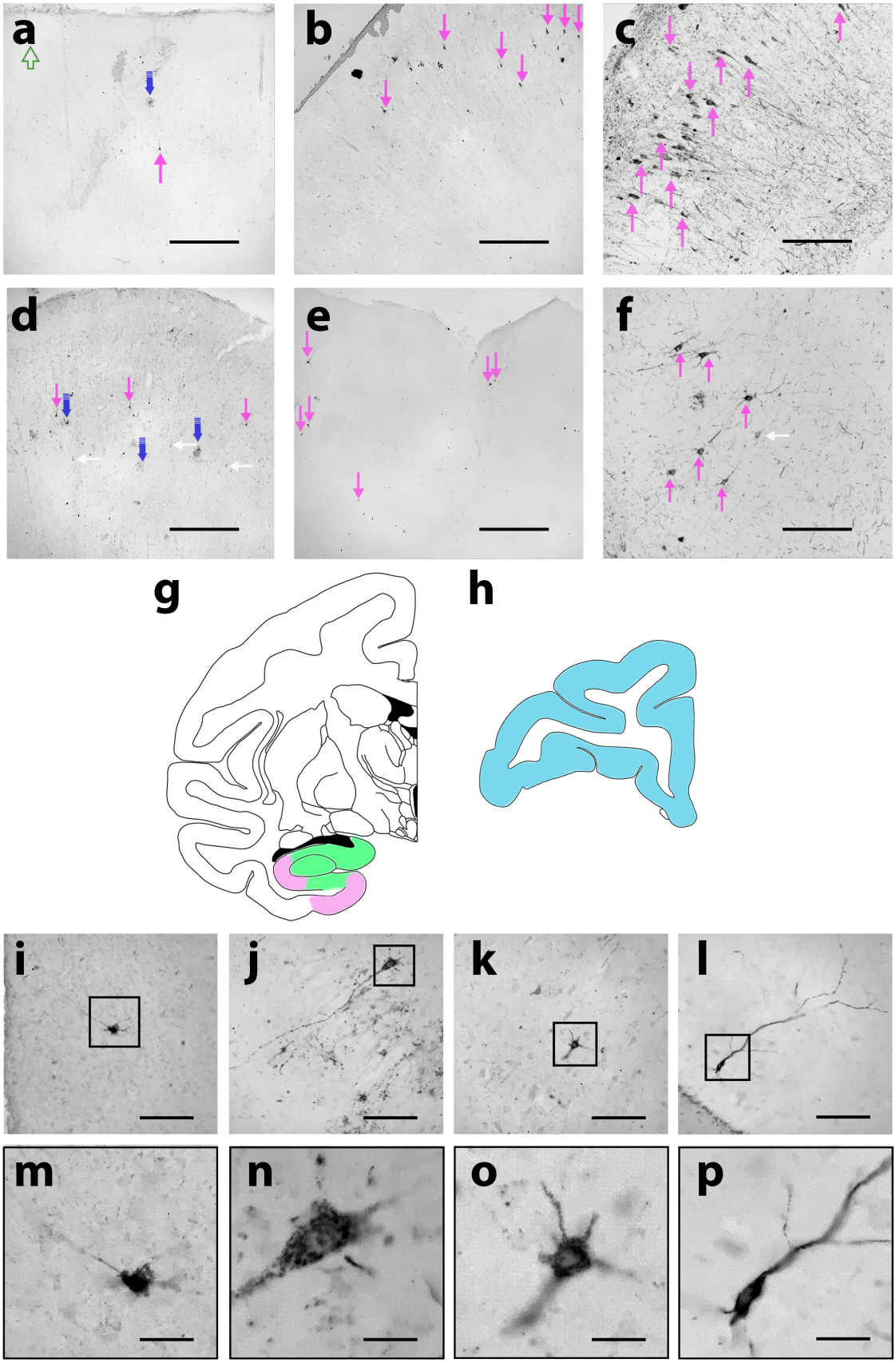

a
b
c
d
e
f
g
h
i
j
k
l
m
n
o
p

Figure 23. Characterization of p-tau staining of NFTs in rhesus macaque brains using primary antibody AT8. Columns in the top two panels (a-f) are examples of each rating in p-tau-positive macaques from this cohort. Pink vertical arrows denote a selection of NFTs, blue vertical broken arrows show examples of p-tau-reactive astroglia, and green open arrows point to examples of immunoreactive oligodendrocytes. (a, d) An animal must have at least one fully developed NFT to earn a p-tau density score of +, and can have, on average, up to 5 tangles per region viewed at a 4x objective. This 4x view contains sparse glial staining and one NFT. (b, e) A ++ rating reaches a threshold of more than five NFTs under a 4x objective, but on average, less than 5 neurons viewed at a 10x objective. This 4x view contains six NFTs as well as an example of an oligodendrocyte. Note that the top left corner may contain five NFTs at a 10x objective; however, this is not consistent throughout the section and therefore this region receives a ++ rating. (c, f) To obtain a +++ score, a region must on average contain more than five NFTs per 10x objective. Not all NFTs are highlighted, as the density is too high to label all cells. This 10x view contains a sufficiently high density to reach a score of +++. (g, h) Classical NFT progression of clinical AD, and areas of analysis. Hemispheric coronal rhesus macaque sections are oriented such that the midline is on the right side of the panel. (g) Example HPC section. Stage A includes the ERC and CA1 regions, highlighted in pink (lighter grey). Stage B includes other HPC regions and the subiculum, highlighted in green (darker grey). (h) Example rhesus macaque PFC section. Stage C include neocortical involvement, which was assessed in the PFC for the current study. Cortical regions are highlighted in blue. Importantly, as regions were given an average rating based on density across the full region(s) for the respective stage. Macaque coronal atlas sections used with opensource permission (BrainInfo, 1991). (i-p) Examples of AT8-positive NFTs; (m-p) are magnifications of the inset directly above the panel. Note dark, fibrillous staining which sometimes excludes the cell nucleus. Neurons lacking dark fibrils were not counted in NFT density ratings, even in the presence of cytoplasmic reactivity.
Scale bar (c, d, f, g): 600 μm. Scale bar (f, h): 200 μm. Scale bar (i-l): 100 μm. Scale bar (m-p): 10 μm

2. Results

2.1 Rhesus macaque NFTs followed clinical AD patterns of spread

Due to the temporal clinical progression from AT8 to PHF1 reactivity (Neddens et al. 2018, Luna-Muñoz et al. 2007, Arbaciauskaite et al. 2021), I predicted that I would detect more AT8 than PHF1, and the animals with the highest AT8 reactivity were most likely to express PHF1. Consistent with the human presentation, more rhesus monkeys showed reactivity to the earlier p-site detected by AT8 than to PHF1, and AT8 reactivity began at younger ages compared to PHF1; i.e., animals showing any PHF1 immunoreactivity also showed positive AY8 staining. This is important, as it validates that tau phosphorylation in the rhesus macaque is similar to that in humans, temporally. Older animals showed more staining overall, with obvious intra- and inter-subject variation (Table 3), just as within the clinical population. The primary antibody AT8 revealed NFTs in nine of the twenty-one animals; conversely, no animals showed labeled NFTs when assessed using PHF1. AT8 staging by age and NFT density rating for each AD stage is displayed in Table 3. Here, one 28.7-year-old animal showed a single NFT in the PFC. All other animals with NFTs were over the age of 30 years at the time of death. Unsurprisingly, three of the four oldest animals show the most extreme NFT pathology. In this cohort, NFTs seem to have appeared earliest in the ERC, then secondarily arose in the HPC, and finally spread to the PFC—a pattern that mimics the clinical spread of p-tau in AD. However, this process did not begin until animals were considerably older than the average lifespan for the species (~26 years; Colman 2018).

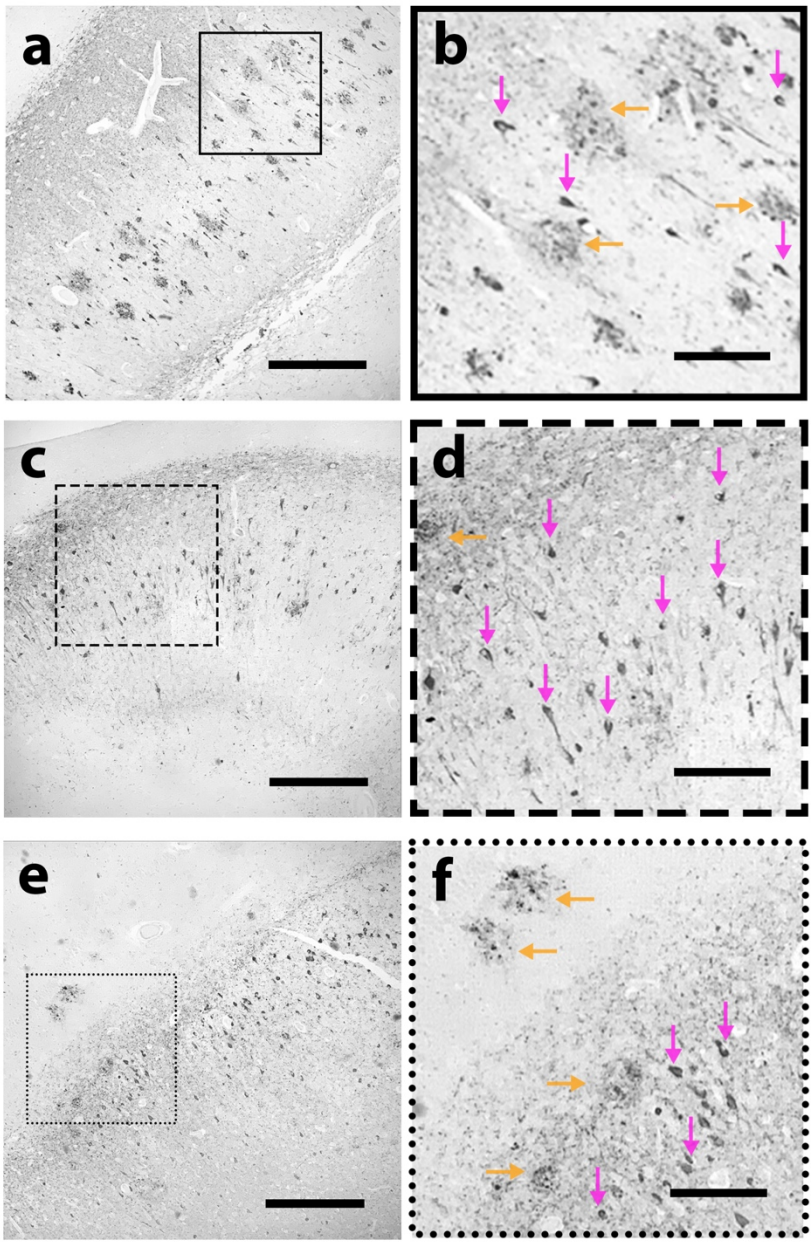


Figure 24: Clinical presentation and progression of "pure" AD. (a-f) human patient HPC sections immunohistochemically stained with primary antibody AT8 against mid-stage p-tau. All three cases had no comorbid neuropathological diagnoses. Panels in the right column are high power views of the inset in the section shown directly to the left. Pink vertical arrows indicate examples of NFTs, and orange horizontal arrows indicate p-tau-positive plaques. (a,b) 51 year-old male. (c,d) 78 year-old male. (e,f) 66 year-old male. Scale bar (a-c): 600 μm. Scale bar (d-f): 200 μm

Animal Number	Age	Sex	Rating: A	Rating: B	Rating: C
CR001	22.4	F	-	-	-
CR020	23.5	F	-	-	-
CR025	26.7	F	-	-	-
CR027	27.9	M	-	-	-
CR026	28.6	M	-	-	-
CR021	28.7	M	-	-	+
CR022	28.7	M	-	-	-
CR023	28.8	M	-	-	-
CR037	30.0	M	-	-	-
CR017	30.1	M	-	-	-
CR033	30.7	M	-	-	-
CR024	30.9	M	-	-	-
CR042	31.9	M	++	+	-
CR034	32.7	M	-	-	-
CR047	32.8	F	-	+	-
CR048	33.0	F	+	-	-
CR039	34.1	M	-	+	+
CR049	39.4	F	+++	+++	++
CR002	40.3	M	+++	+++	+
CR028	41.2	M	+++	+++	++
CR038	44.1	M	+	-	-

Table 3: Spread and density of NFTs in the aged rhesus macaque using AT8. Animals are listed in order of ascending age. Darker cell color indicates a higher density rating. Rating: A indicates the NFT density rating for the ERC and HPC CA1 regions, representing the first regions where NFTs arise in clinical AD. Rating: B indicates average NFT density rating in the HPC and subiculum, which are affected in mid-stage AD. Rating: C refers to NFT density ratings in the PFC, a neocortical area indicative of late-stage AD. Darker cells are indicative of higher NFT density, while a dash indicates that no NFTs were identified in the region. Notably, NFT spread mimics AD progression, but on a delayed timeline compared to clinical AD. Because rhesus macaques age at roughly three times the rate of humans, NFTs would be expected to arise as young as 16-20 years to parallel clinical AD patterns. Density visibly increased across age in this cohort, continuing to support that NFTs accumulate naturally in this species, but not until well beyond the expected lifespan of ~26 years

As + and ++ ratings both denote NFT density far lower than what is seen in AD, or even normal aging, very few animals reached what could be considered a clinically significant, or functionally relevant, NFT load in stages A and B. Even so, only animals over the age of 39 years at death have at least one +++ rating—and, not even the oldest animals show a heavy NFT load in the PFC. The fact that no NFTs were visible in the cohort when using PHF1 also indicates that tau phosphorylation was not as advanced in aged macaques as is seen in humans with AD, among whom PHF1-positive NFTs are common. Due to lack of NFT staining and negligible extra-neuronal immunoreactivity, PHF1 data are not shown. I hypothesized that the presence of NFTs would increase across age and that NFT spread would mimic that seen in clinical AD cases, and both hypotheses were supported. NFTs did not occur until beyond the expected lifespan for a rhesus macaque, and density and spread of NFTs were measurable in only some of the oldest animals, >30 years of age.

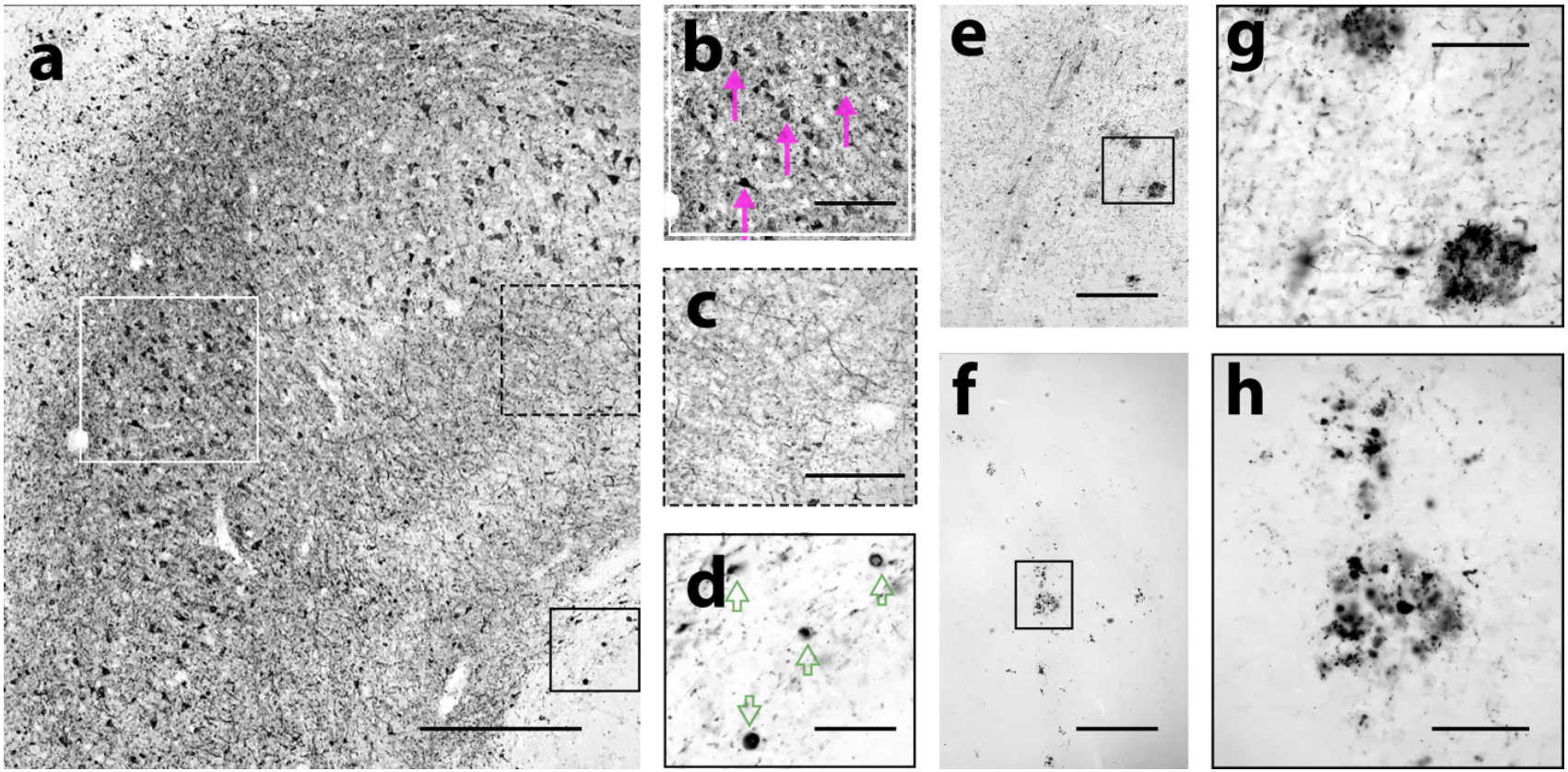


Figure 25. Extracellular tauopathy in the rhesus macaque brain detected immunohistochemically using AT8 antibody in the rhesus macaque brain. (a) example of a heavily stained CA1 region in an aged rhesus macaque. Scale bar (a): 600 μm. (b) Inset labeling examples of high density pyramidal NFTs with pink vertical arrows. (c) inset perspective of a region with no NFTs, but heavy staining of dystrophic processes. Grey and black lines and fibrils are p-tau-reactive neurites. Scale bar (b,c): 200 μm. (d) HPC white matter tract, with green open vertical arrows denoting p-tau positive oligodendrocytes. Scale bar (d): 100 μm. (e,f) Low power examples of HPC (e) and cortical (f) p-tau-containing plaques. Scale bar (e,f): 1 mm. (g,h) magnifications of plaque immunoreactivity of the inset in the left panel. Scale bar (g,h): 100 μm

2.2 AT8 non-NFT phenotypes: intracellular, plaques, dystrophic neurites, and glial tau

P-tau phenotypes outside of NFTs also became evident during analysis—including pre-NFT intraneuronal staining, plaques, dystrophic neurites, and perhaps more interestingly, glial cells. Because only NFTs are used to stage clinical AD, other phenotypes were not herein explicitly quantified. However, they represent important aspects of the model, and therefore I will provide brief characterizations of non-NFT p-tau phenotypes in the aging rhesus macaque brain.

2.2.i Intraneuronal staining

Early cytoplasmic tau aggregations (pretangles) were obvious within neurons when stained for mid-stage tau p-sites (i.e., AT8). Pretangles were evident in some animals with NFTs, but also in some animals with no identifiable NFTs; this is not unexpected as, as indicated by the name, pretangles precede NFTs temporally. Most often, pretangle staining tended to fill the cytoplasm but exclude the nucleus, consistent with clinical observation. Individual p-tau aggregates were visible within the cytoplasmic space of neuronal cells, as is evidenced in images of macaque intraneuronal staining in Figures 25, 26, and 27. In the oldest animals, staining of fully-formed NFTs was evident, as described in the design section. Across ages, many animals had pyramidal neurons with light cytoplasmic staining, which represents a very early aggregation of p-tau, before it has formed large complexes.

2.2.ii Plaques and dystrophic neurites

Two common non-NFT phenotypes of tauopathy in clinical cases are dystrophic neurites and extracellular plaques (Kosik 1990). In the macaque, plaques were most evident in the cortex but also occurred in the HPC (Figure 25[e-h]). Tau-positive neurites can form plaques; some are evident in the plaques shown, for example, in

Figure 25g, or they can exist without coagulating into plaques, as is evident via immunopositive striations in Figure 25c. Examples of these phenotypes are seen in Figures 25 and 26.

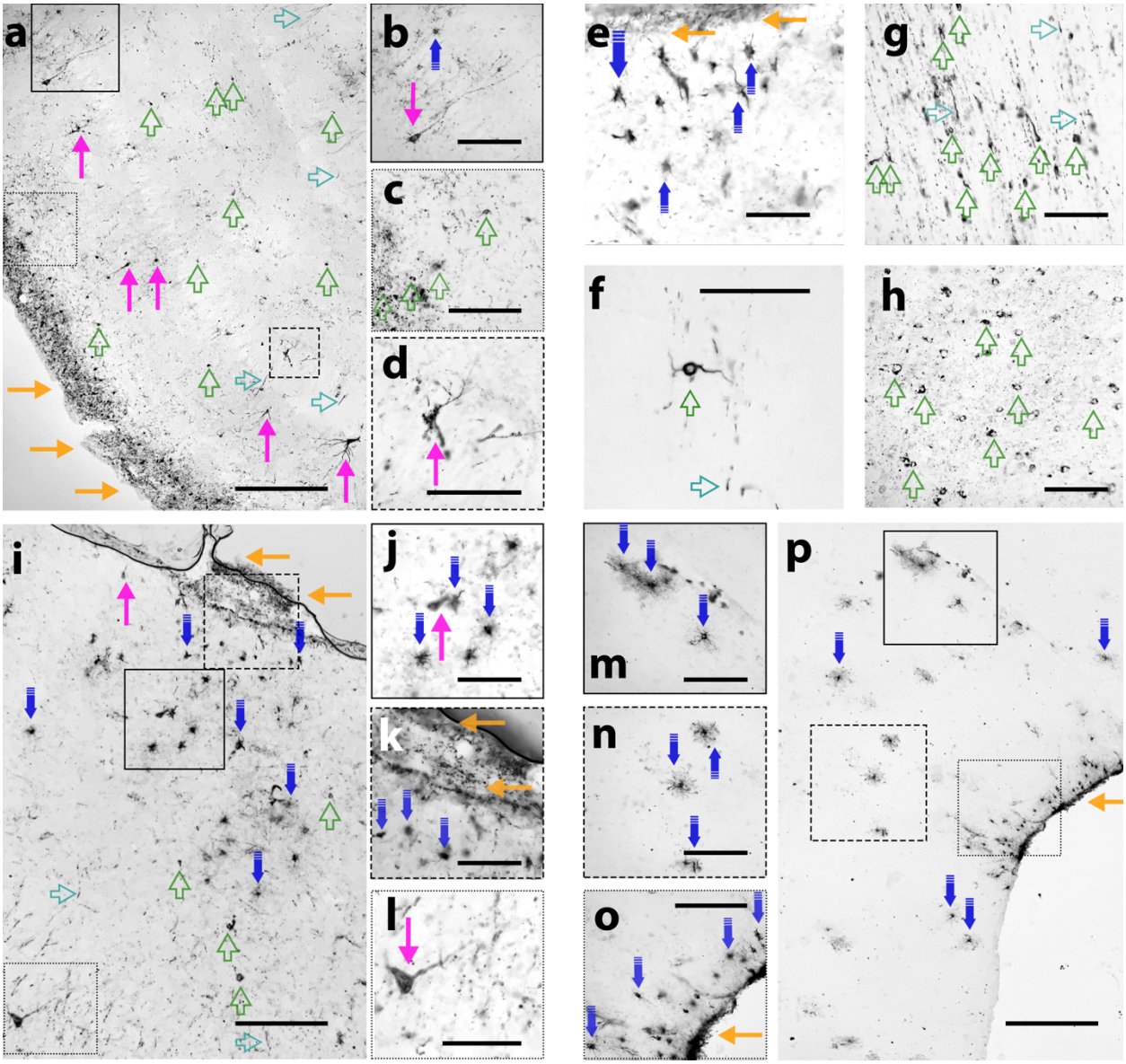


Figure 26: Glial tauopathy in the rhesus macaque brain detected immunohistochemically using AT8 antibody. In all panels, arrows label examples of phenotypes (i.e., not every example of each phenotype is labeled). Pink vertical arrows denote NFTs, blue vertical broken arrows show astrocytic AT8 reactivity, green vertical open arrows label oligodendrocytes, teal open horizonal arrows show dystrophic processes, and orange horizontal arrows denote diffuse p-tau staining, presumed to be astrocytic end feet. (a) HPC section with multiple p-tau phenotypes. Scale bar (a): 1 mm. (b) Inset example of a pyramidal NFT with p-tau positive neurites with a p-tau positive astrocyte. (c) Inset example showing oligodendrocytes near HPC white matter tracts. Scale bar (b,c): 100 μm. (d) Inset example of an HPC NFT. Scale bar (d): 50 μm. (e) Example of thorny astrocytes seen below the pial surface, which contains p-tau reactive astrocytic end feet. This phenotype is seen frequently in clinical glial tau disorders. (f) A coiled body white matter oligodendrocyte surrounded by p-tau positive threads. These phenotypes are the primary oligoglial p-tau-reactive phenotypes found in humans. Scale bar (e, f): 50 μm. (g) P-tau-positive oligodendrocytes and threads in a HPC white matter tract. (h) P-tau-positive oligodendrocyte coiled bodies in subcortical white matter. Scale bar (g,h): 100 μm. (i) Example of an HPC of a different aged monkey with various p-tau reactivity. Scale bar (i): 500 μm. (j) Immuno-positive thorny astrocytes in cortical layers I and II, interior to dense staining of astrocytic end feet. (k) High power view of granular astroglial end feet staining and thorny astrocytes. (l) Deep pyramidal NFT surrounded by dystrophic neurites. Scale bar (j-l): 75 μm. (m-o) Inset views from a cortical section with further astrocytic p-tau reactivity (p). (m) Tufted astrocytes in the cortex, likely surrounding a blood vessel. (n) Individual tufted astrocytes in the grey matter. (o) Thorny astrocytes below the immunoreactive pial surface, made up of astrocytic end feet. Scale bar (m-o): 75 μm. Scale bar (p): 1 mm

2.2.iii Glial tauopathy

Many animals showed marked, identifiable glial tauopathy (Figures 26 and 27). Some exhibited pure glial pathology, with little to no neuronal involvement (i.e., Figure 26p), while others showed glial p-tau in addition to significant neuritic staining (i.e., Figure 26a). There were no cases of neuronal p-tau pathology without some glial involvement. For representative images of glial staining with and without NFTs, and examples of clinically relevant glial cell types such as tufted astrocytes, thorny astrocytes, and coiled body oligodendrocytes, refer to Figures 26 and 27. Additionally, PHF1 shows very light, but morphologically identifiable, staining in glial cells of some very old animals, even though there were no obvious NFTs identified using this antibody (data not shown). Both antibodies revealed stained cells which were morphologically distinguished as astrocytes and oligodendrocytes (Schultz et al. 2000), and in most cases both glial subtypes occurred within the same animal. However, overall reactivity to p-

tau was far more obvious using AT8 to detect mid-stage phosphorylation. The presence of glial staining and absence of neuronal tau phosphorylated at Ser396 supports a p-tau pathway which involves astrocytes and oligodendrocytes earlier than NFTs or even pretangles.

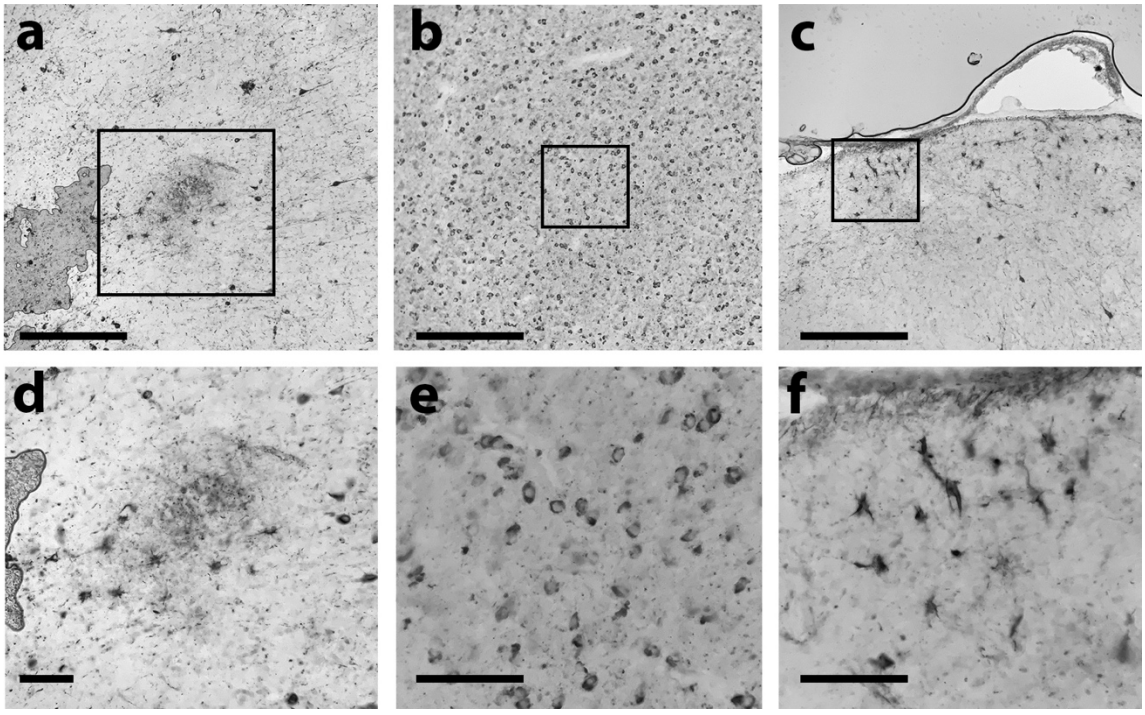


Figure 27: Glial tauopathy in the aged rhesus macaque. Scalebars in (a-c) are 200μm. (a) tau-positive presumed tufted astrocytes at 10x objective. (b) tau-positive presumed oligodendrocytes at 10x objective. (c) tau-positive presumed microglia at 10x objective. Scalebars in (d-f) are 10μm. (d) 20x objective of astrocytes seen in panel (a). (d-f) 40x objective views of tau-positive oligodendroctyes and microglia, corresponding to above panel.

3. Summary

P-tau is a hallmark of Alzheimer's Disease (AD) pathology, but few animal models naturally develop tauopathy. Therefore, it is imperative to characterize natural p-tau spread in the rhesus macaque. Postmortem hippocampal and neocortical sections from very aged rhesus macaques were immunohistochemically stained for p-tau and

characterized with reference to clinical p-tau staging. A subset of animals showed neurofibrillary tangles arising in accordance with the accepted spread of p-tau in AD; however, animals did not develop tangles until beyond the average lifespan (~26 years). Many displayed positive staining in glia, even in the absence of tangles. P-tau tangles were detected in most animals that lived over 31 years, which could phenotypically represent prodromal AD or normative brain aging.

Chapter 4

Discussion

Rhesus macaques are considered to have a lifespan ratio of about 3:1 to that of humans (Tigges et al. 1988; Gearing et al. 1994). The oldest animal in the current cohort lived for more than 44 years, well beyond the average lifespan in captivity of 26 years (Colman 2018) and exceeding an earlier reported maximum lifespan of 40 years (Bodkin et al. 2003). By analyzing tissue from a cohort of the oldest recorded rhesus macaques, the present data extend current knowledge about the aging rhesus macaque brain. The data provide insights into the similarities and differences between the brain of aging rhesus macaques and that of humans undergoing normative and pathological aging. The data in this dissertation represent the oldest reported rhesus macaques, opening exciting new avenues into the exploration of people who live until into the second century of life. Important to note is that the very youngest animal in the cohort represents, using a widely accepted 3:1 ratio of macaque to human aging (Colman 2018), a human who is over 66 years old—already considered aged. Therefore, data herein explore brain changes across the aging process, but not across the lifetime.

1. Staining patterns

1.1 NeuN

In the rhesus monkey PFC, I saw three distinct NeuN immunostaining phenotypes: nuclear staining, cytoplasmic staining, or both, in the same neuron. NeuN (neuronal nuclear antigen) has been identified as the splicing protein Fox-3, which can

be found in varying levels in cytoplasm as well as in neuronal nuclei (Gusel'nikova and Korzchevskiy 2008; Kim et al. 2009), suggesting that the differential NeuN staining observed here may be due to differential expression of Fox-3 splicing protein. While the exact function of Fox-3 is unknown, it is specific to post-mitotic neurons in the brain (Kim et al. 2009). NeuN is traditionally considered a nuclear marker; however, in the current study, animals of both sexes, different ages, and different genetic backgrounds all showed these three phenotypes of NeuN throughout the PFC regions examined. Of note, occipital cortices from the same animals showed more traditional nuclear NeuN staining patterns suggesting this may be a PFC-specific phenomenon (Gittens et al. 2004; Gusel'nikova and Korzchevskiy 2008; Figure 28). Further information on NeuN staining can be found in Duan et al. (Duan et al. 2016)].

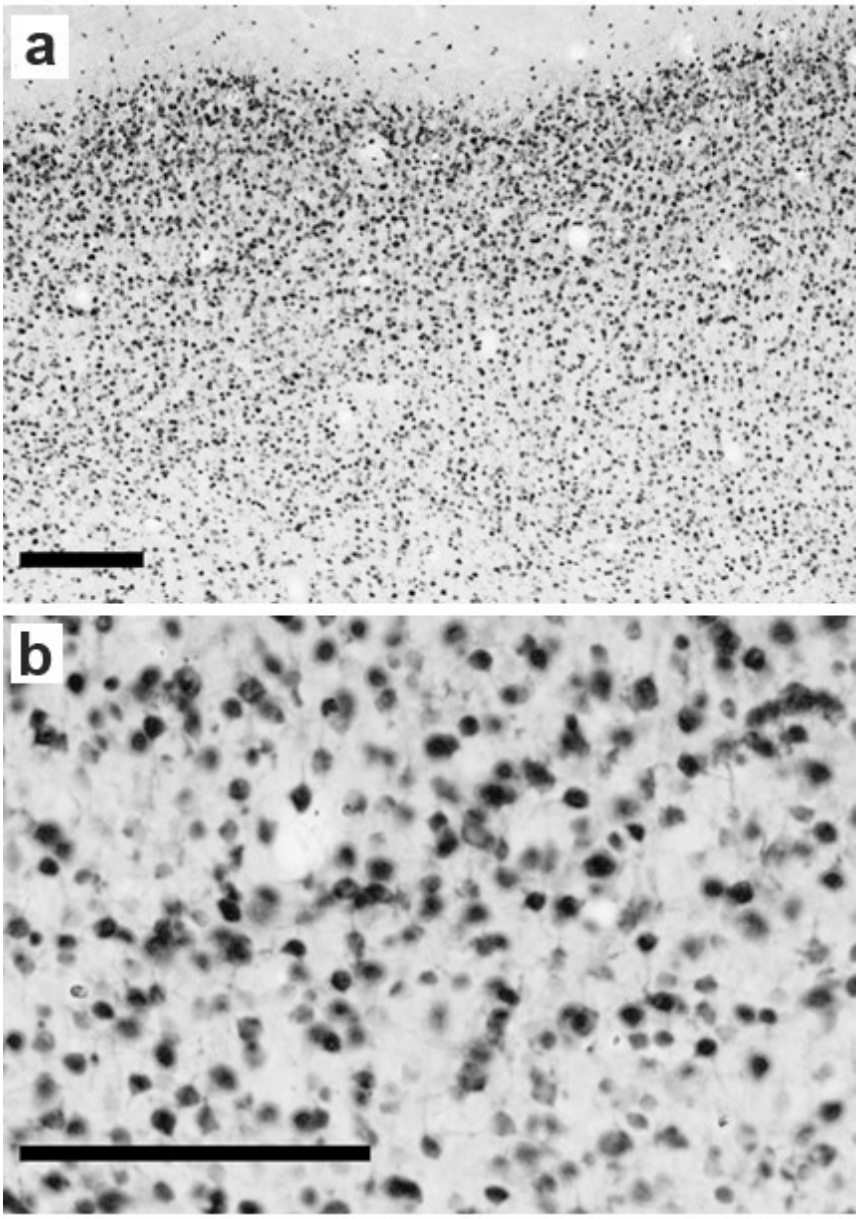


Figure 28. NeuN immunostaining in the occipital cortex of the rhesus macaque. Positive staining exclusively within the cell nuclei conforms to a traditional staining pattern for this antibody, and contrasts with the more widespread cellular staining pattern observed in the PFC (Figure 9). Scale bar (a, b): 200 mm. Published in Stonebarger et al. 2021.

1.2 4G8

Although the focus of the present study was on extracellular Aβ plaques, it was interesting that many animals showed apparent intracellular labeling with the 4G8

antibody. As double-labeling was not performed with NeuN and 4G8, we cannot be completely certain that the observed staining was entirely intraneuronal. However, intraneuronal Aβ has been implicated as a possible precursor to extracellular plaques (Cruz et al. 2018) and has been reported in macaques and humans of varying ages (Kimura et al. 2005; LaFerla and Green 2007). Therefore, it is plausible that light cytoplasmic 4G8 staining indicates labeling of either intraneuronal APP or Aβ (Martin et al. 1991; Kim et al. 2009).

In addition to plaques and presumed intracellular 4G8 labeling, rhesus monkeys showed 4G8 blood vessel staining in both small and large vessels. CAA seemed to be present to some extent in all of the animals in the current study. In humans, vascular Aβ is not uncommon, nor is it specifically related to AD; roughly a quarter of aged adults show this phenotype, regardless of AD status. In the human population, Aβ angiopathy has been linked to several different mutations in the APP gene, and occurs most commonly in larger vessels (Duyckaerts et al. 2009). As shown in Figure 11, both large and small diameter vessels are Aβ-positive within this cohort, and a more in-depth histological exploration of specific phenotypes may reveal more clinically relevant information. CR has been shown in human and animal models to have beneficial cardiovascular effects and delay cardiac aging (Fontaine et al. 2003, Bales and Kraus 2013), which would no doubt effect development of brain angiopathy such as CAA. A primary factor in this conclusion is initial analysis of the Comprehensive Assessment of Long-term Effect of Reducing Intake of Energy (CALERIE) trial in humans, where participants decreased caloric intake by an average of 11.9% from their baseline intake (Kraus et al. 2019). This type of clinical intervention arguably models the control group in the current study; that is, a slight decrease from ad libitum levels. Therefore,

cardiovascular benefits of CR and "light" CR (i.e., inability to overeat) in the NHP could be at play in keeping CAA low in this cohort. These studies together indicate that light CR, or potentially just a lack of overeating, could have the same beneficial effects on amyloidosis as up to 30% CR.

In regard to Aβ plaques, human amyloidosis generally consists of both diffuse (present in macaques) and dense core (not typically observed in macaques) plaques. This is also of interest as dense core plaques are more strongly correlated with cognitive decline in humans (Webster et al. 2014), providing additional support to the idea that the rhesus macaque likely mimics normative aging rather than AD. Another example is that both humans and rhesus macaques have Aβ peptides which are generally cleaved at a length of 40 or 42 (Gearing et al. 1996; Zheng et al. 2017). In humans, $A\beta_{1\text{-}40}$ is found in ten-fold higher concentrations than $A\beta_{1\text{-}42}$ (Gearing et al. 1996), even though the Aβ plaques are predominantly comprised of $A\beta_{1\text{-}42}$. In contrast, in rhesus macaques, $A\beta_{1\text{-}40}$ is the primary component of the Aβ plaques (Gearing et al. 1996). Thus, the relative levels of these peptides seem to be an important differentiator between plaques in monkeys and in AD patients. On a higher level, this study supports others which posit that Aβ plaques are not necessarily an early sign of AD, and may, in fact, be unrelated to more blatantly pathological aspects of the disease, such as loss of cortical neurons and dementia. Clinical data repeatedly shows that many aged humans accumulate Aβ plaques with no signs of mild or overt dementia (Edmonds et al. 2016). In a similar fashion, amyloid levels have not been correlated with cognitive ability in aged monkeys (Sloane et al. 1997).

Aβ levels in this study (~ 1% area coverage in BA 46, and ~ 2–3% coverage in BA 32) also do not reach the 7-20% Aβ area coverage seen in the PFC in late stages of

diagnosed AD in the clinic (Ikonomovic et al. 2008). The existence of a very high plaque load may be necessary before either of cell death or pathological cognitive decline occurs, so the relatively low levels seen here in both PFC regions might indicate that the density is simply insufficient to induce an AD phenotype, especially if the plaques are mainly $A\beta_{1\text{-}40}$ rather than $A\beta_{1\text{-}42}$.

While Aβ plaques are a classical hallmark of AD, some theories suggest that soluble forms of Aβ may be more important for pathological aging than insoluble, plaque-forming confirmations (reviewed in Selkoe and Hardy 2016). While plaque load (i.e., insoluble Aβ) increased across age in this study, there was no evidence of effect on neuron number. Therefore, future studies of soluble Aβ and its interactions with tau phosphorylations may help elucidate the importance of peptide length and solubility in the toxicity of Aβ in humans, and the lack of neurotoxicity in macaques.

1.3 AT8

Detection

Recently, it was posited that the historically uncommon detection of p-tau in the rhesus macaque brain has been due to methodological constraints; namely, that perfusion fixation is necessary to preserve early forms of p-tau (Paspalas et al. 2018). However, tissue in this study was immersion-fixed and still retained antigenicity using primary antibody AT8. Nearly all NFT staining occurred in very old animals—i.e., above the age of 30 years at death—whereas, formerly, younger monkeys were investigated (Härtig et al. 2000, Paspalas et al. 2018, Datta et al., 2021). Now, with a more extensive cohort of old and oldest-old monkeys, I have demonstrated that immersion-fixed tissue also retains antigenicity against primary antibody AT8, with or without specific antigen

retrieval. This is not entirely unexpected as clinical brain tissue is rarely flash frozen and nearly always has a significant post-mortem interval—yet p-tau is still easily detectible in this tissue. These are important considerations, as immersion fixation is a common method of preserving tissue. It is possible to detect and quantify p-tau in fixed macaque tissue, facilitating analysis in previously-preserved tissue—even if it was not flash frozen.

Phenotypes

While NFTs increased across age in this cohort, multiple other phenotypical presentations were obvious, and in many cases more prevalent than NFTs. The most well-known protein to form plaques in AD is Aβ, the primary component in most AD plaques (Duyckaerts 2009). Aβ has been studied in rhesus macaques for decades and forms plaques which are very similar to those in the human brain (Heilbroner 1990, Uno 1993, Stonebarger et al. 2020). In addition to Aβ, many AD patients co-express p-tau in these plaques, and this has been well-validated (Busche and Hyman 2020). Therefore, the presence of p-tau plaques in rhesus macaques was not entirely surprising, as it closely mimics what is seen in the clinic. Further, the initial functional effects of intracellular p-tau seem to be due to the degeneration of axons and dendrites, in both cortical and subcortical structures (Kosik 1990). Some of these processes have "fallen off" of their respective cell bodies and have not been removed by glial cells; in other words, they generally no longer belong to functional neurons (Kosik 1990). Similarly, dystrophic neurites are commonly seen in clinical cases of normative and diseased aging and are potentially the first evidence of functional impairment attributable to p-tau (Vande Weghe et al. 1991). These two phenotypes are unsurprising in either a

pathological or healthy aging context; however, the elevated presence of glial tau was unexpected.

Clinically, p-tau is primarily neuronal in AD, and glial p-tau involvement occurs in specific diagnoses such as aging-related tau astrogliopathy (ARTAG) globular glial tauopathy, Pick's disease, frontotemporal lobar degeneration (FTLD), and others (Kovaks et al. 2013, Kahlson and Colodner 2016, Kovaks 2017, Kovaks et al. 2017, Hirano et al. 2020). While AD can be comorbid with some tauopathies defined by glial p-tau inclusions, clinical diseases that are primarily neuronal and those that are primarily glial likely involve separate pathways (Nolan et al. 2019). In line with observations of human glial tauopathy, the monkeys in the present study showed p-tau reactivity in astrocytes and oligodendrocytes (Figures 26 and 27). Phenotypic presentation of tauopathy in both types of glial cells parallels what is seen in aging humans: oligodendroglial immunoreactivity occurred primarily in coiled bodies and threads, while astrocytic immunoreactivity showed various phenotypes including ramified, thorn-shaped, and tufted astrocytes, as well as astrocytic end feet immunoreactivity which resulted in diffuse staining of the pial surface (Figure 26; indicated by horizontal orange arrows). These inclusions are visually indistinguishable from AT8 staining in postmortem brain tissue from AD patients, for instance (Komori 1999, Kovaks et al. 2013, Kovaks et al. 2017).

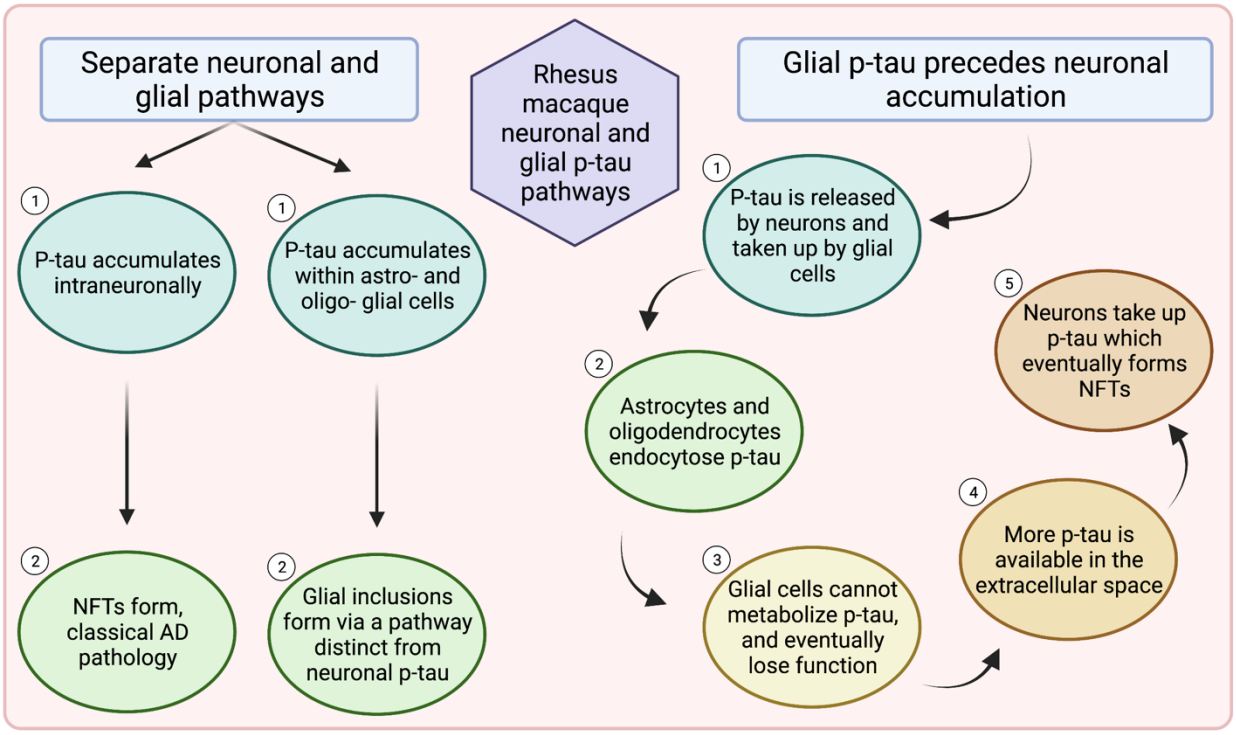


Figure 29: Two proposed pathways by which neuronal and glial p-tau inclusions form. On the left, a representation of two entirely separate pathways by which NFTs form due to a sequence of events, and an unrelated sequence of events culminates in glial p-tau inclusions. A second theory is that, in the NHP brain specifically, glial p-tau may be an earlier indicator of aging. This theory posits that as tau is phosphorylated, it is released into the extracellular matrix. Many glial cells, in particular microglia and astroglia, endocytose pathogenic material, so it stands to reason that p-tau would be taken up by glial cells. This is because p-tau is eventually lethal to neurons, and impedes neuronal function, even without cell death. While microglia were not, upon close inspection, present in the current cohort, astrocytes of multiple subtypes were AT8- and PHF1-positive. If astrocytes are unable to metabolize p-tau, inclusions form intracellularly, which can subsequently be detected *ex vivo* and identified morphologically as glial cells. Once glial cell lose function due to accumulation of p-tau, they can no longer endocytose excess p-tau, and neurons begin to either stop release, or take it back up from the extracellular space. This re-uptake or reversal of the proposed release of p-tau culminates in intraneuronal p-tau in the form of cytoplasmic staining, pretangles, and NFTs. Created with BioRender.com

Another consideration is the occurrence of astrocytic tauopathy in clinical cases following chronic traumatic encephalopathy (CTE). Physical head trauma is known to induce the accumulation of p-tau inclusions in cortical ramified thorny astrocytes alongside pial surface diffuse staining (presumably astrocytic end feet), especially at the

depth of cortical sulci (Bachstetter et al. 2021). This staining pattern occurred in multiple animals, and is virtually indistinguishable from clinical CTE phenotypes (i.e., Figure 26, Bachstetter et al. 2021). Because CTE is not particularly likely in laboratory animals, this phenotype should be investigated further.

2. Presence and spread of NFTs

I have established that NFTs naturally form in very old nonhuman primates and follow a progression that mimics the spread of p-tau in clinical AD. However, it is striking that even at the maximum lifespan for rhesus macaques, mid-stage NFT load did not reach the pathological threshold seen in AD patients. No late-stage NFTs were observed in any monkey, in contrast to the marked PHF1 NFT involvement seen throughout the brain in many humans with AD. This difference in pathology between monkeys and humans is unsurprising, as neuron loss is generally attributed to NFTs, but no neuron loss has been observed in even the oldest macaques (Peters et al. 1994, Giannaris and Rosene 2012, Roberts et al. 2012, Furcila et al. 2018, Stonebarger et al. 2020, Stonebarger et al. 2021). Interestingly however, in contrast to humans, this cohort more commonly showed glial p-tau than neuronal tangles. Glial p-tau in this model should be further characterized to determine whether monkeys exhibit phenotypes most closely related to non-AD tauopathies such as ARTAG or FTLD, as suggested by glial immunoreactivity to AT8. Altogether, this indicates that rhesus monkeys may not develop late-stage NFTs at all, and development of NFTs is not likely until they are aged beyond the expected lifespan for the species. However, some old monkeys present with unexpected glial tauopathy.

Although the aging macaque brain has an age-related increase in amyloid plaques, and p-tau NFT spreading patterns that that are suggestive of human AD pathology, it is not a definitive model of naturally occurring AD for numerous reasons.

3. Lack of diet effects

Animals in the current study represent a subset from a larger study which showed a significant effect of CR on healthspan (Mattison et al. 2017), leading to the hypothesis that these benefits may translate to healthier brain aging in the CR group as well. However, no CR effect on the age-related increase in amyloid load emerged in statistical analyses of BA 46 or 32, or qualitative analysis of staging of neuronal tauopathy. This could be due to the fact that the overall CR effect on other measures of health span is small, or, rather, that CR has effects on other factors such as dendritic atrophy (Luebke et al. 2010), synapse loss (Peters et al. 1996) or inflammation (Willette et al. 2013), as opposed to Aβ plaques. Because Experiment 1 did not show any statistical difference between groups, sexes, or genotypes, animals were combined into one group to represent non-obese aging.

There was large heterogeneity amongst the subjects in this study, as the cohort included both sexes, animals of differing genetic backgrounds (i.e., both Chinese and Indian ancestry), and began CR diets at different stages of life (see Table 1). Small effects were more difficult to detect due to this diversity, in combination with a relatively small sample size compared to human clinical studies, yet this variability is not unlike the heterogeneity found in clinical populations. As ~ 20 additional monkeys from the

original study are still alive, more definitive conclusions about the effects of aging and diet on markers of brain pathology will hopefully become more apparent as these subjects reach the end of life, and their brains are added to the current analysis as well as to future analytic assays.

It also needs to be emphasized that unlike dietary controls in many other calorie restriction studies (Harper et al. 2006; Sridharan et al. 2013; Schafer et al. 2015; Mattison et al. 2017), the control animals in the current study were not fed ad libitum with continuous access to food, but instead receive a standardized caloric intake that was designed to prevent obesity. It has been hypothesized that the benefits of CR are primarily driven by a lack of overeating, i.e., a return to a more evolutionarily relevant state of fewer calories overall, and longer periods of time between feedings (Austad 2001; Le Bourg 2018). If this is the case, we may simply be seeing a "floor" effect, as both the CR and the control group animals escape the deleterious effects of overeating and obesity. This theory is supported by Bodkin et al. (2003), who showed that when caloric intake was only mildly restricted (i.e., restricted enough to prevent obesity), it resulted in reduced morbidity and improved mortality compared to ad libitum control animals. With the assumption that CR is simply a return to evolutionarily relevant dietary standards, restriction beyond recommended caloric intake may not be advantageous in Aβ plaque reduction or overall brain health in primates.

Conversely, the lack of any dietary group differences in CAA or plaques could suggest that amyloidosis across aging is a resilient process that remains unperturbed except under extreme instances. Also supporting this: no differences in extracellular or vascular Aß deposition have been seen in this cohort between dietary groups or innate biological variables outside of age (Stonebarger et al. 2020), which may additionally

indicate that amyloidosis is too robust to be overcome via dietary intervention. This is further evidenced by the parallel NHP CR study at the University of Wisconsin (UW), where amyloid plaque load in the hippocampus increased with age, and also showed no differences between CR and ad libitum groups; however, there was a difference in astrogliosis such that control animals had more (Sridharan et al. 2013). This parallels what has been previously shown in rodents (Major et al. 1997; Sridharan et al. 2013).

This, again, may be an indicator that some brain aging effects may be sensitive to CR, especially compared to a group which overeats, but that the process of amyloid deposition is too resilient. Given similar Aβ findings in both regions, it is likely that CR is not effective at reducing Aβ plaque burden in NHPs, even in the presence of other brain health benefits. This contrasts with transgenic rodent AD models which have shown attenuated plaque formation as well as improved cognitive scores using CR interventions (Halagappa et al. 2007; Schafer et al. 2015; Wahl et al. 2017). Moreover, like some clinical studies (Nelson et al. 2012), prior NHP studies showed no correlation between cognitive scores and Aβ plaques (Sloane et al. 1997), but did show other qualitative and quantitative benefits of CR on brain aging such as reduced iron deposition and beneficial lowering of proinflammatory cytokines (Kastman et al. 2012; Willette et al. 2013). Therefore, it may be pertinent to shift focus in this model to identifying other potential biomarkers of aging and neurodegeneration, which may be more relevant to normative aging. It is also important to distinguish the rhesus model from genetically manipulated rodent models of overt, AD-like damage.

Finally, it is worth noting that even in this cohort of extremely aged subjects, there was no loss of neurons in the PFC, a very vulnerable region in aging. To put this into perspective, other studies of neuron number in BA 46 did not include any animals

over 32 years of age, while all animals in this cohort survived past the age of 22, and six of which were older than the oldest animal with reported neuron counts (i.e., older than 32 years old). For example, in Smith et al. (2004), aged subjects lived an average of 25.4 years, while Peters et al., (1994), had a group of five aged subjects ranging from 25 to 32. In both of these cases, even when compared to young adult groups, there was no evidence of neuron loss in BA 46. Our results extend these findings to reveal that even the oldest-old rhesus macaques do not show any significant loss of neurons in either of the PFC regions examined. Overall, this comparison leaves little doubt that in normal aging rhesus macaques, despite age related amyloid accumulation, there is no age-related loss of neurons in BA 46 of the PFC.

After decades of cognitive aging research in the rhesus macaque, the primary takeaway points of rhesus macaque cognitive aging seem to be that this species does not model overt dementia such as AD, but instead models the natural decline in various cognitive domains seen in healthy aging humans. It remains to be seen whether pathological tauopathy is correlated with cognitive decline in the rhesus macaque, as amyloid plaques are not consistently predictive of cognitive decline in monkeys (Emborg 2017).

4. Summary

Both BA 46 and BA 32 are brain regions that show age-related increases in Aβ plaque load in rhesus macaques, but neither region displays neuron loss, even in the oldest-old rhesus monkeys. Similarly, stability in neuron number across age is shown in PFC BA 8A (Stonebarger et al. 2020). As more brains become available for analysis,

nuances in sex differences, genetic backgrounds, age at CR onset, and more parameters will be explored.

Differential staining patterns of NeuN were observed in the PFC, whereas, the occipital cortices of the same animals contained commonly observed phenotypes. To our knowledge, we are the first group to identify these three immunostaining phenotypes within the rhesus PFC. These patterns are presumed to be due to varying levels of Fox-3; however, for what function is currently unknown.

Finally in the PFC, human data shows that PFC areas like BA 46 and the less well-studied BA 32 are vulnerable to neurodegeneration in AD (Peters et al. 1994; Ikonomovich et al. 2008; Harada et al. 2013; Pimontel et al. 2019). Hence, this first analysis of the cortex of extremely old rhesus monkeys began with BA 46 (Peters et al. 1994), and BA 32. The extreme age of the subjects along with identification of brain areas that are typically affected by aging was quantitatively confirmed, there was no effect of CR nor was any neuron loss observed. Nevertheless, it remains unclear as to whether CR confers any benefit to brain aging in primates as many other factors such as dendritic and synaptic effects remain to be explored.

The percent coverage of Aβ plaques in BA 46 and BA 32 increased significantly with age, but not at a cost to neuron density in the oldest-old individuals. The question is why? Perhaps chronic clinical health issues (obesity, high blood pressure, diabetes etc.) which are suppressed in animal husbandry programs, engage age-related neuropathology. Moreover, regulation of amyloid metabolism in aged monkeys shows a lack of 2-mer amyloid isoforms (Zhang et al. 2019), whereas the addition of amyloid oligomers induces pathology (Beckman et al. 2019, Forny-Germano et al. 2014)

Continued efforts to study the monkey model will provide insights into mechanisms that underlie these differences and could lead to novel preventions and treatments for AD.

In the tauopathy study, I have replicated and extended previous data showing, 1) the natural accumulation of neuronal and non-neuronal p-tau phenotypes in the aging rhesus macaque, 2) the spread of NFTs in the rhesus model mimics clinical AD staging but does not likely reach the threshold necessary for functional impairment, and, 3) the presence of significant astrocytic and oligodendroglial p-tau inclusions, seemingly preceding NFTs. Figure 29 summarizes two potential pathways through which p-tau could accumulate in both neurons and glia. Specifically, accumulation may be via two separate pathways represented by panel (a), or there is also evidence for the pathway described in panel (b), wherein glial p-tau precedes neuronal p-tau, which only begins to accumulate once insoluble p-tau inclusions render glial cells nonfunctional. Evidence from the clinic primarily supports the first theory in AD; however, due to the seemingly chronological nature of NFTs appearing only in the presence of glial tau, it seems likely that in the rhesus monkey, there may be a shared, chronological pathway to NFT aggregation following glial p-tau accumulation. Evidence exists for the role of glial cells in many neurodegenerative disorders, however, so the potential functional role of glial tauopathy itself cannot be dismissed (McConnell et al. 2019).

The knowledge that rhesus macaques NFT pathology follows a similar progression as in AD patients, even if significantly delayed compared to lifespan, brings the possibility for creating induction models of neurodegeneration. Notably, we were still not powered to observe whether differences in tauopathy occur between sexes; as more brains from extremely aged macaques become available, they should be staged to enrich the current dataset, which will also allow for more stringent, statistical analysis.

New NHP AD models would be a more clinically relevant AD model to study disease progression and interventions and can also inform as to which mechanisms induce higher tau accumulation. Specifically, in the future, currently existing macaque models of induced tauopathy (Forny-Germano et al. 2014, Beckmann et al. 2021) should also be scored using the staging methodology detailed herein, to confirm stimulation of the same relevant pathways as in natural p-tau accumulation.

I have herein established that NFTs naturally form in very old nonhuman primates and follow a progression that mimics the spread of p-tau in clinical AD. However, it is striking that even at the maximum lifespan for rhesus macaques, mid-stage NFT load did not reach the pathological threshold seen in AD patients. No late-stage NFTs were observed in any monkey, in contrast to the marked PHF1 NFT involvement seen throughout the brain in many humans with AD. This difference in pathology between monkeys and humans is unsurprising, as neuron loss is generally attributed to NFTs, but no neuron loss has been observed in even the oldest macaques (Peters et al. 1994, Giannaris and Rosene 2012, Roberts et al. 2012, Furcila et al. 2018, Stonebarger et al. 2020, Stonebarger et al. 2021). Interestingly however, in contrast to humans, this cohort more commonly showed glial p-tau than neuronal tangles. Glial p-tau in this model should be further characterized to determine whether monkeys exhibit phenotypes most closely related to non-AD tauopathies such as ARTAG or FTLD, as suggested by glial immunoreactivity to AT8. Altogether, this indicates that rhesus monkeys may not develop late-stage NFTs at all, and development of NFTs is not likely until they are aged beyond the expected lifespan for the species. However, some old monkeys present with unexpected glial tauopathy.

Altogether, the rhesus macaque is a promising model for observation and induction of AD-like pathology and has the potential to serve as an experimental model for lesser-known aging-related tauopathies.

5. Utility of the herein characterization

As the global average and median population ages continue to increase, interventions for diseases of aging such as AD, as well as ways to mediate symptoms of MCI and even normative aging become more urgently needed. Roughly 35% of the clinical population over the age of 85 years has been diagnosed with AD; at an aging rate of 3:1 that of humans, the age equivalent of a rhesus macaque would be nearly 29 years (Le Bourg 2018). Much of the herein cohort (thirteen of twenty-one subjects) survived longer than 29 years, and to mimic clinical prevalence, we would therefore expect to see roughly four or five animals exhibit overt AD symptomology: high plaque load, severe spread of NFTs, and significant neuronal loss. However, no animals showed these characteristics, suggesting that AD does not naturally develop in this species.

The apparent lack of neurodegenerative disease, even in animals that lived into extreme old age, has much potential for informing on clinical AD. Firstly, observing differences in genetics, environmental and lifestyle factors, and other dissimilarities between humans and rhesus macaques can lead to new avenues to examine for protective or deleterious effects in regard to AD or the induction of its various hallmarks. i.e., pathways, proteins, etc. *absent from* rhesus brain aging could point to potential triggers in the human brain. This dissertation begins to categorically

interrogate AD hallmarks across extreme aging to determine whether the rhesus macaque develops Alzheimer's disease naturally.

Both conversely and complimentarily, this characterization begins to open doors for induction models of AD in the rhesus macaque. i.e., the *addition or dysregulation* of pathways suspected to be involved in AD—and, importantly, the outcomes based on those pathway manipulations—give insight into upstream mechanisms driving AD pathology and symptomology. For instance, knowing the progression of NFT spread across age is useful, so that pathology of induction models in younger animals can be compared to pathology of the oldest-old monkeys, even in the absence of control animals with the rarely-seen survival into extreme age. As the species does not naturally develop AD, induced AD-like phenotypes will now be known arise due to the experimental manipulation rather than coincidentally sporadically occurring.

Prior to these studies, there was no baseline characterization of brain aging in an extremely aged population of rhesus macaques. With the current knowledge that they do not develop overt dementia, various pathways can be probed and experimentally manipulated in a model incredibly similar to the clinical population, and the development of overt dementia due to an induced brain alteration could lead to insight into novel treatment pathways. The insights from this dissertation contribute to a full understanding of natural NHP brain aging, which is of increasing translational importance as the global population ages.

6. Future directions

As of yet, there has been no quantification of HPC neuron loss or stability across extreme age in rhesus macaques. Until now, various regions have shown no cell loss. Because p-tau correlates with neuronal death and cognitive decline, however, and some animals had a significant NFT load in regions of the HPC and entorhinal cortex, there is reason to investigate whether enough p-tau has accumulated to kill a significant number of pyramidal neurons. If any HPC regions indeed show a decline in neuronal density, a safe assumption would be that a full AD phenotype can be induced with the correct parameters, as the mechanisms for each hallmark already exist; they just don't become pathological until well after average time of survival. Of note, there were very few to no p-tau ghost cells visible in the present tissue, which alludes to the fact that neurons are likely intact. However, a stereological cell count in the HPC of extremely old animals will be a "nail in the coffin" in determining the absence of aging-related neuron death in this model.

Another complementary direction is to correlate IHC measures with CSF and/or serum levels of circulating biomarkers. $Aß_{1\text{-}40}$ and $Aß_{1\text{-}42}$, as well as the ratio of the two species, are used commonly as predictors and biomarkers of AD. Physiological tau as well as multiple of its post-translational modification variants are also studied as clinical biomarkers. It has been proposed that a mechanism by which NHPs are protected from overt dementia is the ratio of $Aß_{1\text{-}40}$ to $Aß_{1\text{-}42}$ in both the brain and serum; we were able to obtain female serum for hormone assays, so this may be a practical next step.

Because the study from which these animals were sourced is a longitudinal metabolic study, animals were unfortunately not behaviorally tested, so there is no way

to know whether any animals with particularly high plaque or NFT loads are more cognitively impaired than their peers with less aggregation of pathological protein. As previously stated, multiple monkeys in the study are still living, and a collaborator is currently beginning to train them perform learning and memory tasks; to our knowledge, animals this old have never been probed for cognition. Therefore, this will be an exciting continued characterization of extreme aging. Logically, if rhesus macaques model healthy, normative aging, working memory and other types of fluid intelligence should be impaired and/or delayed compared to young, middle-aged, and likely even old macaques, but not severely so. These cognitive measures could also be observed in the context of histology that has been performed on this cohort. In addition to neuronal, Aß, and p-tau sets of stained tissue discussed herein, I have stained parallel stereological sets of tissue from the same animals with multiple glial markers (in the PFC; iba-1 for microglia, and GFAP for activated astroglia) as well as more 4G8 staining for Aß in the HPC. Others in the lab are quantifying other proteins of interest, including aquaporin 1, which is astrocytic and upregulated with age in clinical populations; both physiologically relevant and phosphorylated TDP-43, glial cytoskeletal protein vimentin, which is also upregulated across clinical aging, and other markers of both pathology and visible morphology. Cognitive testing will enable a functional correlate to any changes that are observed cross-sectionally, even if by proxy. Due to longevity being a key outcome of the study, animals live until natural death, so building a collection of brains from animals that have been tested will be a multi-year undertaking. However, changes across age could still be correlated with any histological measures (i.e., does Braak stage determine working memory capacity? Does processing speed negatively correlated with Aß plaque load?). The inherent reason that aged adults seek treatment or a diagnosis is

due to cognitive problems (rather than a buildup of any protein, which is undetectable *in vivo* without a PET scan); therefore, assessing cognition against proteins known to be involved in brain aging will open the door to potential therapeutic interventions into age-related cognitive decline.

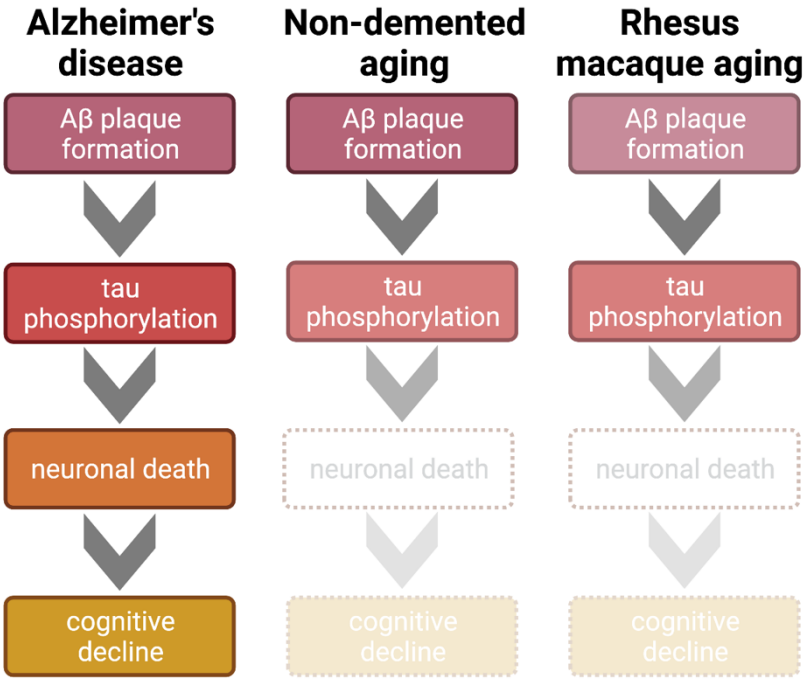


Figure 30: Hallmarks of AD compared to non-pathological human aging and the naturally aging rhesus macaque. In AD, a commonly accepted hypothesis is the Amyloid Cascade hypothesis, which posits that Aβ plaques accumulate, which leads to phosphorylation of tau protein, which in turn causes cell death, driving a severe decline in cognition. In the healthy aging human, Aβ plaques form, sometimes to the degree they are present in AD cases, but tau is not generally seen to the same degree as in tauopathies such as AD. Neuronal death is absent across clinical aging, but some decline in certain cognitive areas is expected. The rhesus macaque model parallels non-demented aging humans in all of these hallmarks, but Aβ plaques form to an even lesser degree. Created with BioRender.com

7. Conclusion

Clinical studies can guide future directions of rodent behavioral and molecular research with regard to normal and pathological aging, which in turn can inform non-human primate research thereby potentially impacting clinical outcomes. This cross-species integrative approach is impractical, however, without detailed characterization of aging and AD-like symptomology in the most common preclinical non-human primate: the rhesus macaque. Importantly, in the rhesus macaque model of aging, all four major hallmarks of AD—significant cognitive decline, amyloid beta plaques, p-tau tangles, and neuronal death—do not reach the pathological levels seen in clinical AD. Cognitive decline in aged rhesus monkeys parallels the healthy aging human very well, in that gradual, incremental decline is seen across age, beginning in middle age or later, depending on the task. Amyloid beta plaques do naturally accumulate in the rhesus macaque brain, especially in sensitive areas such as the PFC. Importantly, however, the area coverage of these plaques in rhesus monkey brains is not high enough to be considered an AD phenotype relative to diagnostic hallmarks in the clinic. While the recent discovery of naturally occurring p-tau in the rhesus monkey brain is indeed exciting, data thus far indicate that the amount of p-tau detected is not in line with the classically accepted progression and advanced conditions of neurofibrillary tangles that represent hallmarks of AD. However, four distinct patterns of tau progression have recently been proposed; therefore, it is unclear which of these trajectories monkey p-tau most closely resembles (Vogel et al., 2021). Finally, neuronal death is an established AD phenotype, but this hallmark has not been obvious even in the very oldest rhesus macaques in studies to date. Taken altogether, it is evident that the rhesus macaque

does not develop overt AD, even though the CNS conditions represent subclinical variations of AD hallmarks, as visualized in Figure 30. Notably, this environment can be experimentally leveraged in a systematic fashion, setting the stage for induction or mitigation models in which various methods can be employed to exacerbate or attenuate existing pathology (i.e., Beckman et al., 2021).

Acknowledgements

Firstly, thank you to the monkeys used in this study, as well as all other biomedical studies. I extend heartfelt gratitude to veterinary and animal care personnel at both NIA and ONPRC; without you none of this would be possible. My research and publications were funded by multiple insititutes including the National Institutes of Health (NIH) grants AG043640, AG055378, AG062220, OD011092 and the Intramural Research Program, National Institute on Aging, NIH. Thank you for early funding from the Achievement Rewards for College Scholars (ARCS) scholarship.

Throughout my career as a graduate student, I've received generous help from multiple faculty and core facilities at OHSU and ONPRC, especially from Dr. Sathya Srnivasan at the OHSU Imaging and Morphology core, and Dr. Byung Park at the Biostatistics and Bioinformatics core at ONPRC. Serum hormone data in Experiment 2 was acquired by the Endocrine Technologies core at ONPRC.

Thank you to Dr. Donald Ingram, who initiated the NIA CR program in the rhesus colony, and Dr. Julie Mattison who leads the program currently. Dr. Kelli Vaughan at NIA has graciously provided consult, veterinary information, and analyses regarding the herein subjects. Thank you to Dr. Douglas Rosene at Boston University and his laboratory, including Samantha Calderazzo, Dr. Penny Shultz, Dr. Tara Moore, and too many others to list, for sectioning, sorting, and cryoprotecting brain tissue used in this dissertation.

Thank you to my mentor, Dr. Henryk Urbanksi (just one last typo). I know I have not been a stereotypical graduate student, and I appreciate you taking the time to learn mentoring styles that work well for both of us, and for trusting my independence. You've taught me so much about writing, and fastidious copy editing, and I know I'm carrying so many skills with me into the world.

My past and present dissertation advisory committee members: Dr. Matthew Ford, Dr. Jacob Raber, Dr. Randy Woltjer, Dr. Bonnie Nagel, Dr. Deborah Finn, and Dr. Heather Bimonte-Nelson. Thank you for your continued guidance and individual conversations and meetings. You're all incredibly busy with entire rap sheets of impressive activities, and I'm humbled that you all make time to support me and my research. Deb, when I came to OHSU you were the first faculty member mentioned to me as a student advocate, and you have proven that to me time and time again. I'm constantly in awe of your resilience, fierceness, poise, and determination. Heather, you've now been my science mom for over a decade! I would never have discovered behavioral neuroscience had it not been for your Behavioral Endocrinology class (which is still my favorite neuroscience topic). I have too many anecdotes and thank yous for this group, but I appreciate you and your dedication to my growth immensely.

Thank you to OHSU non-faculty support I've received over the years, including Amanda Asbrock, Josh Merrick, Louise Sacha, Erin Bickler, Jeanne Sutter, Jackie Wirz, Antoinette Foster, and many, many others. My labmates throughout my time in the Urbanski lab, including Dr. Steve Dash, Dr. Donald Brown, Dr. Leticia Luna, Ben Nilaver, Opal Stayer-Wilburn, Dr. Luisa Appleman, and Dr. Steven Kohama all deserve so many thank yous.

A deep thank you to everyone involved in supporting me throughout my journey to get here. My family has always encouraged my passion for science, and tolerated my passion for communicating, from my first memories of playing with bugs and rocks.

Thank you to my little sister Alex, who left this life a few months ago. You were my first psychology study test subject, and grew into my best friend. My love of mentorship probably started from bossing you around as a toddler. I wouldn't have made it through my first few years of grad school without the hundreds of hours we spent on the phone and weekends you visited me, I love you, I miss you.

My brothers, Michael and Jack, are two of the only men in the world that I trust. I love you so, so much, and I'm so proud of who you've both grown into. I can't wait to see what you both continue to do in the world. acab, we keep each other safe.

Thank you to my dog Moose, for not only saving my life literally, but continuing to be a source of endless love and comfort, even when I have to redo data for the fourth time.

Mom and Dad, I don't have the time or space to even begin. You are my role models and favorite people, and I can't imagine more loving, supportive, unbelievably strong parents. It's made the biggest difference in the world.

Dozens of friends, in Portland and across the country and world, have kept me afloat throughout the last six years. Far too many to list (if you're wondering, it probably includes you), but this department has brought me three of the best women I've ever known: Dr. Rebecca Hood, Dr. Sydney Boutros, and Dr. Sheena Potretzke. We finally did it, y'all.

References

Adams JC. Biotin amplification of biotin and horseradish peroxidase signals in histochemical stains. *J Histochem Cytochem*. 1992;40(10):1457-1463. doi:10.1177/40.10.1527370

Aguiar S, Borowski T. Neuropharmacological Review of the Nootropic Herb *Bacopa monnieri*. *Rejuvenation Research*. 2013;16(4):313-326. doi:10.1089/rej.2013.1431

Albert MS, DeKosky ST, Dickson D, et al. The diagnosis of mild cognitive impairment due to Alzheimer's disease: Recommendations from the National Institute on Aging-Alzheimer's Association workgroups on diagnostic guidelines for Alzheimer's disease. *Alzheimer's & Dementia*. 2011;7(3):270-279. doi:10.1016/j.jalz.2011.03.008

Antonsdottir IM, Leoutsakos JM, Sloan D, et al. The associations between unmet needs with protective factors, risk factors and outcomes among care partners of community-dwelling persons living with dementia. *Aging & Mental Health*. Published online March 24, 2022:1-9. doi:10.1080/13607863.2022.2046698

Arbaciauskaite M, Lei Y, Cho YK. High-specificity antibodies and detection methods for quantifying phosphorylated tau from clinical samples. *Antibody Therapeutics*. 2021;4(1):34-44. doi:10.1093/abt/tbab004

Arnsten AFT, Datta D, Preuss TM. Studies of aging nonhuman primates illuminate the etiology of early-stage Alzheimer's-like neuropathology: An evolutionary perspective. *Am J Primatol*. 2021;83(11). doi:10.1002/ajp.23254

Arriagada PV, Marzloff K, Hyman BT. Distribution of Alzheimer-type pathologic changes in nondemented elderly individuals matches the pattern in Alzheimer's disease. *Neurology*. 1992;42(9):1681-1681. doi:10.1212/WNL.42.9.1681

Attems J, Jellinger K, Thal DR, Van Nostrand W. Review: sporadic cerebral amyloid angiopathy. *Neuropathology and applied neurobiology*. 2011;37(1):75-93. doi:10.1111/j.1365-2990.2010.01137.x

Austad SN. Does Caloric Restriction in the Laboratory Simply Prevent Overfeeding and Return House Mice to Their Natural Level of Food Intake? *Sci Aging Knowl Environ*. 2001;2001(6). doi:10.1126/sageke.2001.6.pe3

Austad SN, Kristan DM. Are mice calorically restricted in nature? *Aging Cell*. 2003;2(4):201-207. doi:10.1046/j.1474-9728.2003.00053.x

Bachstetter AD, Garrett FG, Jicha GA, Nelson PT. Space-occupying brain lesions, trauma-related tau astrogliopathy, and ARTAG: a report of two cases and a literature review. *acta neuropathol commun*. 2021;9(1):49. doi:10.1186/s40478-021-01152-3

Bailey ZD, Krieger N, Agénor M, Graves J, Linos N, Bassett MT. Structural racism and health inequities in the USA: evidence and interventions. *The Lancet*. 2017;389(10077):1453-1463. doi:10.1016/S0140-6736(17)30569-X

Bales CW, Kraus WE. Caloric Restriction: IMPLICATIONS FOR HUMAN CARDIOMETABOLIC HEALTH. *Journal of Cardiopulmonary Rehabilitation and Prevention*. 2013;33(4):201-208. doi:10.1097/HCR.0b013e318295019e

Bartus RT, Fleming D, Johnson HR. Aging in the Rhesus Monkey: Debilitating Effects on Short-term Memory. *Journal of Gerontology*. 1978;33(6):858-871. doi:10.1093/geronj/33.6.858

Baxter A, Wood EK, Jarman P, Cameron AN, Capitanio JP, Higley JD. Sex Differences in Rhesus Monkeys' Digit Ratio (2D:4D Ratio) and Its Association With Maternal Social Dominance Rank. *Front Behav Neurosci*. 2018;12:213. doi:10.3389/fnbeh.2018.00213

Beckman D, Chakrabarty P, Ott S, et al. A novel tau-based rhesus monkey model of Alzheimer's pathogenesis. *Alzheimer's & Dementia*. 2021;17(6):933-945. doi:10.1002/alz.12318

Beckman D, Ott S, Donis-Cox K, et al. Oligomeric Aβ in the monkey brain impacts synaptic integrity and induces accelerated cortical aging. *Proc Natl Acad Sci U S A*. Published online December 23, 2019:201902301. doi:10.1073/pnas.1902301116

Bhattacherjee A, Djekidel MN, Chen R, Chen W, Tuesta LM, Zhang Y. Cell type-specific transcriptional programs in mouse prefrontal cortex during adolescence and addiction. *Nat Commun*. 2019;10(1):4169. doi:10.1038/s41467-019-12054-3

Bierer LM, Hof PR, Purohit DP, et al. Neocortical Neurofibrillary Tangles Correlate With Dementia Severity in Alzheimer's Disease. *Archives of Neurology*. 1995;52(1):81-88. doi:10.1001/archneur.1995.00540250089017

Bodkin NL, Alexander TM, Ortmeyer HK, Johnson E, Hansen BC. Mortality and morbidity in laboratory-maintained rhesus monkeys and effects of long-term dietary restriction. *J Geron*. 2003;58A:212-219.

Boyle PA, Yu L, Wilson RS, Gamble K, Buchman AS, Bennett DA. Poor Decision Making Is a Consequence of Cognitive Decline among Older Persons without Alzheimer's Disease or Mild Cognitive Impairment. Reddy H, ed. *PLoS ONE*. 2012;7(8):e43647. doi:10.1371/journal.pone.0043647

Braak H, Braak E. Neuropathological stageing of Alzheimer-related changes. *Acta Neuropathol*. 1991;82(4):239-259.

Brown DL. Practical Stereology Applications for the Pathologist. *Vet Pathol*. 2017;54(3):358-368. doi:10.1177/0300985817695781

Bufalini J, Eslinger P, Lehman E, George DR. Effects of a Personalized Music Intervention for Persons with Dementia and their Caregivers. *ADR*. 2022;6(1):43-48. doi:10.3233/ADR-210043

Busche MA, Hyman BT. Synergy between amyloid-β and tau in Alzheimer's disease. *Nat Neurosci*. 2020;23(10):1183-1193. doi:10.1038/s41593-020-0687-6

Byrne A, Torrens-Burton A, Sivell S, et al. Early palliative interventions for improving outcomes in people with a primary malignant brain tumour and their carers. Cochrane Gynaecological, Neuro-oncology and Orphan Cancer Group, ed. *Cochrane Database of Systematic Reviews*. 2022;2022(1). doi:10.1002/14651858.CD013440.pub2

Calabrese C, Gregory WL, Leo M, Kraemer D, Bone K, Oken B. Effects of a Standardized *Bacopa monnieri* Extract on Cognitive Performance, Anxiety, and Depression in the Elderly: A Randomized, Double-Blind, Placebo-Controlled Trial. *The Journal of Alternative and Complementary Medicine*. 2008;14(6):707-713. doi:10.1089/acm.2008.0018

Cera N, Esposito R, Cieri F, Tartaro A. Altered Cingulate Cortex Functional Connectivity in Normal Aging and Mild Cognitive Impairment. *Front Neurosci*. 2019;13(857). doi:10.3389/fnins.2019.00857.

Chang W, Weaver Cm, Medalla M, Moore Tl, Luebke Ji. Age-related alterations to working memory and to pyramidal neurons in the prefrontal cortex of rhesus monkeys begin in early middle-age and are partially ameliorated by dietary curcumin. *Neurobiology of Aging*. 2022;109:113-124. doi:10.1016/j.neurobiolaging.2021.09.012

Colman RJ. Non-human primates as a model for aging. Biochim Biophys Acta. *Mol Basis Dis*. 2018;1864:2733-2741. doi:10.1016/j.bbadis.2017.07.008

Cordone S, Annarumma L, Rossini PM, De Gennaro L. Sleep and β-Amyloid Deposition in Alzheimer Disease: Insights on Mechanisms and Possible Innovative Treatments. *Front Pharmacol*. 2019;10:695. doi:10.3389/fphar.2019.00695

Crestini A, Santilli F, Martellucci S, et al. Prions and Neurodegenerative Diseases: A Focus on Alzheimer's Disease. *JAD*. 2022;85(2):503-518. doi:10.3233/JAD-215171

Cummings JL, Cohen S, van Dyck CH, et al. ABBY: A phase 2 randomized trial of crenezumab in mild to moderate Alzheimer disease. *Neurology*. 2018;90(21):e1889-e1897. doi:10.1212/WNL.0000000000005550

Cunnane SC, Trushina E, Morland C, et al. Brain energy rescue: an emerging therapeutic concept for neurodegenerative disorders of ageing. *Nat Rev Drug Discov*. 2020;19(9):609-633. doi:10.1038/s41573-020-0072-x

Datta D, Leslie SN, Wang M, et al. Age-related calcium dysregulation linked with tau pathology and impaired cognition in non-human primates. *Alzheimer's & Dementia*. 2021;17(6):920-932. doi:10.1002/alz.12325

Dawkins E, Small DH. Insights into the physiological function of the β-amyloid precursor protein: beyond Alzheimer's disease. *J Neurochem*. 2014;129(5):756-769. doi:10.1111/jnc.12675

Deb A, Thornton JD, Sambamoorthi U, Innes K. Direct and indirect cost of managing alzheimer's disease and related dementias in the United States. *Expert Review of Pharmacoeconomics & Outcomes Research*. 2017;17(2):189-202. doi:10.1080/14737167.2017.1313118

Decourt B, Boumelhem F, Pope ED, Shi J, Mari Z, Sabbagh MN. Critical Appraisal of Amyloid Lowering Agents in AD. *Curr Neurol Neurosci Rep*. 2021;21(8):39. doi:10.1007/s11910-021-01125-y

Decourt B, D'Souza GX, Shi J, Ritter A, Suazo J, Sabbagh MN. The Cause of Alzheimer's Disease: The Theory of Multipathology Convergence to Chronic Neuronal Stress. *Aging and disease*. 2022;13(1):37. doi:10.14336/AD.2021.0529

Devore EE, Kang JH, Breteler MMB, Grodstein F. Dietary intakes of berries and flavonoids in relation to cognitive decline. *Ann Neurol*. 2012;72(1):135-143. doi:10.1002/ana.23594

Dey A, Bhattacharya R, Mukherjee A, Pandey DK. Natural products against Alzheimer's disease: Pharmaco-therapeutics and biotechnological interventions. *Biotechnology Advances*. 2017;35(2):178-216. doi:10.1016/j.biotechadv.2016.12.005

Dickstein DL, Kabaso D, Rocher AB, Luebke JI, Wearne SL, Hof PR. Changes in the structural complexity of the aged brain. *Aging Cell*. 2007;6(3):275-284. doi:10.1111/j.1474-9726.2007.00289.x

Dickstein DL, Weaver CM, Luebke JI, Hof PR. Dendritic spine changes associated with normal aging. *Neuroscience*. 2013;251:21-32. doi:10.1016/j.neuroscience.2012.09.077

Downs JL, Urbanski HF. Neuroendocrine Changes in the Aging Reproductive Axis of Female Rhesus Macaques (Macaca mulatta)1. *Biology of Reproduction*. 2006;75(4):539-546. doi:10.1095/biolreprod.106.051839

Drummond E, Wisniewski T. Alzheimer's disease: experimental models and reality. *Acta Neuropathol*. 2017;133(2):155-175. doi:10.1007/s00401-016-1662-x

Duan W, Zhang YP, Hou Z, et al. Novel insights into NeuN: from neuronal marker to splicing regulator. *Mol Neurobiol*. 2016;53:1637-1647. doi:10.1007/s12035-015-9122-5

Dumas JA. What Is Normal Cognitive Aging? Evidence from Task-Based Functional Neuroimaging. *Curr Behav Neurosci Rep*. 2015;2(4):256-261. doi:10.1007/s40473-015-0058-x

Dutta S, Sengupta P. Men and mice: Relating their ages. *Life Sciences*. 2016;152:244-248. doi:10.1016/j.lfs.2015.10.025

Duyckaerts C, Delatour B, Potier MC. Classification and basic pathology of Alzheimer disease. *Acta Neuropathol*. 2009;118(1):5-36. doi:10.1007/s00401-009-0532-1

Dye L, Boyle NB, Champ C, Lawton C. The relationship between obesity and cognitive health and decline. *Proc Nutr Soc*. 2017;(v;76(4):443-454). doi:10.1017/S0029665117002014.

Edler MK, Munger EL, Meindl RS, et al. Neuron loss associated with age but not Alzheimer's disease pathology in the chimpanzee brain. *Phil Trans R Soc B*. 2020;375(1811):20190619. doi:10.1098/rstb.2019.0619

Edmonds EC, Bangen KJ, Delano-Wood L, et al. for the Alzheimer's Disease Neuroimaging Initiative Patterns of cortical and subcortical amyloid burden across stages of preclinical Alzheimer's disease. *J Int Neuropsychol Soc*. 2016;22:978-990. doi:10.1017/S1355617716000928.

Egan MF, Kost J, Voss T, et al. Randomized Trial of Verubecestat for Prodromal Alzheimer's Disease. *N Engl J Med*. 2019;380(15):1408-1420. doi:10.1056/NEJMoa1812840

Emborg ME. Nonhuman Primate Models of Neurodegenerative Disorders. *ILAR Journal*. 2017;58(2):190-201. doi:10.1093/ilar/ilx021

Estrada LI, Robinson AA, Amaral AC, et al. Evaluation of Long-Term Cryostorage of Brain Tissue Sections for Quantitative Histochemistry. *J Histochem Cytochem*. 2017;65(3):153-171. doi:10.1369/0022155416686934

Farlow M, Arnold SE, Dyck CH, et al. Safety and biomarker effects of solanezumab in patients with Alzheimer's disease. *Alzheimer's & Dementia*. 2012;8(4):261-271. doi:10.1016/j.jalz.2011.09.224

Fish PV, Steadman D, Bayle ED, Whiting P. New approaches for the treatment of Alzheimer's disease. *Bioorganic & Medicinal Chemistry Letters*. 2019;29(2):125-133. doi:10.1016/j.bmcl.2018.11.034

Fjell AM, McEvoy L, Holland D, Dale AM, Walhovd KB. What is normal in normal aging? Effects of aging, amyloid and Alzheimer's disease on the cerebral cortex and the hippocampus. *Progress in Neurobiology*. 2014;117:20-40. doi:10.1016/j.pneurobio.2014.02.004

Fjell AM, Westlye LT, Amlien I, et al. High Consistency of Regional Cortical Thinning in Aging across Multiple Samples. *Cerebral Cortex*. 2009;19(9):2001-2012. doi:10.1093/cercor/bhn232

Fontaine KR, Yang D, Gadbury GL, et al. Results of soy-based meal replacement formula on weight, anthropometry, serum lipids & blood pressure during a 40-week clinical weight loss trial. *Nutr J*. 2003;2:14. doi:10.1186/1475-2891-2-14

Fontana L, Meyer TE, Klein S, Holloszy JO. Long-term calorie restriction is highly effective in reducing the risk for atherosclerosis in humans. *Proc Natl Acad Sci USA*. 2004;101(17):6659-6663. doi:10.1073/pnas.0308291101

Forny-Germano L, Lyra e Silva NM, Batista AF, et al. Alzheimer's Disease-Like Pathology Induced by Amyloid-β Oligomers in Nonhuman Primates. *J Neurosci*. 2014;34(41):13629-13643. doi:10.1523/JNEUROSCI.1353-14.2014

Fracassi A, Marcatti M, Zolochevska O, et al. Oxidative Damage and Antioxidant Response in Frontal Cortex of Demented and Nondemented Individuals with Alzheimer's Neuropathology. *J Neurosci*. 2021;41(3):538-554. doi:10.1523/JNEUROSCI.0295-20.2020

Franklin MS, Kraemer GW, Shelton SE, Baker E, Kalin NH, Uno H. Gender differences in brain volume and size of corpus callosum and amygdala of rhesus monkey measured from MRI images. *Brain Research*. 2000;852(2):263-267. doi:10.1016/S0006-8993(99)02093-4

Freeman SH, Kandel R, Cruz L, et al. Preservation of Neuronal Number Despite Age-Related Cortical Brain Atrophy in Elderly Subjects Without Alzheimer Disease. *J Neuropathol Exp Neurol*. 2008;67(12):1205-1212. doi:10.1097/NEN.0b013e31818fc72f

Fricker M, Tolkovsky AM, Borutaite V, Coleman M, Brown GC. Neuronal Cell Death. *Physiological Reviews*. 2018;98(2):813-880. doi:10.1152/physrev.00011.2017

Furcila D, DeFelipe J, Alonso-Nanclares L. A Study of Amyloid-β and Phosphotau in Plaques and Neurons in the Hippocampus of Alzheimer's Disease Patients. *JAD*. 2018;64(2):417-435. doi:10.3233/JAD-180173

Gardener H, Caunca M, Dong C, et al. Obesity Measures in Relation to Cognition in the Northern Manhattan Study. *JAD*. 2020;78(4):1653-1660. doi:10.3233/JAD-201071

Gazzaley AH, Thakker MM, Hof PR, Morrison JH. Preserved number of entorhinal cortex layer II neurons in aged macaque monkeys. *Neurobiol Aging*. 1997;18:549-553. doi:10.1016/S0197-4580(97)00112-7

Gearing M, Rebeck GW, Hyman BT, Tigges J, Mirra SS. Neuropathology and apolipoprotein E profile of aged chimpanzees: implications for Alzheimer disease. *Proc Natl Acad Sci USA*. 1994;91(20):9382-9386. doi:10.1073/pnas.91.20.9382

Gearing M, Tigges J, Mori H, Mirra SS. Aβ40 is a major form of β-amyloid in nonhuman primates. *Neurobiology of Aging*. 1996;17(6):903-908. doi:10.1016/S0197-4580(96)00164-9

Giannakopoulos P, Silhol S, Jallageas V, et al. Quantitative analysis of tau protein-immunoreactive accumulations and β amyloid protein deposits in the cerebral cortex of the mouse lemur, Microcebus murinus. *Acta Neuropathologica*. 1997;94(2):131-139. doi:10.1007/s004010050684

Giannaris EL, Rosene DL. A stereological study of the numbers of neurons and glia in the primary visual cortex across the lifespan of male and female rhesus monkeys. *J Comp Neurol*. 2012;520:3492-3508. doi:10.1002/cne.23101

Gibbs RA, Rogers J, Katze MG, et al. Evolutionary and biomedical insights from the rhesus macaque genome. *Science*. 2007;316:222-234. doi:10.1126/science.1139247.

Gigi A, Babai R, Katzav E, Atkins S, Hendler T. Prefrontal and parietal regions are involved in naming of objects seen from unusual viewpoints. *Behavioral Neuroscience*. 2007;121(5):836-844. doi:10.1037/0735-7044.121.5.836

Gittins R, Harrison PJ. Neuronal density, size and shape in the human anterior cingulate cortex: A comparison of Nissl and NeuN staining. *Brain Res Bull*. 2004;63:155-160. doi:10.1016/j.brainresbull.2004.02.005

Gómez-Isla T, Hollister R, West H, et al. Neuronal loss correlates with but exceeds neurofibrillary tangles in Alzheimer's disease: Neuronal Loss in the Superior Temporal Sulcus in Alzheimer's Disease. *Ann Neurol*. 1997;41(1):17-24. doi:10.1002/ana.410410106

González-Granillo AE, Gnecco D, Díaz A, et al. Curcumin induces cortico-hippocampal neuronal reshaping and memory improvements in aged mice. *Journal of Chemical Neuroanatomy*. 2022;121:102091. doi:10.1016/j.jchemneu.2022.102091

Gregorini A, Di Canio A, Palmucci E, Tomasetti M, Rocchi MBL, Colomba M. Effects of Animal-Assisted Therapy (AAT) in Alzheimer's Disease: A Case Study. *Healthcare*. 2022;10(3):567. doi:10.3390/healthcare10030567

Gültekin F, Nazıroğlu M, Savaş HB, Çiğ B. Calorie restriction protects against apoptosis, mitochondrial oxidative stress and increased calcium signaling through inhibition of TRPV1 channel in the hippocampus and dorsal root ganglion of rats. *Metab Brain Dis*. 2018;33(5):1761-1774. doi:10.1007/s11011-018-0289-0

Gundersen HJG. Stereology of arbitrary particles*: A review of unbiased number and size estimators and the presentation of some new ones, in memory of William R. Thompson. *Journal of Microscopy*. 1986;143(1):3-45. doi:10.1111/j.1365-2818.1986.tb02764.x

Gusel'nikova VV, Korzhevskiy DE. NeuN As a Neuronal Nuclear Antigen and Neuron Differentiation Marker. *Acta Naturae*. 2015;7(2):42-47. doi:10.32607/20758251-2015-7-2-42-47

Haass C, Levin J. Hat die Alzheimer-Forschung versagt?: Das Scheitern amyloidbasierter klinischer Studien. *Nervenarzt*. 2019;90(9):884-890. doi:10.1007/s00115-019-0751-1

Hadad N, Unnikrishnan A, Jackson JA, et al. Caloric restriction mitigates age-associated hippocampal differential CG and non-CG methylation. *Neurobiol Aging*. 2018;67:53-66. doi:10.1016/j.neurobiolaging.2018.03.009

Halagappa VK, Guo Z, Pearson M, et al. Intermittent fasting and caloric restriction ameliorate age-related behavioral deficits in the triple-transgenic mouse model of Alzheimer's disease. *Neurobiol Dis*. 2007;26:212-220. doi:10.1016/j.nbd.2006.12.019

Han ZZ, Kang SG, Arce L, Westaway D. Prion-like strain effects in tauopathies. *Cell Tissue Res*. Published online April 23, 2022. doi:10.1007/s00441-022-03620-1

Haque RU, Levey AI. Alzheimer's disease: A clinical perspective and future nonhuman primate research opportunities. *Proc Natl Acad Sci U S A*. 2019;23;116(52):26224–9. doi:10.1073/pnas.1912954116.

Hara Y, Rapp PR, Morrison JH. Neuronal and morphological bases of cognitive decline in aged rhesus monkeys. *AGE*. 2012;34(5):1051-1073. doi:10.1007/s11357-011-9278-5

Harada CN, Natelson Love MC, Triebel KL. Normal cognitive aging. *Clin Geriatr Med*. 2013;29:737-752. doi:10.1016/j.cger.2013.07.002

Hardy J, Allsop D. Amyloid deposition as the central event in the aetiology of Alzheimer's disease. *Trends in Pharmacological Sciences*. 1991;12:383-388. doi:10.1016/0165-6147(91)90609-V

Hardy JA, Higgins GA. Alzheimer's Disease: The Amyloid Cascade Hypothesis. *Science*. 1992;256(5054):184-185. doi:10.1126/science.1566067

Harper JM, Leathers CW, Austad SN. Does caloric restriction extend life in wild mice? *Aging Cell*. 2006;5:441-449. doi:10.1111/j.1474-9726.2006.00236.x

Härtig W, Klein C, Brauer K, et al. Abnormally phosphorylated protein tau in the cortex of aged individuals of various mammalian orders. *Acta Neuropathologica*. 2000;100(3):305-312. doi:10.1007/s004010000183

Heilbroner PL, Kemper TL. The cytoarchitectonic distribution of senile plaques in three aged monkeys. *Acta Neuropathol*. 1990;81(1):60-65. doi:10.1007/BF00662638

Herndon JG, Moss MB, Rosene DL, Killiany RJ. Patterns of cognitive decline in aged rhesus monkeys. *Behavioural Brain Research*. 1997;87(1):25-34. doi:10.1016/S0166-4328(96)02256-5

Hirano M, Iritani S, Fujishiro H, et al. Globular glial tauopathy Type I presenting with behavioral variant frontotemporal dementia. *Neuropathology*. 2020;40(5):515-525. doi:10.1111/neup.12668

Hof PR, Nimchinsky EA, Young WG, Morrison JH. Numbers of Meynert and layer IVB cells in area V1: A stereologic analysis in young and aged macaque monkeys. *J Comp Neurol*. 2000;420:113-126. doi:10.1002/(SICI)1096-9861(20000424)420:1

Houthoofd K, Vanfleteren JR. Public and private mechanisms of life extension in Caenorhabditis elegans. *Mol Genet Genomics*. 2007;277(6):601-617. doi:10.1007/s00438-007-0225-1

Huffman KM, Parker DC, Bhapkar M, et al. Calorie restriction improves lipid-related emerging cardiometabolic risk factors in healthy adults without obesity: Distinct influences of BMI and sex from CALERIE™ a multicentre, phase 2, randomised controlled trial. *eClinicalMedicine*. 2022;43:101261. doi:10.1016/j.eclinm.2021.101261

Ihara R, Vincent BD, Baxter MR, et al. Relative neuron loss in hippocampal sclerosis of aging and Alzheimer's disease. *Ann Neurol*. 2018;84(5):741-753. doi:10.1002/ana.25344

Ikonomovic MD, Klunk WE, Abrahamson EE, et al. Post-mortem correlates of in vivo PiB-PET amyloid imaging in a typical case of Alzheimer's disease. *Brain*. 2008;131:1630-1645. doi:10.1093/brain/awn016

Ingram DK, de Cabo R. Calorie restriction in rodents: Caveats to consider. *Ageing Research Reviews*. 2017;39:15-28. doi:10.1016/j.arr.2017.05.008

Ingram DK, Cutler RG, Weindruch R, et al. Dietary Restriction and Aging: The Initiation of a Primate Study. *Journal of Gerontology*. 1990;45(5):B148-B163. doi:10.1093/geronj/45.5.B148

Ingram DK, Weindruch R, Spangler EL, Freeman JR, Walford RL. Dietary Restriction Benefits Learning and Motor Performance of Aged Mice. *Journal of Gerontology*. 1987;42(1):78-81. doi:10.1093/geronj/42.1.78

Kahlson MA, Colodner KJ. Glial Tau Pathology in Tauopathies: Functional Consequences. *J Exp Neurosci*. 2015;9s2:JEN.S25515. doi:10.4137/JEN.S25515

Kastman EK, Willette AA, Coe CL, et al. A Calorie-Restricted Diet Decreases Brain Iron Accumulation and Preserves Motor Performance in Old Rhesus Monkeys. *Journal of Neuroscience*. 2012;32(34):11897-11904. doi:10.1523/JNEUROSCI.2553-12.2012

Kemnitz JW, Weindruch R, Roecker EB, Crawford K, Kaufman PL, Ershler WB. Dietary Restriction of Adult Male Rhesus Monkeys: Design, Methodology, and Preliminary Findings From the First Year of Study. *Journal of Gerontology*. 1993;48(1):B17-B26. doi:10.1093/geronj/48.1.B17

Kennedy BK, Steffen KK, Kaeberlein M. Ruminations on dietary restriction and aging. *Cell Mol Life Sci*. 2007;64(11):1323-1328. doi:10.1007/s00018-007-6470-y

Kępka A, Ochocińska A, Borzym-Kluczyk M, et al. Healthy Food Pyramid as Well as Physical and Mental Activity in the Prevention of Alzheimer's Disease. *Nutrients*. 2022;14(8):1534. doi:10.3390/nu14081534

Keuker JIH, Luiten PGM, Fuchs E. Preservation of hippocampal neuron numbers in aged rhesus monkeys. *Neurobiol Aging*. 2003;24:157-165. doi:10.1016/S0197-4580(02)00062-3

Kim HY, Frongillo EA, Han SS, et al. Academic performance of Korean children is associated with dietary behaviours and physical status. *Asia Pac J Clin Nutr*. 2003;12(2):186-192.

Kim KK, Adelstein RS, Kawamoto S. Identification of neuronal nuclei (NeuN) as Fox-3, a new member of the Fox-1 gene family of splicing factors. *J Biol Chem*. 2009;284:31052-31061. doi:10.1074/jbc.M109.052969

Kimura N, Yanagisawa K, Terao K, et al. Age-related changes of intracellular Aβ in cynomolgus monkey brains. *Neuropathol Appl Neurobiol*. 2005;31:170-180. doi:10.1111/j.1365-2990.2004.00624.x

Kishi T, Hirooka Y, Nagayama T, et al. Calorie restriction improves cognitive decline via up-regulation of brain-derived neurotrophic factor: Tropomyosin-related kinase B in hippocampus of obesity-induced hypertensive rats. *Int Heart J*. 2015;56:110-115. doi:10.1536/ihj.14-168

Kok FK, van Leerdam SL, de Lange ECM. Potential Mechanisms Underlying Resistance to Dementia in Non-Demented Individuals with Alzheimer's Disease Neuropathology. Taglialatela G, ed. *JAD*. Published online March 7, 2022:1-31. doi:10.3233/JAD-210607

Komori T. Tau-positive dial Inclusions in Progressive Supranuclear Palsy, Corticobasal Degeneration and Pick's Disease. *Brain Pathology*. 1999;9(4):663-679. doi:10.1111/j.1750-3639.1999.tb00549.x

Korf JM, Ganesh BP, McCullough LD. Gut dysbiosis and age-related neurological diseases in females. *Neurobiology of Disease*. 2022;168:105695. doi:10.1016/j.nbd.2022.105695

Kosik KS. Tau protein and neurodegeneration. *Mol Neurobiol*. 1990;4(3-4):171-179. doi:10.1007/BF02780339

Kovacs GG. Tauopathies. In: *Handbook of Clinical Neurology*. Vol 145. Elsevier; 2018:355-368. doi:10.1016/B978-0-12-802395-2.00025-0

Kovacs GG, Lee VM, Trojanowski JQ. Protein astrogliopathies in human neurodegenerative diseases and aging: Protein astrogliopathies. *Brain Pathology*. 2017;27(5):675-690. doi:10.1111/bpa.12536

Kraus WE, Bhapkar M, Huffman KM, et al. 2 years of calorie restriction and cardiometabolic risk (CALERIE): exploratory outcomes of a multicentre, phase 2, randomised controlled trial. *The lancet Diabetes & endocrinology*. 2019;7(9):673-683. doi:10.1016/S2213-8587(19)30151-2

LaFerla FM, Green KN. Animal Models of Alzheimer Disease. *Cold Spring Harbor Perspectives in Medicine*. 2012;2(11):a006320-a006320. doi:10.1101/cshperspect.a006320

LaFerla FM, Green KN, Oddo S. Intracellular amyloid-β in Alzheimer's disease. *Nat Rev Neurosci*. 2007;8:499-509. doi:10.1038/nrn2168

Lai ZC, Moss MB, Killiany RJ, Rosene DL, Herndon JG. Executive system dysfunction in the aged monkey: Spatial and object reversal learning. *Neurobiology of Aging*. 1995;16(6):947-954. doi:10.1016/0197-4580(95)02014-4

Le Bourg E. Does calorie restriction in primates increase lifespan? Revisiting studies on macaques (Macaca mulatta) and mouse lemurs (Microcebus murinus. *BioEssays*. 2018;40:e1800111. doi:10.1002/bies.201800111.

Letenneur L, Proust-Lima C, Le Gouge A, Dartigues J, Barberger-Gateau P. Flavonoid Intake and Cognitive Decline over a 10-Year Period. *American Journal of Epidemiology*. 2007;165(12):1364-1371. doi:10.1093/aje/kwm036

Lewis J, Dickson DW. Propagation of tau pathology: hypotheses, discoveries, and yet unresolved questions from experimental and human brain studies. *Acta Neuropathol*. 2016;131(1):27-48. doi:10.1007/s00401-015-1507-z

Li R, Robinson M, Ding X, et al. Genistein: A focus on several neurodegenerative diseases. *Journal of Food Biochemistry*. Published online April 22, 2022. doi:10.1111/jfbc.14155

Liang SY, Wang ZT, Tan L, Yu JT. Tau Toxicity in Neurodegeneration. *Mol Neurobiol*. Published online March 31, 2022. doi:10.1007/s12035-022-02809-3

Lim GP, Chu T, Yang F, Beech W, Frautschy SA, Cole GM. The Curry Spice Curcumin Reduces Oxidative Damage and Amyloid Pathology in an Alzheimer Transgenic Mouse. *J Neurosci*. 2001;21(21):8370-8377. doi:10.1523/JNEUROSCI.21-21-08370.2001

Lucey BP. It's complicated: The relationship between sleep and Alzheimer's disease in humans. *Neurobiology of Disease*. 2020;144:105031. doi:10.1016/j.nbd.2020.105031

Luebke J, Barbas H, Peters A. Effects of normal aging on prefrontal area 46 in the rhesus monkey. *Brain Res Rev*. 2010;62:212-232. doi:10.1016/j.brainresrev.2009.12.002

Luna SL, Brown DI, Kohama SG, Urbanski HF. Lack of effect of short-term DHEA supplementation on the perimenopausal ovary†. *Biology of Reproduction*. 2020;103(6):1209-1216. doi:10.1093/biolre/ioaa160

Major DE, Kesslak JP, Cotman CW, Finch CE, Day J. Life-long dietary restriction attenuates age-related increases in hippocampal glial fibrillary acidic protein mRNA. *Neurobiol Aging*. 1997;18:523-526. doi:10.1016/s0197-4580(97)00102-4

Mancuso C, Bates TE, Butterfield DA, et al. Natural antioxidants in Alzheimer's disease. *Expert Opinion on Investigational Drugs*. 2007;16(12):1921-1931. doi:10.1517/13543784.16.12.1921

Marner L, Nyengaard JR, Tang Y, Pakkenberg B. Marked loss of myelinated nerve fibers in the human brain with age. *J Comp Neurol*. 2003;462(2):144-152. doi:10.1002/cne.10714

Martin CK, Bhapkar M, Pittas AG, et al. Effect of calorie restriction on mood, quality of life, sleep, and sexual function in healthy nonobese adults the CALERIE 2 randomized clinical trial. *JAMA Intern Med*. 2016;176:743-752. doi:10.1001/jamainternmed.2016.1189

Martin LJ, Sisodia SS, Koo EH, et al. Amyloid precursor protein in aged nonhuman primates. *Proc Natl Acad Sci USA*. 1991;88:1461-1465.

Matthews KA, Xu W, Gaglioti AH, et al. Racial and ethnic estimates of Alzheimer's disease and related dementias in the United States (2015–2060) in adults aged ≥65 years. *Alzheimer's & Dementia*. 2019;15(1):17-24. doi:10.1016/j.jalz.2018.06.3063

Mattison JA, Black A, Huck J, et al. Age-related decline in caloric intake and motivation for food in rhesus monkeys. *Neurobiol Aging*. 2005;26:1117-1127. doi:10.1016/j.neurobiolaging.2004.09.013

Mattison JA, Colman RJ, Beasley TM, et al. Caloric restriction improves health and survival of rhesus monkeys. *Nat Commun*. 2017;8:1-12. doi:10.1038/ncomms14063

Mattison JA, Roth GS, Beasley TM, et al. Impact of caloric restriction on health and survival in rhesus monkeys from the NIA study. *Nature*. 2012;489:318-321. doi:10.1038/nature11432

Mattison JA, Vaughan KL. An overview of nonhuman primates in aging research. *Exp Gerontol*. 2017;94:41-45. doi:10.1016/j.exger.2016.12.005

Maust DT, Solway E, Langa KM, et al. Perception of Dementia Risk and Preventive Actions Among US Adults Aged 50 to 64 Years. *JAMA Neurol*. 2020;77(2):259. doi:10.1001/jamaneurol.2019.3946

McCay CM, Crowell MF. Prolonging the Life Span. *Science*. 1934;39:405-414.

McConnell HL, Li Z, Woltjer RL, Mishra A. Astrocyte dysfunction and neurovascular impairment in neurological disorders: Correlation or causation? *Neurochemistry International*. 2019;128:70-84. doi:10.1016/j.neuint.2019.04.005

McDade E. Why Amyloid Is Still a Target for Alzheimer Disease Clinical Trials: AMYLOID AS A THERAPEUTIC TARGET. *J Am Geriatr Soc*. 2019;67(4):845-847. doi:10.1111/jgs.15829

Mehla J, Gupta P, Pahuja M, Diwan D, Diksha D. Indian Medicinal Herbs and Formulations for Alzheimer's Disease, from Traditional Knowledge to Scientific Assessment. *Brain Sciences*. 2020;10(12):964. doi:10.3390/brainsci10120964

Merrill DA, Roberts JA, Tuszynski MH. Conservation of neuron number and size in entorhinal cortex layers II, III, and V/VI of aged primates. *J Comp Neurol*. 2000;422:396-401. doi:10.1002/1096-9861(20000703)422:3

Messaoudi I, Estep R, Robinson B, Wong SW. Nonhuman Primate Models of Human Immunology. *Antioxidants & Redox Signaling*. 2011;14(2):261-273. doi:10.1089/ars.2010.3241

Miller AA, Spencer SJ. Obesity and neuroinflammation: a pathway to cognitive impairment. *Brain Behav Immun*. 2014;(v;42:10-21). doi:10.1016/j.bbi.2014.04.001.

Miziak B, Błaszczyk B, Czuczwar SJ. Some Candidate Drugs for Pharmacotherapy of Alzheimer's Disease. *Pharmaceuticals*. 2021;14(5):458. doi:10.3390/ph14050458

Moloney CM, Lowe VJ, Murray ME. Visualization of neurofibrillary tangle maturity in Alzheimer's disease: A clinicopathologic perspective for biomarker research. *Alzheimer's & Dementia*. 2021;17(9):1554-1574. doi:10.1002/alz.12321

Moore T. Impairment in abstraction and set shifting in aged Rhesus monkeys. *Neurobiology of Aging*. 2003;24(1):125-134. doi:10.1016/S0197-4580(02)00054-4

Moore TL, Bowley BGE, Shultz PL, et al. Oral curcumin supplementation improves fine motor function in the middle-aged rhesus monkey. *Somatosens Mot Res*. 2018;35(1):1-10. doi:10.1080/08990220.2018.1432481

Moore TL, Killiany RJ, Herndon JG, Rosene DL, Moss MB. Executive system dysfunction occurs as early as middle-age in the rhesus monkey. *Neurobiology of Aging*. 2006;27(10):1484-1493. doi:10.1016/j.neurobiolaging.2005.08.004

Morrison JH, Hof PR. Chapter 37 Selective vulnerability of corticocortical and hippocampal circuits in aging and Alzheimer's disease. In: *Progress in Brain Research*. Vol 136. Elsevier; 2002:467-486. doi:10.1016/S0079-6123(02)36039-4

Morrison JH, Hof PR. Life and Death of Neurons in the Aging Brain. *Science*. 1997;278(5337):412-419. doi:10.1126/science.278.5337.412

Moss MB, Moore TL, Schettler SP, Killiany R, Rosene D. Successful vs. Unsuccessful Aging in the Rhesus Monkey. In: Riddle DR, ed. *Brain Aging: Models, Methods, and Mechanisms*. Frontiers in Neuroscience. CRC Press/Taylor & Francis; 2007. Accessed April 24, 2022. http://www.ncbi.nlm.nih.gov/books/NBK1833/

Murphy KR. Is the Relationship Between Cognitive Ability and Job Performance Stable Over Time? *Human Performance*. 1989;2(3):183-200. doi:10.1207/s15327043hup0203_3

Nagahara AH, Bernot T, Tuszynski MH. Age-related cognitive deficits in rhesus monkeys mirror human deficits on an automated test battery. *Neurobiology of Aging*. 2010;31(6):1020-1031. doi:10.1016/j.neurobiolaging.2008.07.007

Neddens J, Temmel M, Flunkert S, et al. Phosphorylation of different tau sites during progression of Alzheimer's disease. *acta neuropathol commun*. 2018;6(1):52. doi:10.1186/s40478-018-0557-6

Nelson PT, Alafuzoff I, Bigio EH, et al. Correlation of Alzheimer Disease Neuropathologic Changes With Cognitive Status: A Review of the Literature. *J Neuropathol Exp Neurol*. 2012;71(5):362-381. doi:10.1097/NEN.0b013e31825018f7

Nolan A, De Paula Franca Resende E, Petersen C, et al. Astrocytic Tau Deposition Is Frequent in Typical and Atypical Alzheimer Disease Presentations. *Journal of*

Neuropathology & Experimental Neurology. 2019;78(12):1112-1123. doi:10.1093/jnen/nlz094

O'Brien RJ, Wong PC. Amyloid Precursor Protein Processing and Alzheimer's Disease. *Annu Rev Neurosci*. 2011;34(1):185-204. doi:10.1146/annurev-neuro-061010-113613

Oikawa N, Kimura N, Yanagisawa K. Alzheimer-type tau pathology in advanced aged nonhuman primate brains harboring substantial amyloid deposition. *Brain Research*. 2010;1315:137-149. doi:10.1016/j.brainres.2009.12.005

Ooms S, Overeem S, Besse K, Rikkert MO, Verbeek M, Claassen JAHR. Effect of 1 Night of Total Sleep Deprivation on Cerebrospinal Fluid β-Amyloid 42 in Healthy Middle-Aged Men: A Randomized Clinical Trial. *JAMA Neurol*. 2014;71(8):971. doi:10.1001/jamaneurol.2014.1173

Oster H. The interplay between stress, circadian clocks, and energy metabolism. *Journal of Endocrinology*. 2020;247(1):R13-R25. doi:10.1530/JOE-20-0124

Ostrowitzki S, Lasser RA, Dorflinger E, et al. A phase III randomized trial of gantenerumab in prodromal Alzheimer's disease. *Alz Res Therapy*. 2017;9(1):95. doi:10.1186/s13195-017-0318-y

Park DC, Reuter-Lorenz P. The Adaptive Brain: Aging and Neurocognitive Scaffolding. *Annu Rev Psychol*. 2009;60(1):173-196. doi:10.1146/annurev.psych.59.103006.093656

Parrella E, Maxim T, Maialetti F, et al. Protein restriction cycles reduce IGF-1 and phosphorylated Tau, and improve behavioral performance in an Alzheimer's disease mouse model. *Aging Cell*. 2013;12(2):257-268. doi:10.1111/acel.12049

Paspalas CD, Carlyle BC, Leslie S, et al. The aged rhesus macaque manifests Braak stage III/IV Alzheimer's-like pathology. *Alzheimer's & Dementia*. 2018;14(5):680-691. doi:10.1016/j.jalz.2017.11.005

Pavez-Fox MA, Negron-Del Valle JE, Thompson IJ, et al. Sociality predicts individual variation in the immunity of free-ranging rhesus macaques. *Physiology & Behavior*. 2021;241:113560. doi:10.1016/j.physbeh.2021.113560

Perez SE, Raghanti MA, Hof PR, et al. Alzheimer's disease pathology in the neocortex and hippocampus of the western lowland gorilla (*Gorilla gorilla gorilla*): AD Pathology in the Gorilla Brain. *J Comp Neurol*. 2013;521(18):4318-4338. doi:10.1002/cne.23428

Peters A, Morrison JH, Rosene DL, Hyman BT. Feature article are neurons lost from the primate cerebral cortex during normal aging? *Cereb Cortex*. 1998;8:295-300. doi:10.1093/cercor/8.4.295

Peters A, Rosene DL, Moss MB, et al. Neurobiological bases of age-related cognitive decline in the rhesus monkey. *J Neuropath Exp Neuro*. 1996;55:861-874. doi:10.1097/00005072-199608000-00001

Pimontel MA, Kanellopoulos D, Gunning FM. Neuroanatomical Abnormalities in Older Depressed Adults With Apathy: A Systematic Review. *J Geriatr Psychiatry Neurol*. 2020;33(5):289-303. doi:10.1177/0891988719882100

Pittas AG, Das SK, Hajduk CL, et al. A Low-Glycemic Load Diet Facilitates Greater Weight Loss in Overweight Adults With High Insulin Secretion but Not in Overweight Adults With Low Insulin Secretion in the CALERIE Trial. *Diabetes Care*. 2005;28(12):2939-2941. doi:10.2337/diacare.28.12.2939

Poddar J, Pradhan M, Ganguly G, Chakrabarti S. Biochemical deficits and cognitive decline in brain aging: Intervention by dietary supplements. *Journal of Chemical Neuroanatomy*. 2019;95:70-80. doi:10.1016/j.jchemneu.2018.04.002

Price JL. Tangles and plaques in healthy aging and Alzheimer's disease: independence or interaction? *Seminars in Neuroscience*. 1994;6(6):395-402. doi:10.1006/smns.1994.1051

Price JL, Morris JC. So what if tangles precede plaques? *Neurobiology of Aging*. 2004;25(6):721-723. doi:10.1016/j.neurobiolaging.2003.12.017

Price JL, Morris JC. Tangles and plaques in nondemented aging and "preclinical" Alzheimer's disease. *Ann Neurol*. 1999;45(3):358-368. doi:10.1002/1531-8249(199903)45:3<358::AID-ANA12>3.0.CO;2-X

Primiani CT, Ryan VH, Rao JS, et al. Coordinated Gene Expression of Neuroinflammatory and Cell Signaling Markers in Dorsolateral Prefrontal Cortex during Human Brain Development and Aging. Sirén AL, ed. *PLoS ONE*. 2014;9(10):e110972. doi:10.1371/journal.pone.0110972

Rapp P, Amaral D. Evidence for task-dependent memory dysfunction in the aged monkey. *J Neurosci*. 1989;9(10):3568-3576. doi:10.1523/JNEUROSCI.09-10-03568.1989

Rastogi M, Ojha RP, Prabu PC, Devi BP, Agrawal A, Dubey GP. Prevention of age-associated neurodegeneration and promotion of healthy brain ageing in female Wistar rats by long term use of bacosides. *Biogerontology*. 2012;13(2):183-195. doi:10.1007/s10522-011-9367-y

Raz N, Lindenberger U, Rodrigue KM, et al. Regional Brain Changes in Aging Healthy Adults: General Trends, Individual Differences and Modifiers. *Cerebral Cortex*. 2005;15(11):1676-1689. doi:10.1093/cercor/bhi044

Resnick SM, Pham DL, Kraut MA, Zonderman AB, Davatzikos C. Longitudinal Magnetic Resonance Imaging Studies of Older Adults: A Shrinking Brain. *J Neurosci*. 2003;23(8):3295-3301. doi:10.1523/JNEUROSCI.23-08-03295.2003

Rickman AD, Williamson DA, Martin CK, et al. The CALERIE Study: Design and methods of an innovative 25% caloric restriction intervention. *Contemporary Clinical Trials*. 2011;32(6):874-881. doi:10.1016/j.cct.2011.07.002

Roberts DE, Killiany RJ, Rosene DL. Neuron numbers in the hypothalamus of the normal aging rhesus monkey: Stability across the adult lifespan and between the sexes. *J Comp Neurol*. 2012;520(6):1181-1197. doi:10.1002/cne.22761

Roberts R, Knopman DS. Classification and Epidemiology of MCI. *Clinics in Geriatric Medicine*. 2013;29(4):753-772. doi:10.1016/j.cger.2013.07.003

Robinson LM, Coleman K, Capitanio JP, et al. Rhesus macaque personality, dominance, behavior, and health. *Am J Primatol*. 2018;80(2):e22739. doi:10.1002/ajp.22739

Rosene DL, Roy NJ, Davis BJ. A cryoprotection method that facilitates cutting frozen sections of whole monkey brains for histological and histochemical processing without freezing artifact. *J Histochem Cytochem*. 1986;34:1301-1315.

Salat DH. Thinning of the Cerebral Cortex in Aging. *Cerebral Cortex*. 2004;14(7):721-730. doi:10.1093/cercor/bhh032

Saleem KS, Logothetis NK. *A Combined MRI and Histology Atlas of the Rhesus Monkey Brain in Stereotaxic Coordinates*. Academic Press; 2012.

Salloway S, Sperling R, Fox NC, et al. Two Phase 3 Trials of Bapineuzumab in Mild-to-Moderate Alzheimer's Disease. *N Engl J Med*. 2014;370(4):322-333. doi:10.1056/NEJMoa1304839

Salthouse TA. Trajectories of normal cognitive aging. *Psychology and Aging*. 2019;34(1):17-24. doi:10.1037/pag0000288

Salvia E, Petit C, Champely S, Chomette R, Di Rienzo F, Collet C. Effects of Age and Task Load on Drivers' Response Accuracy and Reaction Time When Responding to Traffic Lights. *Front Aging Neurosci*. 2016;8. doi:10.3389/fnagi.2016.00169

Sambataro F, Safrin M, Lemaitre HS, et al. Normal aging modulates prefrontoparietal networks underlying multiple memory processes: Aging of prefrontoparietal memory networks. *Eur J Neurosci*. 2012;36(11):3559-3567. doi:10.1111/j.1460-9568.2012.08254.x

Schafer MJ, Alldred MJ, Lee SH, et al. Reduction of β-amyloid and γ-secretase by calorie restriction in female Tg2576 mice. *Neurobiology of Aging*. 2015;36(3):1293-1302. doi:10.1016/j.neurobiolaging.2014.10.043

200. Schindelin J, Arganda-Carreras I, Frise E, et al. Fiji: an open-source platform for biological-image analysis. *Nat Methods*. 2012;9(7):676-682. doi:10.1038/nmeth.2019

Schliebs R, Arendt T. The cholinergic system in aging and neuronal degeneration. *Behavioural Brain Research*. 2011;221(2):555-563. doi:10.1016/j.bbr.2010.11.058

Schott JM. The neurology of ageing: what is normal? *Pract Neurol*. 2017;17(3):172-182. doi:10.1136/practneurol-2016-001566

Schultz C, Dehghani F, Hubbard GB, et al. Filamentous Tau Pathology in Nerve Cells, Astrocytes, and Oligodendrocytes of Aged Baboons. *J Neuropathol Exp Neurol*. 2000;59(1):39-52. doi:10.1093/jnen/59.1.39

Selkoe DJ. The molecular pathology of Alzheimer's disease. *Neuron*. 1991;6(4):487-498. doi:10.1016/0896-6273(91)90052-2

Senderovich H, Gardner S, Berall A, Shultz R, Grant B, Santaguida V. Therapeutic Touch in the Management of Responsive Behaviors in Patients with Dementia. *Dement Geriatr Cogn Disord*. Published online March 25, 2022:1-8. doi:10.1159/000523752

Sevigny J, Chiao P, Bussière T, et al. The antibody aducanumab reduces Aβ plaques in Alzheimer's disease. *Nature*. 2016;537(7618):50-56. doi:10.1038/nature19323

Shamy JL, Habeck C, Hof PR, et al. Volumetric Correlates of Spatiotemporal Working and Recognition Memory Impairment in Aged Rhesus Monkeys. *Cerebral Cortex*. 2011;21(7):1559-1573. doi:10.1093/cercor/bhq210

Sharma G, Huo A, Kimura T, et al. Tau isoform expression and phosphorylation in marmoset brains. *Journal of Biological Chemistry*. 2019;294(30):11433-11444. doi:10.1074/jbc.RA119.008415

Sloane JA, Pietropaolo MF, Rosene DL, et al. Lack of correlation between plaque burden and cognition in the aged monkey. *Acta Neuropathologica*. 1997;94(5):471-478. doi:10.1007/s004010050735

Smith DE. Memory Impairment in Aged Primates Is Associated with Focal Death of Cortical Neurons and Atrophy of Subcortical Neurons. *Journal of Neuroscience*. 2004;24(18):4373-4381. doi:10.1523/JNEUROSCI.4289-03.2004

Smith R, Wibom M, Pawlik D, Englund E, Hansson O. Correlation of In Vivo [^{18}F]Flortaucipir With Postmortem Alzheimer Disease Tau Pathology. *JAMA Neurol*. 2019;76(3):310. doi:10.1001/jamaneurol.2018.3692

Sorwell KG, Garten J, Renner L, et al. Hormone Supplementation During Aging: How Much and When? *Rejuvenation Research*. 2012;15(2):128-131. doi:10.1089/rej.2011.1251

Squire LR, Genzel L, Wixted JT, Morris RG. Memory Consolidation. *Cold Spring Harb Perspect Biol*. 2015;7(8):a021766. doi:10.1101/cshperspect.a021766

Stonebarger GA, Bimonte-Nelson HA, Urbanski HF. The Rhesus Macaque as a Translational Model for Neurodegeneration and Alzheimer's Disease. *Front Aging Neurosci*. 2021;13:734173. doi:10.3389/fnagi.2021.734173

Stonebarger GA, Urbanski HF, Woltjer RL, et al. Amyloidosis increase is not attenuated by long-term calorie restriction or related to neuron density in the prefrontal cortex of extremely aged rhesus macaques. *GeroScience*. 2020;42(6):1733-1749. doi:10.1007/s11357-020-00259-0

Takahashi RH, Capetillo-Zarate E, Lin MT, Milner TA, Gouras GK. Accumulation of Intraneuronal β-Amyloid 42 Peptides Is Associated with Early Changes in Microtubule-Associated Protein 2 in Neurites and Synapses. Iijima KM, ed. *PLoS ONE*. 2013;8(1):e51965. doi:10.1371/journal.pone.0051965

Tanaka H, Gourley DD, Dekhtyar M, Haley AP. Cognition, Brain Structure, and Brain Function in Individuals with Obesity and Related Disorders. *Curr Obes Rep*. 2020;9(4):544-549. doi:10.1007/s13679-020-00412-y

Thal DR, Capetillo-Zarate E, Del Tredici K, Braak H. The Development of Amyloid β Protein Deposits in the Aged Brain. *Sci Aging Knowl Environ*. 2006;2006(6). doi:10.1126/sageke.2006.6.re1

Thal DR, Rüb U, Schultz C, et al. Sequence of Aβ-Protein Deposition in the Human Medial Temporal Lobe. *J Neuropathol Exp Neurol*. 2000;59(8):733-748. doi:10.1093/jnen/59.8.733

Tigges J, Gordon TP, McClure HM, Hall EC, Peters A. Survival rate and life span of rhesus monkeys at the Yerkes regional primate research center. *Am J Primatol*. 1988;15(3):263-273. doi:10.1002/ajp.1350150308

Todorov OS, Weisbecker V, Gilissen E, Zilles K, de Sousa AA. Primate hippocampus size and organization are predicted by sociality but not diet. *Proc R Soc B*. 2019;286(1914):20191712. doi:10.1098/rspb.2019.1712

Trejo-Lopez JA, Yachnis AT, Prokop S. Neuropathology of Alzheimer's Disease. *Neurotherapeutics*. Published online November 2, 2021. doi:10.1007/s13311-021-01146-y

Uno H. The incidence of senile plaques and multiple infarction in aged Macaque brain. *Neurobiology of Aging*. 1993;14(6):673-674. doi:10.1016/0197-4580(93)90067-L

Uprety A, Moss MB, Rosene DL, Killiany RJ, Moore TL. Curcumin improves reversal learning in middle-aged rhesus monkeys. *Behavioral Neuroscience*. 2022;136(2):126-138. doi:10.1037/bne0000497

Vakulin A, D'Rozario A. Does sleep apnea exacerbate adverse driving behaviours and accident risk in drivers with preclinical markers of Alzheimer's Disease? *Sleep*. Published online April 22, 2022:zsac093. doi:10.1093/sleep/zsac093

Varholick JA, Pontiggia A, Murphy E, et al. Social dominance hierarchy type and rank contribute to phenotypic variation within cages of laboratory mice. *Sci Rep*. 2019;9(1):13650. doi:10.1038/s41598-019-49612-0

Vogel JW, Young AL, Oxtoby NP, et al. Four distinct trajectories of tau deposition identified in Alzheimer's disease. *Nat Med*. 2021;27(5):871-881. doi:10.1038/s41591-021-01309-6

Voytko ML. Impairments in acquisition and reversals of two-choice discriminations by aged rhesus monkeys. *Neurobiology of Aging*. 1999;20(6):617-627. doi:10.1016/S0197-4580(99)00097-4

Wahl D, Coogan SCP, Solon-Biet SM, et al. Cognitive and behavioral evaluation of nutritional interventions in rodent models of brain aging and dementia. *Clin Interv Aging*. 2017;12:1419-1428. doi:10.2147/CIA.S145247

Webster SJ, Bachstetter AD, Nelson PT, Schmitt FA, Van Eldik LJ. Using mice to model Alzheimer's dementia: an overview of the clinical disease and the preclinical behavioral changes in 10 mouse models. *Front Genet*. 2014;5. doi:10.3389/fgene.2014.00088

Weghe JV, Cras P, Kawai M, et al. Dystrophic neurites infiltrate extracellular neurofibrillary tangles in Alzheimer disease. *Brain Research*. 1991;560(1-2):303-305. doi:10.1016/0006-8993(91)91247-X

Weindruch R, Walford RL. Dietary Restriction in Mice Beginning at 1 Year of Age: Effect on Life-Span and Spontaneous Cancer Incidence. *Science*. 1982;215(4538):1415-1418. doi:10.1126/science.7063854

Weindruch R, Walford RL, Fligiel S, Guthrie D. The Retardation of Aging in Mice by Dietary Restriction: Longevity, Cancer, Immunity and Lifetime Energy Intake. *The Journal of Nutrition*. 1986;116(4):641-654. doi:10.1093/jn/116.4.641

Wesseling H, Mair W, Kumar M, et al. Tau PTM Profiles Identify Patient Heterogeneity and Stages of Alzheimer's Disease. *Cell*. 2020;183(6):1699-1713.e13. doi:10.1016/j.cell.2020.10.029

West MJ, Kawas CH, Stewart WF, Rudow GL, Troncoso JC. Hippocampal neurons in pre-clinical Alzheimer's disease. *Neurobiology of Aging*. 2004;25(9):1205-1212. doi:10.1016/j.neurobiolaging.2003.12.005

Willette AA, Coe CL, Birdsill AC, et al. Interleukin-8 and interleukin-10, brain volume and microstructure, and the influence of calorie restriction in old rhesus macaques. *AGE*. 2013;35(6):2215-2227. doi:10.1007/s11357-013-9518-y

Wooddell LJ, Kaburu SSK, Dettmer AM. Dominance rank predicts social network position across developmental stages in rhesus monkeys. *Am J Primatol.* 2020;82(11). doi:10.1002/ajp.23024

Yuan Y, Chen YP, Boyd-Kirkup J, Khaitovich P, Somel M. Accelerated aging-related transcriptome changes in the female prefrontal cortex. *Aging Cell.* 2012;11(5):894-901. doi:10.1111/j.1474-9726.2012.00859.x

Zhang J, Chen B, Lu J, et al. Brains of rhesus monkeys display Aβ deposits and glial pathology while lacking Aβ dimers and other Alzheimer's pathologies. *Aging Cell.* 2019;18(4). doi:10.1111/acel.12978

Zhang Y, Wu KM, Yang L, Dong Q, Yu JT. Tauopathies: new perspectives and challenges. *Mol Neurodegeneration.* 2022;17(1):28. doi:10.1186/s13024-022-00533-z

Zheng W, Tsai MY, Wolynes PG. Comparing the Aggregation Free Energy Landscapes of

Amyloid Beta(1–42) and Amyloid Beta(1–40). *J Am Chem Soc.* 2017;139(46):16666-

16676. doi:10.1021/jacs.7b08089